EX LIBRIS
UNIVERSITATIS
ALBERTENSIS

The Bruce Peel
Special Collections
Library

University of Alberta

Library Release Form

Name of Author: Kristine Moir Haug

Title of Thesis: Density Dependent Numerical Modelling of a Saline Plume in the Mannville Group Aquifer, Alberta Basin

Degree: Master of Science

Year this Degree Granted: 2003

Permission is hereby granted to the University of Alberta Library to reproduce single copies of this thesis and to lend or sell such copies for private, scholarly, or scientific research purposes only.

The author reserves all other publication and other rights in association with the copyright in the thesis, and except as hereinbefore provided, neither the thesis nor any substantial portion thereof may be printed or otherwise reproduced in any material form whatever without the author's prior written permission.

University of Alberta

Density Dependent Numerical Modelling of a Saline Plume in the Mannville Group Aquifer, Alberta Basin

By

Kristine Moir Haug ©

A THESIS SUBMITTED TO THE FACULTY OF GRADUATE STUDIES AND RESEARCH IN PARTIAL FULFILLMENT OF THE REQUIREMENTS FOR THE DEGREE OF MASTER OF SCIENCE.

DEPARTMENT OF EARTH AND ATMOSPHERIC SCIENCES

Edmonton, Alberta

Spring 2003

Digitized by the Internet Archive
in 2025 with funding from
University of Alberta Library

https://archive.org/details/0162017203082

University of Alberta

Faculty of Graduate Studies and Research

The undersigned certify that they have read, and recommended to the Faculty of Graduate Studies and Research for acceptance, a thesis entitled “Density Dependent Numerical Modelling of a Saline Plume in the Mannville Group Aquifer, Alberta Basin” submitted by Kristine Moir Haug in partial fulfillment of the requirements for the degree of Master of Science.

DEDICATION

For Blair

ABSTRACT

Numerical simulations were used to determine the timing, flow path and driving forces controlling the movement of a high total dissolved solids (TDS) plume presently observed in the Mannville Group Aquifer (MGA). The present day and paleo-hydrogeology of Upper Devonian to Lower Cretaceous strata in south-central Alberta was simulated using a two-dimensional, variable-density, finite-element flow and transport model (SUTRA). The plume originated in the Cooking Lake Formation, then ascended through the Leduc reefs, travelled along and through the Nisku Formation and entered the MGA at the Wabamun subcrop. The results from the numerical simulations showed that a present-day topographic gradient (0.001) was insufficient to create the plume during the past 30 million years of tectonic dormancy. The results from paleo simulations (hydraulic gradients of 0.01, 0.007, and 0.004) showed that after 5 million years a hydraulic gradient of 0.007 created the best representation of the salinity distribution observed today. A sensitivity analysis supported the parameters used in the base case.

ACKNOWLEDGEMENTS

I would like to thank my supervisor, Dr. Ben Rostron, for the opportunity to work on this project and for his guidance and encouragement throughout.

I would also like to thank my other committee members, Dr. Carl Mendoza and Dr. Andrew Bush. A special thanks to Dr. Mendoza for the sharing of his technical expertise to help this project along.

I would like to thank my fellow grad students: Jennifer Adams, Tannis Sharp, Heather Iampen and Heather von Hauff for their friendship and support over the years. A special thanks to Jennifer Adams for sharing her expertise and for all her help in getting this thesis completed.

Also, I would like to thank Nancy for her help and encouragement in this last year.

I would like to thank my husband Blair for his unwavering support and patience. Also, my very supportive parents Moir and Corrine, and the rest of my family Elling, Jocelyn, Ian, and Avery.

TABLE OF CONTENTS

Chapter 1 Introduction **1**

1.1 Previous Work/Setting 1

1.2 Research Objectives 3

1.3 Study Area 4

1.4 Thesis Organization 4

Chapter 2 Fluid Flow Mechanisms **8**

2.1 Variable Density Fluid Flow 8

2.1.1 Hydraulic Heads Formatulation 8

2.1.2 Driving Force Ratio (DFR) 9

2.1.3 Density-driven Flow 11

Chapter 3 Geological Background **17**

3.1 Regional Setting 17

3.1.1 The Alberta Basin 17

3.2 Stratigraphy 18

3.2.1 Upper Devonian Strata 19

3.2.2 Mississippian Strata 20

3.2.3 Jurassic Strata 20

3.2.4 Cretaceous Strata 20

3.3 Hydrostratigraphy and Hydrogeology 22

3.3.1 Upper Devonian Hydrogeologic Group (UDHG) 22

3.3.2 Mississippian Aquitard 23

3.3.3 Mannville Group Aquifer (MGA) 23

3.3.4 Viking Group Aquifer (VGA) 24

3.4 Regional Fluid Flow in the Alberta Basin 24

3.5 Chapter Summary 27

Chapter 4 Numerical Model and Approach **33**

4.1 Numerical Model Evaluation 33

4.2 The SUTRA Model 33

4.2.1 Fluid Mass Balance 34

4.2.2 Subsurface Solute Transport Mechanisms 35
4.3 Numerical Model Parameters 36
4.3.1 Numerical Model Grid 36
4.3.2 Boundary Conditions 39
4.3.3 Non-Spatial Parameters 40
4.3.4 Spatial Parameters 41
4.4 Temporal Discretization 42
4.5 Initial Conditions 42
4.6 Simulation Approach 43
4.6.1 Importance of Density Effects 43
4.6.2 Today's Gradient 44
4.6.3 Choosing the Paleo-topographic Gradient 44
4.6.4 Bustin's Paleo-topography 45
4.6.5 Nurkowski's Paleo-topography 46
4.6.6 Base Case Paleo-topographic Gradient 46
4.7 Chapter Summary 47

Chapter 5 Numerical Results 59
5.1 Mapping of the Brine Plume 59
5.2 Numerical Simulations 60
5.2.1 Results Criteria 60
5.2.2 Physical Pathway of Flow 60
5.2.3 Importance of Density Effects 60
5.2.4 Present Day Topography Results 61
5.2.5 Paleo Topography Results 62
5.2.5.1 Bustin's Paleo-topography 63
5.2.5.2 Nurkowski's Paleo-topography 63
5.2.5.3 Paleo-topographic Flow Discussion 64
5.2.5.4 Base Case Results 65
5.3 Discussion and Results Summary 65

Chapter 6 Sensitivity Analysis 81
6.1 Vertical Gradient 81
6.2 Permeability 82

6.2.1 Ireton Conduit 83
6.2.2 Wabamun Aquitard 84
6.2.3 Mannville Group Aquifer 85
6.2.4 Aquitard Permeabilities 86
6.3 Anisotropy 87
6.4 Discussion and Summary 89

Chapter 7 Conclusion 107
7.1 Recommendations 109

Reference 110
Appendix A 118

List of Tables

Table 3.1 - Stratigraphy and equivalent hydrostratigraphic units for the study area. 28

Table 4.1 - Various variable density numerical codes. 48

Table 4.2 - Sample results from the Courant number evaluation of a base-case simulation. 48

Table 4.3 - Comparison between a coarse grid and a refined grid. 48

Table 4.4 - Non-Spatial Model Parameters. 49

Table 4.5 - Aquifer Spatial Model Parameters. 49

Table 4.6 - Boundary conditions used in the density dependent and non-density dependent cases. 50

Table 4.7 - Hydraulic parameters used in the density dependent and non-density dependent cases. 50

Table 6.1 - Simulations run in the sensitivity analysis. 91

Table 6.2 - Aquitard permeability for the low permeability sensitivity analysis. 92

Table 6.3 - Varied Anisotropies from Beleke (1999). 92

List of Figures

Figure 1.1 - Map of Alberta basin showing the structure top of the Mannville Group Aquifer (Adapted from Mossop and Shetson, 1994). 5

Figure 1.2 - Total dissolved solids distribution for the Mannville Group Aquifer, west-central Alberta (modified from Rostron and Toth, 1997). 6

Figure 1.3 - Summary of cross-formational flow systems and their influence on the Mannville Group Aquifer, west-central Alberta (modified after Rostron and Toth, 1997). 7

Figure 2.1 - Measurement of hydraulic heads in groundwater of variable density (modified after Luszynski, 1961). 14

Figure 2.2 - Schematic diagram showing the relationship between pressure related driving force component, density related driving force component, and total driving force (modified after Davies, 1987). 15

Figure 2.3 - Driving Force Ratios as a function of $|\nabla E|/|\nabla Hf|$ for a family of fluid density curves (modified from Davies, 1987). 16

Figure 3.1 - Map of Western Canada showing the thickness of the Phanerozoic cover (Adapted from Mossop and Shetson, 1994). 29

Figure 3.2 - Subcrop edges below the sub-cretaceous unconformity in the central part of the Alberta basin (modified after Mossop and Shetson, 1994). 30

Figure 3.3 - Basinal flow regimes: a) Topography-driven flow due to tectonic rebound; b) Erosional-rebound flow; c) Thermo-haline convection during rifting; and d) Tectonically-driven flow during orogenic activity (Modified from Garven, 1995; Adams, 2001). 31

Figure 3.4 - Diagrammatic model of steady-state topographic-driven flow of formation waters in the Alberta basin (after Hitchon, 1984). 32

Figure 4.1 - Numerical model grid containing 22410 nodes and 21942 quardrilateral elements. 51

Figure 4.2 - The conceptual model used in the numerical solution. 52

Figure 4.3 - Longitudinal dispersivity versus scale with data classified by reliability (modified after Gelhar, 1986). 53

Figure 4.4 - Schematic of present day topography above the study area, hydraulic gradient 0.001. 54

Figure 4.5 - Reconstructed thickness of overburden (eroded section) in the

WCSB (Modified from Bustin, 1991). 55

Figure 4.6 - Schematic of Bustin's paleo-topography above the study area, paleo hydraulic gradient 0.01. 56

Figure 4.7 - Thickness of removed sediments from plains area of Alberta (Modified from Nurkowski, 1984). 57

Figure 4.8 - Schematic of Nurkowski's paleo-topography above the study area, paleo hydraulic gradient of 0.004. 58

Figure 5.1 - Flow diagram of numerical simulation organization. 68

Figure 5.2 - Mapped distribution of total dissolved solids (TDS) in the Mannville Group Aquifer, south-central Alberta. 69

Figure 5.3 - Modelled cross section and location of the observation point. 70

Figure 5.4 - Comparison of hydraulic head distributions after the first time step (500 years) between (a) non-density dependent and (b) density dependent cases. (c) shows the concentration differences between the cases. 71

Figure 5.5 - Comparison of brine concentration distribution after 2.5 million years between (a) non-density dependent and (b) density dependent cases. (c) shows the contour map of the concentration differences between the cases. 72

Figure 5.6 - Hydraulic head distribution results based on today's topography gradient of 0.001. 73

Figure 5.7 - Results of density dependent simulation using today's gradient of 0.001 after (a) 10 million, (b) 20 million, and (c) 30 million years. 74

Figure 5.8 - Change in concentration over time using today's hydraulic gradient of 0.001 at the observation point in the MGA. 75

Figure 5.9 - Comparison between hydraulic head distribution based on variations in hydraulic gradients (a) 0.004, (b) 0.01, and (c) 0.007. 76

Figure 5.10 - Results of density dependent simulation with a hydraulic gradient of 0.01after (a) 1 million, (b) 1.5 million, and (c) 2.5 million years. 77

Figure 5.11 - Results of density dependent simulation with a hydraulic gradient of 0.004 after (a) 1 million, (b) 2.5 million, and (c) 5 million years. 78

Figure 5.12 - Comparison of the effect of established paleo-topographic gradient on the concentration over time at the observation point in the MGA. 79

Figure 5.13 - Results of density dependent simulation with a hydraulic gradient of 0.007 after (a) 1 million, (b) 2.5 million, and (c) 5 million years. 80

Figure 6.1 - Results of sensitivity analysis to determine the effects of a vertical gradient of 0.05 forcing water up the west boundary after (a) 1 million, (b) 2.5 million, and (c) 5 million years. 93

Figure 6.2 - Comparing the effect of a vertical gradient on concentration over time at an observation point in the MGA. 94

Figure 6.3 - Results of the sensitivity analysis to determine the effects of the Ireton aquitard conduit permeability (a) 1×10^{-14}, (b) 1×10^{-16}, and (c) 1×10^{-18} m^2. 95

Figure 6.4 - Comparing the effect of the Ireton conduit permeability on the concentration over time at an observation point in the MGA. 96

Figure 6.5 - Results of the sensitivity analysis to determine the effects of the Wabamun aquitard permeability (a) 1×10^{-17}, (b) 1×10^{-16}, and (c) 1×10^{-18} m^2. 97

Figure 6.6 - Comparing the effect of the Wabamun permeability on the concentration over time at an observation point in the MGA. 98

Figure 6.7 - Results of the sensitivity analysis to determine the effects of the Mannville Group aquifer permeability (a) 4×10^{-15}, (b) 4×10^{-14}, and (c) 4×10^{-16} m^2. 99

Figure 6.8 - Comparing the effect of the MGA permeability on the concentration over time at an observation point in the MGA. 100

Figure 6.9 - Results of the sensitivity analysis to determine the effects of low aquitard permeability in the study area after (a) 1 million, (b) 2.5 million, and (c) 5 million years. 101

Figure 6.10 - Comparing the effect of the aquifer permeability on the concentration over time at an observation point in the MGA. 102

Figure 6.11 - Results of the sensitivity analysis to determine the effects of anisotropy (a) 10:1, (b) 1:1, and (c) 100:1. 103

Figure 6.12 - Comparing the effect of anisotropy on the concentration over time at an observation point in the MGA. 104

Figure 6.13 - Results of the sensitivity analysis to determine the effects of anisotropy (a) 10:1 and (b) varied anisotropy. 105

Figure 6.14 - Comparing the effect of varied anisotropy on the concentration over time at an observation point in the MGA. 106

Chapter 1 Introduction

Regional-scale flow of formation waters plays an important role in the migration and accumulation of hydrocarbons and ore deposits (Hubbert, 1953; Tóth, 1980; Cathles, 1981; Hitchon, 1984; Sharp and Kyle, 1988; Russell, 1992; Bachu, 1995a; Garven, 1995). Numerical modelling of regional-scale flow helps to provide an understanding of the mechanism(s) that form these resources. The mechanisms for flow are a function of the following factors: 1) the pathway, 2) driving forces, 3) the properties of the porous media through which the flow occurs, and 4) time (Hitchon, 1969a,b; Senger and Fogg, 1987; Belitz and Bredehoeft, 1988). Understanding the relationship between these factors can improve the evaluation of valuable economic resources and advance exploration techniques.

One example of a basin with an active flow system influencing resource generation is the Alberta basin (Figure 1.1). The Alberta basin is one of the most studied basins in Canada due to its abundance of non-renewable resources. This basin contains large reserves of coal, natural gas, and conventional and heavy oils (AEUB, 2001). A large portion of these resources is concentrated within this basin in the Lower Cretaceous Mannville Group. Estimates of reserves in the Mannville Group aquifer are 2.0 x 10^9 m^3 of conventional crude oil, 9.4x 10^{11} m^3 gas and 2.6 x 10^{11} m^3 of heavy oil, bitumen and oil sands (ERCB, 1991).

Numerous studies of the formation fluids within the Mannville Group Aquifer (MGA) have been conducted (Hitchon, 1969a; b; Hitchon, 1984; Abercrombie and Fullmer, 1992; Abercrombie *et al.,* 1994; Cody and Hutcheon, 1994; Bachu, 1995a; Rostron and Tóth, 1997; Bachu, 1999; Anfort *et al.,* 2001). These studies have provided valuable data on fluid flow within this basin and have helped establish a large collection of published aquifer parameters. For this reason, the Alberta basin provides an excellent opportunity for the application of numerical models to investigate the mechanism of formation water flow.

1.1 Previous Work/Setting

Regional flow systems in the Alberta basin have been mapped in considerable detail (Tóth, 1962; Hitchon, 1969a; b, 1984; Bachu, 1995a, 1999; Anfort *et al.,* 2001). This

mapping has identified the existence of several major systems acting in the basin today which play a unique role in distributing chemical species, heat, and hydrocarbons throughout the basin. Currently, the regional groundwater flow in the Alberta basin is thought to be made up of three flow systems:

a) A basin-scale topography-driven flow system originating in Montana, where Cambrian to Cretaceous strata crop out at a topographic high, travelling northward and discharging at the Peace River (Bachu and Underschultz, 1993).
b) A secondary updip flow system of connate waters from the southwest to central portion of the basin (Bachu, 1999; Anfort *et al.,* 2001).
c) A downdip flow of meteoric water driven by the Grosmont drain from the Northeast to central portion of the basin (Bachu, 1999; Anfort *et al.,* 2001).

One manifestation of flow in the Alberta basin is the presence of anomalous brine zones within the MGA (Rostron and Tóth, 1997). Zones of water with high total dissolved solids (TDS) (>120 g/L) are found today in the MGA above the northeast corner of the Bashaw reef complex (Figure 1.2). Rostron and Tóth (1997) mapped TDS and found that there were two distinct signatures of formation waters present in the MGA. The background MGA waters had TDS values ranging from 20 to 60 g/L. The second were classified as a brine ‘plume’, containing TDS values exceeding 120 g/L.

Rostron (1995) proposed that cross-formational flow was the mechanism by which a saline plume was created in the MGA. This plume of saline waters is thought to have originated in Upper Devonian strata, specifically, in the Cooking Lake-Leduc aquifer (Figure 1.3). The chemical composition of the brine plume water in the MGA was found to be similar to the chemical composition of formation waters in the Leduc and Nisku aquifers. Analysis of hydraulic data (i.e., pressure versus depth plots) showed that the saline waters from the Cooking Lake-Leduc aquifer were ascending, allowing the plume to migrate vertically through the Ireton aquitard.

Pathways for cross-formational flow are thought to be through fractured, thin or absent sections in the Ireton aquitard cap-rock above the Leduc Formation (Rostron and Tóth, 1997). These breaches allow the reef to act as a conduit for vertical flow of brines into the overlying Nisku aquifer. Breaches in the Ireton aquitard sealing the Bashaw reef complex occur in two principal areas (Hearn, 1996):

a) where the Ireton aquitard is effectively absent (0-4 m thick); and
b) through an Ireton aquitard drape that is 4-10 m thick, but only where the average carbonate content exceeds >80%.

Reidiger *et al.*'s (1999) study of the origin and migration of Mannville Group oils from the Provost oil field supports the theory of cross-formational flow further. Family D oil (Upper Devonian Duvernay source) is interpreted to have accessed the Mannville Group through these breaches in the Ireton aquitard.

Once in the Nisku aquifer the plume migrates updip. The plume is then thought to enter the MGA by flowing across the subcroping Wabamun aquitard (Figure 1.3; Rostron and Tóth, 1997) .

There are several forces known to drive regional-scale flow (Garven, 1995). Topography-driven flow is the primary driving force for deep fluid migration across Canada (Tòth, 1962; Freeze and Witherspoon, 1967; van Everdingen, 1968; Hitchon, 1969a,b; Larson, 1971; Tòth, 1978; Downey, 1984; Garven, 1985; Belitz and Bredehoeft, 1988; and Ingebritsen and Sanford, 1998). The dormant nature of today's flow system in the study area is a function of the existing relatively small topographic relief, a result of Late Cenozoic erosion over the past 10 million years (Cody and Hutcheon, 1994; Garven, 1995).

1.2 Research Objectives

Previous studies have established both the origin and the flow path of the brine plume. However, the time frame in which the plume migrated into the MGA is unknown. The timing of the plume migration is important since it links the flow systems that were active in the basin at the time of the plume creation. Based on previous studies it was hypothesized that a strong paleo topography-driven flow system was necessary to drive the dense brine. The time frame for plume emplacement is dependent on both the driving forces acting on the flow system and, the porous media parameters.

The objectives of this study were:

1) map the full extent of the brine plume in the central portion of the MGA, since previous work did not define the full extent of the boundary (e.g. Figure 1.2);

2) conduct a numerical simulation of the development of the MGA brine plume in a topography-driven flow system;
3) determine the magnitude of the driving forces required to produce the present observed salinity distribution; and,
4) determine a general time frame for brine plume emplacement in the MGA.

1.3 Study Area

The study area is located in the south-central portion of the Alberta basin between 52° N and 54° N and 110° W and 114° W (DLS 028-35W4 to 058-1W4) (Figure 1.1). It was chosen to capture the full extent of the MGA plume not mapped in detail previously (Rostron and Tóth, 1997). The TDS and hydraulic head maps of the study area indicate a SW-NE flow direction along the A-A' cross section. The cross-section is oriented along the presumed paleo regional flow direction and intersects the anomalous brine plume above the Bashaw reef complex.

1.4 Thesis Organization

The objective of this thesis was to model the flow of formation fluids from the Upper Devonian to Lower Cretaceous aquifers to simulate the emplacement of the brine plume currently observed in the Lower Cretaceous MGA.

To start, a brief review of the mathematical theory of fluid flow and the numerical model used in these simulations is presented. The following chapter discusses the relevant geological background, most importantly the stratigraphy and hydrogeology of the study area. This is followed by a description of the numerical simulations, which includes a discussion of the specific parameters used in the analysis. The results from the simulation are discussed in Chapter 5, followed by a discussion of the sensitivity of the results to the input parameters.

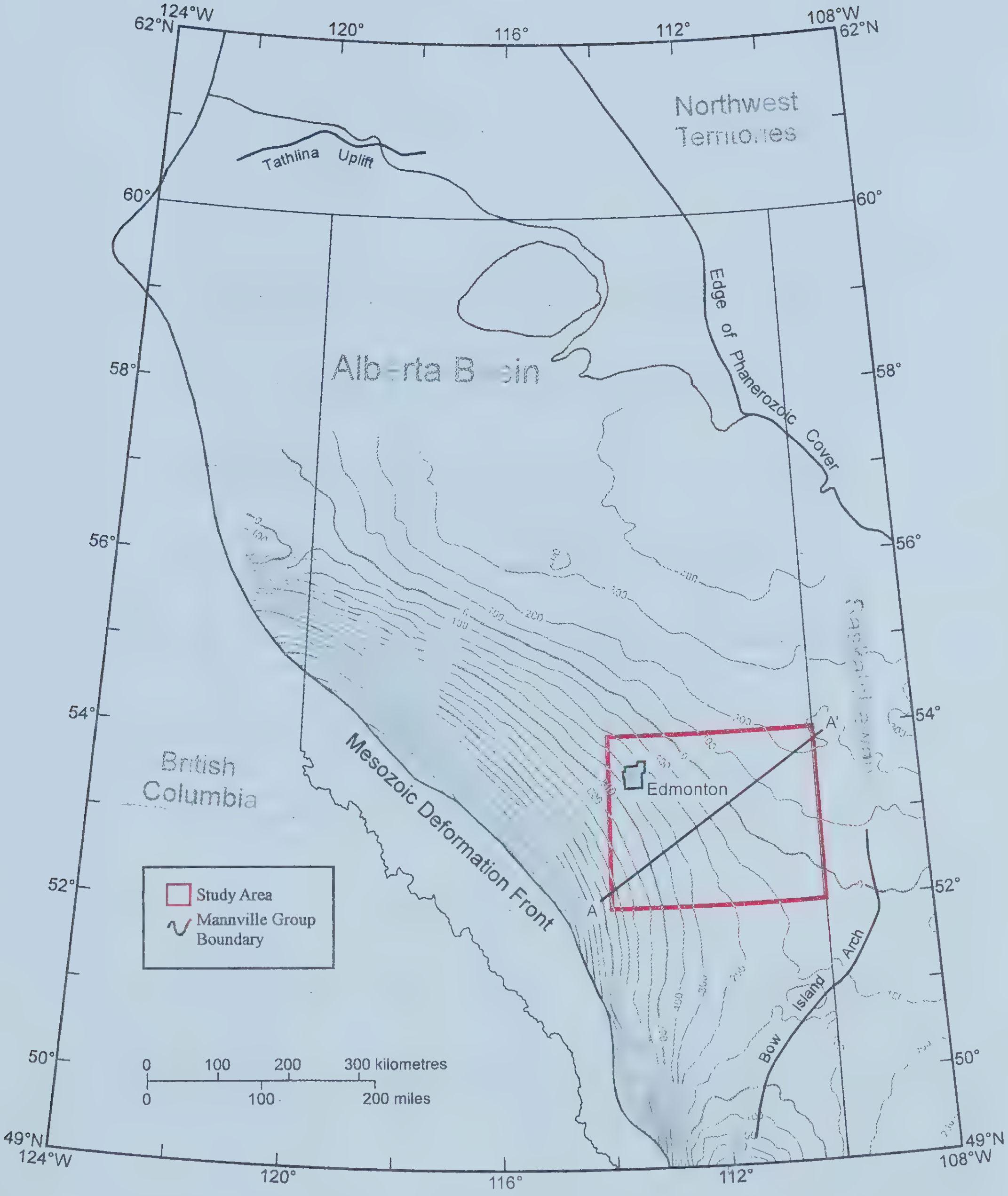

Figure 1.1 - Map of Alberta basin showing the structure top of the Mannville Group Aquifer (Adapted from Mossop and Shetson, 1994). Contour interval of 100 m. A-A' indicates the cross-section used in the numerical model.

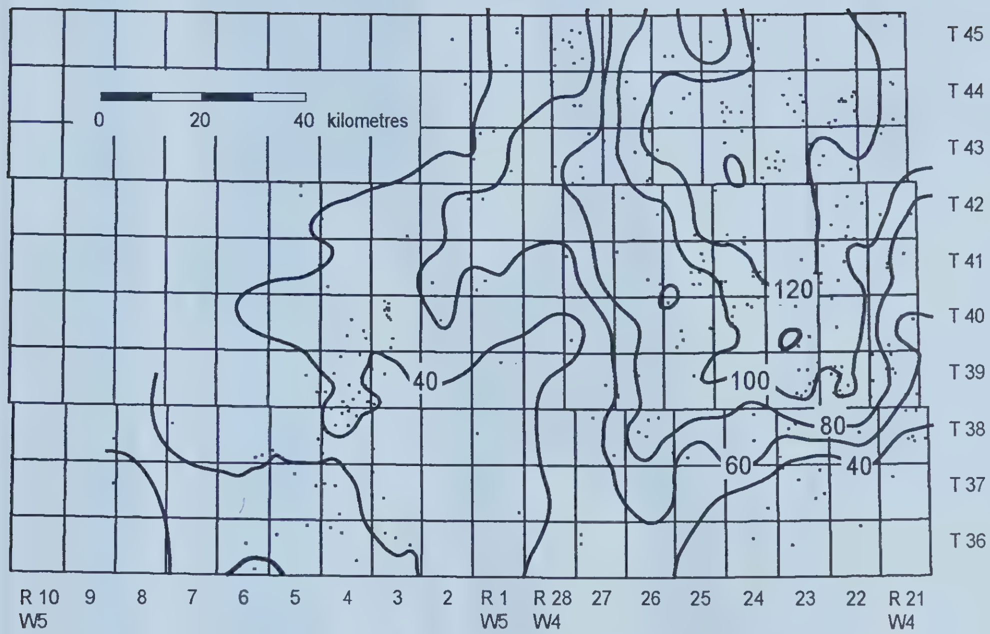

Figure 1.2 - Total dissolved solids distribution in the Mannville Group Aquifer, west-central Alberta. Contour interval 20 g/L (modified after Rostron and Tóth, 1997).

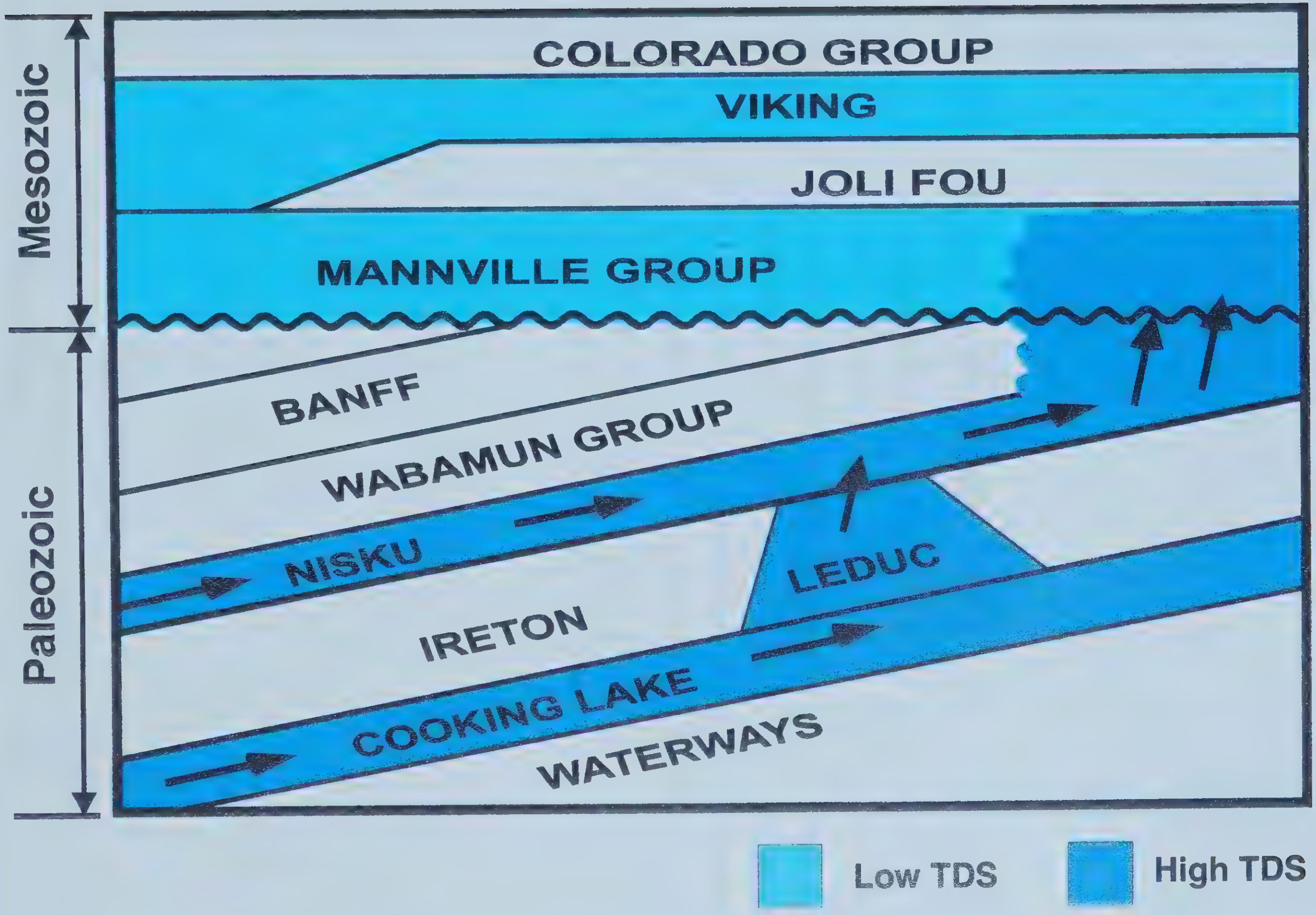

Figure 1.3 – Summary of cross-formational flow systems and their influence on the Mannville Group Aquifer, west-central Alberta (modified after Rostron and Tóth, 1997).

Chapter 2 Fluid Flow Mechanism

The objective of this chapter is to provide the theoretical background for the hydrogeology used in this thesis. The density of fluids in sedimentary basins is variable, due to the salinity and temperatures associated with basinal fluids (Hanor 1994). There are many practical complications associated with the flow of variable density fluids. Evaluation of the effects of density on fluid flow has been well established (Lusczynski, 1961; Jorgensen *et al.,* 1982; Davies, 1987; Bachu, 1995b; and others). Errors associated with variable density flow and the methods for quantifying those errors are discussed.

2.1 Variable-Density Fluid Flow

The vast majority of hydrogeological problems analyzed to date have assumed that formation waters have a constant density and thus gradients of hydraulic head alone drive fluid flow. For many circumstances, such as shallow flow systems, the assumption of small or negligible variation in formation water density is valid (Bachu, 1995). Lusczynski (1961) and DeWiest (1965) determined, analytically, that strictly horizontal flow is driven by gradients of equivalent freshwater head (defined below) and that density-related gravity effects are only important in the vertical direction. Therefore, under these circumstances, it is valid to use equivalent freshwater heads to determine flow direction.

In deeper flow systems the density effects cannot necessarily be ignored. Numerous studies have focused on the density effects on fluid flow (Luscynski, 1961; Jorgensen, 1982; Davies, 1987; Bachu, 1995b; and others). These studies have shown that analyzing variable-density-fluid flow using equivalent freshwater heads can lead to erroneous interpretations of fluid flow direction due to various combinations of sloping strata (vertical flow) and significant density variations.

2.1.1 Hydraulic Heads Formulation

A widely used concept in evaluating variable-density groundwater flow-systems is equivalent freshwater head (Figure 2.1). The fluid level is given by the water level elevation in a well filled with freshwater to a level high enough to balance the existing

fluid pressure at a given point (Davies 1987). The calculation of equivalent freshwater head is given by:

$$H_f = \frac{P}{\rho_f g} + z \tag{1}$$

Where:

H_f = freshwater head (L)

P = pressure $(M/L*T^2)$

ρ_f = density of freshwater $(M/L^3) = 1000\ kg \cdot m^{-3}$

g = magnitude of gravitational acceleration (L/T^2)

z = elevation (L)

Equivalent freshwater heads are unreliable for representing the hydraulic potential of a saline groundwater flow system (Lusczynski, 1961). Lusczynski (1961) analytically determined that equivalent freshwater head can only represent strictly horizontal flow. In practice, equivalent freshwater heads are used to characterize variable density flow if the aquifer dip does not exceed a few degrees or density contrast is small (Davies, 1987). This assumption is justified when fluid flow in aquifers is approximately horizontal and the associated density related effects are small.

However, in sedimentary basins, the flow of formation waters (fluxes and velocities) cannot be directly represented by equivalent freshwater head surfaces because of the absence of either flow or force potentials due to the typical sloping strata (Bachu, 1995; Bachu and Michael, 2002). The question that often arises is, when does one need to account for density? An elegant solution to this is the Driving Force Ratio (DFR) method given by Davies (1987).

2.1.2 Driving Force Ratio (DFR)

The driving force ratio (DFR) is a dimensionless value that quantifies the relative importance of the density-driven flow component. It is defined as the ratio between the gravity-driven flow component and the magnitude of the pressure term (Davies, 1987):

$$DFR = \frac{\Delta\rho |\nabla E|}{\rho_o |\nabla H_f|} \tag{2}$$

Where:

$\Delta\rho$ = $\rho - \rho_o$ = difference between ambient and reference density

ρ_o = fluid density at reference concentration (M/L^3)

∇E = magnitude of the gradient of elevation (dimensionless)

∇H_f = magnitude of the gradient of equivalent freshwater head (dimensionless)

The DFR illustrates the possible errors associated with using equivalent freshwater heads in the analysis of variable density fluid flow (Davies, 1987). Figure 2.2 shows the relationship between the pressure-related driving force component (∇H_f), the density-related driving force component ($(\Delta\rho/\rho_f)*\nabla E$) and the total driving force (T_{df}), which is the resultant of the two vectors. The two flow components usually vary in magnitude and direction. By using equivalent freshwater heads the density-dependent driving-force component is ignored and this, subsequently, creates errors in predicting the flow direction (ψ) and magnitude ($|T_{df}| - |\nabla H_f|$)

It is difficult to define a DFR value in sloping confined aquifers, which are typically found in sedimentary basins (Bachu, 1995b). Buoyancy is the main force driving lighter waters to the top of the aquifer and heavier water to the bottom. From there the water moves along the upper confining aquitard. If the potential driving gradient force is strong, assuming isotropic hydraulic conductivity, the flow will be mainly along the freshwater hydraulic gradient. If this force is weak, when compared with the buoyancy force, the flow will be along the main elevation gradient of the confining top or bottom surface. This also depends on whether the buoyancy force is driving flow updip or downdip. If the gradient of elevation is equal to the slope of the aquifer, then ($|\nabla E|/|\nabla H_f|$) is the ratio of aquifer slope to the slope of the equivalent freshwater head surface.

The threshold for DFR is approximately 0.5. The density-related gravity effects may become significant (Davies, 1987) if the DFR is above this value (Figure 2.3). The threshold value is dependent on the actual flow conditions and on the accuracy required by a particular study.

In practice, the DFR concept can be further refined. For a specified fluid, there will exist at each point a macroscopic impelling force vector F, defined as the force per unit mass that would act upon a macroscopic element of the fluid if placed at that point. The impelling force is a function of both buoyancy and hydraulic head gradients. F_e is the impelling force along a two-dimensional slope (Barson *et al.,* 1998):

$$F_e = -\nabla H_f + \left(\frac{\Delta\rho}{\rho_o}\right)\nabla E \qquad (3)$$

When the strata are horizontal ($\nabla E=0$) or when the formation contains completely freshwater ($\Delta\rho=0$), the driving force is equal to the negative of the equivalent freshwater head (∇H_f). When the strata are sloped the buoyancy effects need to be taken into account to determining the 'true' gradient driving the fluid.

2.1.3 Density-driven Flow

The previous sections discussed how to determine if variable density flow was significant in a flow system. In the cases where the variation in density is such that the resulting buoyancy forces are large enough to affect the fluid velocities, Darcy's Law is written as:

$$v = -\frac{k}{n_e\mu}(\nabla P + \rho g \nabla E) \qquad (4)$$

v = fluid velocity (L/T)
P = fluid pressure ($M/L{*}T^2$)
k = intrinsic permeability (L^2)
μ = fluid dynamic viscosity (M/L*T)
n_e = porosity

In most cases, density can be defined as a linear function of a conservative major dissolved constituent (e.g., chloride) for an isothermal case (Ingebritsen and Sanford, 1998). Thus, density can be defined as:

$$\rho = \rho_o + \gamma(C - C_o) \qquad (5)$$

C_o = reference concentration (mass fraction)

C = concentration (mass fraction)

γ = constant coefficient of density variability (dimensionless)

Using a basic continuity equation, assuming single-phase flow, fully saturated conditions, and using a general form of Darcy's law gives rise to the following general form of the groundwater flow equation (Ingebritsen and Sanford, 1998):

$$\frac{\partial(n_e\rho)}{\partial t} = \nabla \cdot \left[\frac{k\rho_o}{\mu} (\nabla P + \rho_o g \nabla E) \right] \qquad (6)$$

t = time (T)

The flow equation for variable-density solute transport is determined by incorporating the variable density form of Darcy's law into equation 6:

$$\nabla \cdot \left[\frac{\rho k}{\mu} (\nabla P + \rho g \nabla E) \right] = \rho \frac{\partial n_e}{\partial P} \frac{\partial P}{\partial t} + n_e \frac{\partial \rho}{\partial P} \frac{\partial P}{\partial t} + \gamma n_e \frac{\partial C}{\partial t} \qquad (7)$$

The terms on the right hand side of the equation refer to changes in mass over time through changes in porosity with respect to pressure, changes in fluid density with respect to pressure, and changes in fluid density with respect to concentration (Ingebritsen and Sanford, 1998).

Solving the governing equation (equation 7) in a variable-density flow system involves the simultaneous calculation of the coupled transport and flow equations. Fluid flow is a function of density (equation 7), and density is a function of concentration (equation 5). Also, the solute concentration is a function of transport, which is controlled by fluid flow.

It is possible to use equivalent freshwater heads to compute and represent velocity vectors using a numerical model. A numerical model calculates fluid properties at every grid node and time-step based on the assigned hydraulic properties. A numerical model couples the density equation, as a function of concentration, with the fluid velocity

equation at every node and time step. These velocities are then used to calculate solute and mass distribution in the model domain.

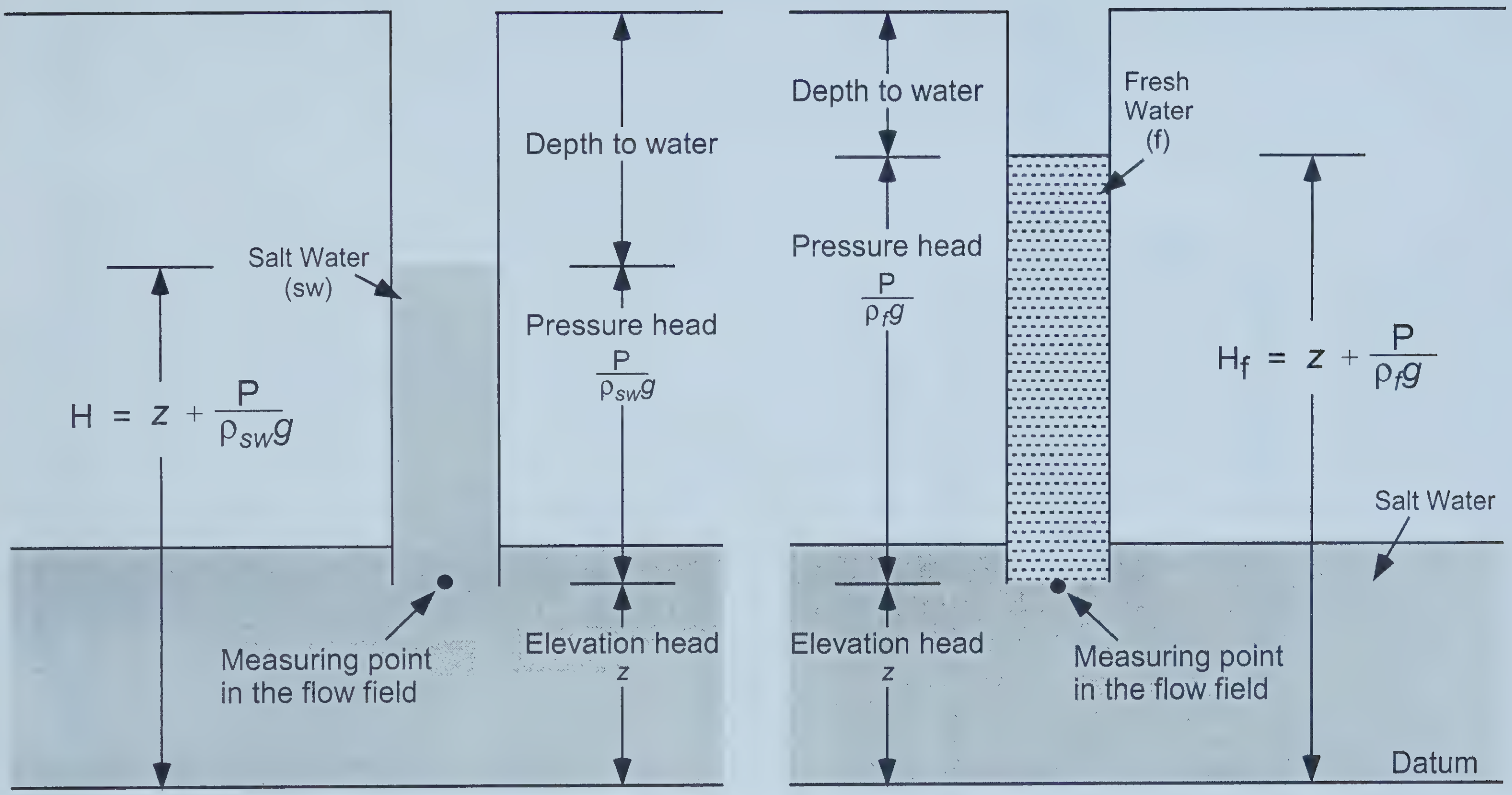

Figure 2.1 - Measurement of hydraulic heads in groundwater of variable density (modified after Luszynski, 1961).

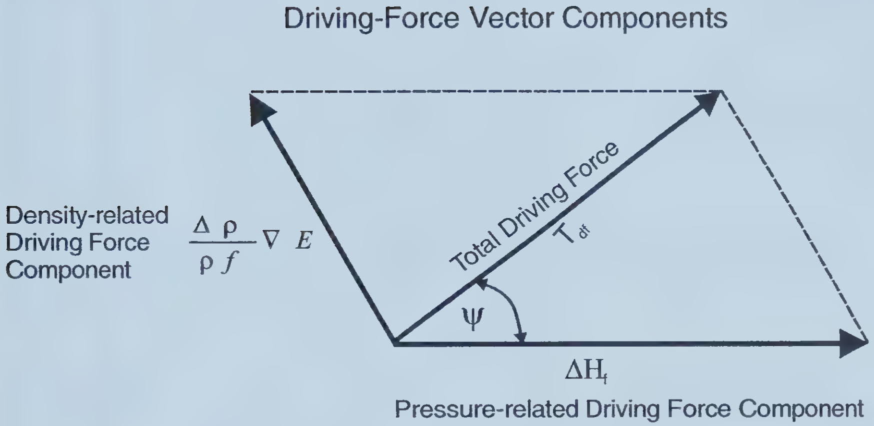

Figure 2.2 – Schematic diagram showing the relationship between pressure related driving force component, density related driving force component, and total driving force (modified from Davies, 1987).

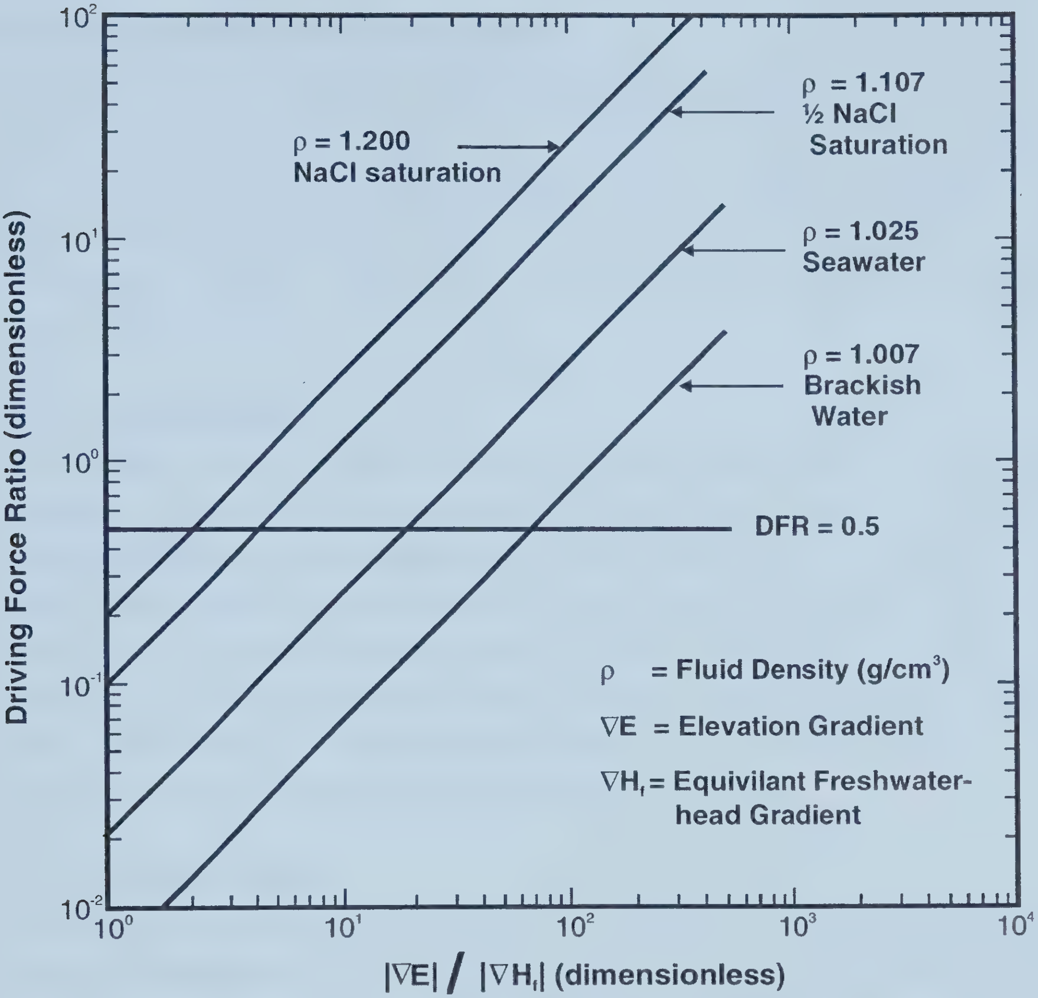

Figure 2.3 – Driving Force Ratios as a function of |∇E|/|∇Hf| for a family of fluid density curves (modified from Davies, 1987). The DFR=0.5 is the approximate threshold at which density-related gravity effects may become significant.

Chapter 3 Geological Background

The objective of this chapter is to introduce the geological framework for this study. First, the large-scale tectonic history of the basin is reviewed as it relates to the paleo-flow systems in the study area. Next, the specific geological stratigraphy and hydrostratigraphy are outlined, followed by a review of previous studies of the hydrogeology in the area. This sets the stage for the numerical modelling discussed in the following chapters.

3.1 Regional Setting

The Western Canada Sedimentary basin (WCSB) is comprised of two major sedimentary basins, the northwest-trending Alberta basin (Figure 3.1) and the intracratonic Williston basin (Wright *et al.,* 1994). These basins are separated by a broad, northeast-trending, positive feature, which includes the Bow Island Arch. The northern limit of the Alberta basin is bounded by the Tathlina uplift in the Northwest Territories and the southern limit is conventionally taken as the Canada-USA border (49°N). The Alberta basin thickens westward from 0 km in the northeast to more than 6 km at the boundary within the Cordilleran deformation front (Figure 3.1).

3.1.1 The Alberta Basin

The creation of the Alberta basin was initiated during the late Proterozoic era by rifting of the North American craton. The basin has evolved sequentially since Precambrian time from a passive margin to a foreland basin stage due to a compressive orogen (Porter *et al.,* 1982; Beaumont *et al.*, 1993).

The Paleozoic and earliest Mesozoic sequences in the basin were dominated by extensional tectonics, typically associated with an open ocean to the west (Wright, 1994). The bottom portion of the undeformed basin consists of a package of Middle Cambrian to Middle Jurassic passive-margin sediments dominated by shallow-water carbonates and evaporites with some intervening shales (Porter *et al.*, 1982). The Cratonic Platform's depositional sequences ended in Middle Jurassic time, about 158 million years ago (Wright *et al.*, 1994).

The foreland portion of the basin formed as a consequence of deformation along the western edge of the North American Craton, which began in the late Early Jurassic with

the accretion of terranes from the west (Wright *et al.*, 1994). The Columbian and Laramide orogenies (Late Jurassic to Early Tertiary) are characterised by discrete episodes of terrane accretion along the western margin of the craton, which resulted in the deformation and structural thickening of western parts of the succession. The resulting tectonically induced subsidence and isostatic flexure tilted the Precambrian basement westward (Porter *et al.,* 1982). This resulted in a gentle slope of 7 m/km in the east, near the Canadian Shield, increasing up to 12 m/km in the west, near the deformation front. The basement tilting and significant pre-Cretaceous erosion resulted in successive subcrops of Jurassic to Middle Devonian strata along sub-Cretaceous unconformity (Figure 3.2).

During the early Cretaceous, ongoing sedimentation and subsidence along the western margin formed the foredeep of the Alberta basin after a period of erosion. Deposition during the foreland stage of basin development is dominated by clastics, sandstones and shales derived from the evolving Cordillera and marine sediments from the north, respectively (Hayes *et al.,* 1994).

The transition from compressional to extensional stress regimes in the Cordilleran orogen marks the time of maximum burial in the basin (Willett *et al.,* 1997). Geochronological, structural and stratigraphic data indicate that maximum burial most likely occurred between 50-60 Ma (Willett *et al.*, 1997), during the Laramide orogeny in the Paleocene. Tertiary to Recent erosion has removed 2000 to 3800 m of sediments in the southwest, but only up to 1000 m in the North (Nurkowski, 1984; Kalkreuth and McMechan, 1988; Bustin, 1991). The deposition of sediments was predominately clastics, muds and silts, derived from the evolving Cordillera. The basin was subsequently uplifted during the late Paleocene and Eocene as erosion reduced the sediment load (Wright *et al.*, 1994).

3.2 Stratigraphy

The tectonic history of the basin has produced the varied package of sediments found in the basin today. The geology of the Alberta basin has been well documented at regional scales in the Geological Atlas of the Western Canadian Sedimentary basin (Ricketts, 1989; Mossop and Shetson, 1994). In the study area, the section of interest consists of 2 packages of Upper Devonian and Lower Cretaceous strata (Table 3.1), separated by an

angular unconformity. The stratigraphy of the study area is a key factor in the creation of the saline plume as it relates directly to the hydraulic parameters of the formations.

3.2.1 Upper Devonian Strata

Beaverhill Lake Group

At the base of the section of interest is the Beaverhill Lake Group, which consists of an extensive platform with carbonate-evaporitic cycles in its interior (Moore, 1988). In the study area the group consists of calcareous shales and limestones of the Waterways Formation. This formation ranges in thickness from 150 to 200 metres across the study area.

Woodbend Group

Overlying the Waterways Formation is the Cooking Lake Formation which is the lower interval of the Woodbend Group. This formation is comprised of a sheet-like unit of shallow water platform carbonates. The Cooking Lake Formation is primarily limestone, but within the lower third of the formation there are variable amounts of dolostone present (Wendte, 1994). In the study area, the Cooking Lake Formation is approximately 75 metres thick (Switzer *et al.*, 1994).

Attached to the western margin of the Cooking Lake Formation are the Leduc Formation platform margin reef buildups or “pinnacle reefs” (Hugo, 1990). These reefs are either isolated or grouped together in complexes (e.g., the Bashaw reef complex in the study area). Leduc Formation reefs are mostly comprised of coarse-crystalline, highly porous and permeable dolostones and reach a thickness in excess of 275 m (Hugo, 1990).

Uppermost in the Woodbend Group are the thick shales and marls that make up the Ireton Formation. This formation drapes over the Cooking Lake and Leduc Formations. The Ireton Formation is believed to represent a drowning of the underlying reef complexes and reaches a thickness of 280 metres in the study area (Mossop and Shetson, 1994).

Winterburn Group

The Winterburn Group overlies the Woodbend Group and its deposition is characterised by the shallowing and continued filling of the basin (Switzer *et al.*, 1994). The base of

the group is the Nisku Formation. The interval in which the Nisku Formation was deposited began with an apparent rise in sea level. This marine transgression resulted in the deposition of a widespread carbonate ramp consisting of permeable, shallow-water, shelf carbonates approximately 40 metres thick, which have been subsequently dolomitized in the study area (Switzer *et al.*, 1994).

The Wabamun Group strata sits above the Winterburn Group and represents the uppermost limits of the Upper Devonian strata. This group represents an overall regressive sequence punctuated by several important transgressive pulses (Halbertsma, 1994), and as such has a highly variable lithology. In the study area, the Wabamun Group strata consist of two lithofacies (Halbertsma, 1994). A more westerly lithofacies consists of interbedded brown microcrystalline dolomite and anhydrite with a slightly argillaceous top (Settler Formation) and the east lithofacies is a dolomitic anhydrite overlain by interbedded anhydrite and dolomite with minor bioclastic limestone on top (Big Valley Formation). The thickness of this group in the study area ranges from 0 to 150 metres (Halbertsma, 1994).

3.2.2 Mississippian Strata

The Mississippian strata in the study area consists of series of trangressive-regressive cycles, which formed the present Banff/Exshaw formations (Richards *et al.,* 1994). The Banff/Exshaw formations consist of limestone with subordinate fine-grained siliciclastics, marlstone and dolostone. Erosion removed much of the Mississippian strata during the creation of the sub-Cretaceous unconformity. In the study area the thickness varies from 0-120 metres (Richards *et al.,* 1994).

3.2.3 Jurassic Strata

There are no rocks of Jurassic age present in the study area.

3.2.4 Cretaceous Strata

Mannville Group

The Mannville Group forms the base of the Lower Cretaceous strata in the study area and consists of the Upper and Lower Mannville formations (Hayes *et al.,* 1994). This group is a depositional response to the Columbian orogeny. The strata from the Mannville Group covers the entire basin and represents a major episode of subsidence

and sedimentation following a long period of uplift, exposure and erosion of older strata (Hayes *et al.,* 1994). The Mannville Group is 160 to 200 metres thick in the study area.

In the study area, the Lower Mannville Formation consists of three types of lithofacies (Hayes *et al.,* 1994):

1) fine to medium grained grey and brown sandstone, moderately sorted, very porous with interbedded silty shale;
2) fine-grained grey brown sandstone, silty, moderately sorted; and,
3) fine-grained interbedded grey carbonaceous shale and silty sandstone, moderately to poorly sorted.

The Upper Mannville Formation also consist of three types of lithofacies (Hayes *et al.,* 1994):

1) silty shale with interbedded fine-grained, poorly sorted, silty sandstone;
2) shale interbedded with fine-grained moderately sorted, silty, sandstone; and,
3) moderate to well sorted, fine-grained sandstone with interbedded shale and siltstone.

Colorado Group

Above the Mannville Group is the uppermost unit in the study area, the Colorado Group, consisting of the Joli Fou and Viking formations. The Colorado Group was deposited during the Cretaceous when global sea levels were high. This group consists of predominately thick shales that form aquitards, more specifically, mudstones interspersed with relatively thin sandstone and conglomerate beds (Leckie *et al.,* 1994). This marine shale is 250 to 625 metres thick in the study area.

The shales of the Joli Fou Formation disconformably overlie the Mannville Group where the Basal Colorado/Spinney Hill formations are absent (Leckie *et al.,* 1994). The shale of the Joli Fou Formation is a dark grey, noncalcareous, marine shale with a small proportion of interbedded fine to medium grain sandstone (Leckie *et al.,* 1994). This formation is continuously 20 to 40 metres thick across the area.

The Viking Formation represents a wedge-shaped coarse clastic interval that prograded from the Cordilleran orogenic belt eastward into the foreland basin (Reinson *et al.,*

1994). These clastic sediments were deposited during the Albian stage when the basin was flooded by a shallow epicontinental seaway extending from the Arctic Ocean to the Gulf of Mexico (Caldwell, 1984). In the study area, the Viking Formation is comprised of shale, with some sandstone and siltstone, and is 20 to 50 metres thick.

3.3 Hydrostratigraphy and Hydrogeology

Fluids follow permeable pathways through the subsurface, therefore rock units need to be grouped into units of similar hydraulic properties. Based on the hydraulic properties of the rock hydrostratigraphic units are classified as aquifers, aquicludes, and aquitards. Previous studies on the hydrogeology and hydrochemistry of the area were used to create a hydrostratigraphic classification consisting of 3 groups (Rostron and Tóth, 1997; Rostron *et al.,* 1997; Anfort *et al.,* 2001):

1) Upper Devonian Hydrogeologic Group (UDHG),
2) Mannville Group Aquifer (MGA), and
3) Viking Group Aquifer (VGA).

3.3.1 Upper Devonian Hydrogeologic Group (UDHG)

The Upper Devonian Hydrogeologic Group (UDHG) consists of two main aquifers: the Cooking Lake and Nisku formation aquifers. The lower boundary of the UDHG is the thick aquitard of the Waterways Formation. Separating the Cooking Lake and Nisku aquifers is the Ireton aquitard and the Leduc Formation reefs. At the top of the Upper Devonian strata, the Wabamun Group is classified as an aquitard, because of the presence of dolomite and anhydrite (Halbertsma, 1994).

Previous studies on the potentiometric surface in the Cooking Lake-Leduc aquifer show substantial variations in hydraulic head in the study area (Rostron and Tóth, 1997; Anfort *et al.,* 2001). As mentioned in the previous section, the Leduc Formation reefs are in direct contact with the underlying Cooking Lake Formation. These highly permeable formations are classified as aquifers and are in hydraulic communication. Rostron and Tóth's (1997) potentiometric map indicates that the highest values of hydraulic heads in the Cooking Lake aquifer reach 860 metres and are located at the east edge of the study area. Adjacent to these areas of high hydraulic head, values of hydraulic heads in the Leduc aquifer range between 700 and 750 metres. The approximately 100-metre

differences in hydraulic head in this study area, between connected aquifers, indicates that vertical fluid flow occurs in the Leduc reefs (Rostron and Tóth, 1997).

The Ireton Formation consists of low permeability marly shale and primarily acts as an aquitard and partially hydraulically confines the Cooking Lake and Leduc aquifers from the overlying flow system. However, fractures and thin sections are located within the shales above the reefs (Rostron, 1995; Hearn, 1996; and Rostron and Tóth, 1997). These breaches have established local hydraulic communication between the Cooking Lake aquifer and the overlying Winterburn Group Nisku aquifer, therefore creating the Upper Devonian Hydrogeologic Group (UDHG).

The Nisku Formation forms the upper part of the UDHG. It is a permeable carbonate aquifer and contains two flow systems (Rostron and Tóth, 1997). The first flow system is identified by the mounding of hydraulic heads in the potentiometric surface in the Nisku aquifer. This illustrates that horizontal flow radiates outward over the area of the underlying Bashaw reef complex. The hydraulic heads in the Nisku aquifer in this area are mapped to be approximately 750 metres. The second flow system is the regional up-dip flow along the Nisku aquifer across this study area with hydraulic head between 600 and 400 metres. These hydraulic heads indicate that the regional flow system within the Nisku Formation aquifer flows to the northeast.

3.3.2 Mississippian Aquitard

The Exshaw/Banff formations act together as a minor aquitard, consisting of a thin, tight shale overlain by a low permeability limestone (Rostron and Tóth, 1997). The effects of the aquitard are minimal due to the limited extent of the Exshaw/Banff formations in the study area.

3.3.3 Mannville Group Aquifer (MGA)

The MGA is a basin-scale, sandstone-dominated aquifer, overlain by the Joli Fou aquitard. The regional-scale potentiometric surfaces of the MGA illustrate the trends of flow in the study area (Hitchon, 1969b; Abercrombie and Fullmer; 1992; Anfort *et al.*, 2001). Those surfaces show lateral flow from the southwest to northeast across the WCSB. The approximate values of hydraulic heads in the study area range from 650 metres in the southwest corner of the area and decrease to approximately 400 metres to

the northeast. The potentiometric surface also illustrates another major component of flow in the MGA (Rostron and Tóth, 1997). A noticeable flattening of the potentiometric surface in this area indicates the intersection of the UDHG and the MGA in the vicinity of the Bashaw reef complex. This is caused by a large component of fluid flow occurring in the vertical direction.

3.3.4 Viking Group Aquifer (VGA)

The sandstone bodies of the Viking Group aquifer (VGA) are extensively inter-connected and create one of the most hydraulically conductive regional aquifers in the entire Western Canadian Sedimentary basin (Hitchon, 1969a; b; Creaney and Allan, 1990; Bekele *et al.,* 2002). In the study area, the base of the VGA is the Joli Fou Formation, a regionally extensive weak aquitard. The Joli Fou aquitard is overlain by the laterally extensive Viking aquifer. The Colorado shale acts is designated the impermeable upper boundary for the numerical model and isolates the flow regime from the overlying aquifers.

3.4 Regional Fluid Flow in the Alberta Basin

The mechanisms driving regional fluid flow in the Alberta basin have been extensively studied and documented (Hitchon, 1969a; b, 1984; Bachu 1995a, 1999; Anfort *et al.,* 2001). This section will discuss the past and present day driving forces to show the most likely mechanism driving the high TDS plume into the Mannville aquifer. The possible mechanisms driving flow in the basin are as follows (Figure 3.3): topography, erosional rebound, thermo-haline convection (buoyancy), tectonics, and hydrocarbon generation.

Topography

Topography-driven flow is generated by variations in elevation of the land surface, which translates into fluid potential gradients in the subsurface. In topography-driven flow systems, fluid movement occurs because hydraulic heads decrease from high-elevation recharge areas (highest head) to low-elevation discharge areas (lowest head) (Figure 3.3a) (Tóth, 1962; 1963; Freeze and Witherspoon, 1967). Tóth (1962, 1963) delineated the different scales of topography-driven flow: local, intermediate and regional (Figure 3.4). Regional topographic relief allows for fluids to be driven through deep strata over long periods of time at maximum flow rates of approximately 1 to 10 m/yr.

The present day flow system in the Alberta basin contains two basin-scale topography-driven flow systems (Bachu, 1999). These are open-flow systems driven by topography which are recharged at the fold belt and discharge in the north at the Great Slave Lake. One exists in the central part of the basin where the fluids discharge under a thin Quaternary cover at Great Slave Lake and along the edge of the Precambrian shield. This flow system also contains semi-open flow in which the formations are recharged at the surface but discharge into adjacent confining aquitards (Bachu, 1999).

The second topography-driven flow system involves the recharge of meteoric waters in Devonian, Carboniferous, and Cretaceous aquifers near the 49th parallel and in Montana where these aquifers outcrop at high elevations. This flow system is driven by the progression of the meteoric water flowing from south to north across the basin and discharges at an outcrop of the Grosmont aquifer along the Peace River (Schwartz *et al.*, 1981; Hitchon, 1989a; b; Cody and Hutcheon, 1994; Bachu, 1995a; Anfort *et al.*, 2001).

Erosional Rebound

Compaction of strata due to rapid sedimentation of a basin can create highly overpressured zones in shaly aquitards (Figure 3.3b; Bekele *et al.*, 2000). This creates a deep flow regime resulting from fluid displaced in those zones as the strata compacts under the weight of the accumulating sediments (Bethke, 1989). These fluids flow into the adjacent sandstone aquifers and then laterally out into the basin. When the load is removed, either by erosion of overburden or retreat of glaciers, underpressuring is generated due to elastic dilation of rock-pore volumes (Tóth, 1986). This disequibrium of fluid pressure between the shales and the adjacent strata drives an inward-oriented fluid flow (Figure 3.3c). The maximum flow rates of this driving force are 0.01 to 0.1 m/yr. This flow mechanism has been documented in the aquifers of the Cretaceous succession (Tóth and Corbet, 1986; Corbet and Bethke, 1992; Bachu, 1995a; Parks and Tóth, 1995).

Buoyancy

The effect of salinity concentration and temperature on the density of formation fluids can generate thermo-haline convection (Bethke, 1989). Increases in fluid temperatures

decrease the fluid density and increases of salinity concentration increase the fluid density. It is possible, due to thermal expansion, for a dense saline brine to become less dense and to therefore overlain by a more dense, fresher, shallower fluid. Fluid flow convection cells can then be generated in areas where there are large temperature and salinity gradients, such as, coastal aquifers, geothermal areas and deeply buried formations (Figure 3.3c). Given a sufficient driving force the hydraulic gradient in deeper aquifers can overwhelm buoyant forces and displace brines into shallower strata (Bethke, 1989). The maximum flow rates range from 0.1 to 1 m/yr.

Within the Alberta basin, Paleozoic waters and freshwaters of meteoric origin are present in the Lower Mannville aquifer in the south-central part of the basin, in the region where Devonian aquifers subcrop at the sub-Cretaceous unconformity (Bachu, 1995a; Rostron and Tóth, 1997; Anfort *et al.,* 2001). It is thought that buoyancy induces these high salinity and density fluids to move down dip in the Lower Mannville aquifer.

Tectonic Compression

During orogenic events the tectonic compression in the deformed belt of the WCSB may have created lateral stresses and pressure pulses that caused the lateral expulsion of fluid from the overburden and thrusted strata (Figure 3.3d) (Oliver, 1986; Shi and Wang, 1986; Ge and Garven, 1989, 1994; Bachu, 1999; Machel and Cavell, 1999). This expulsion forced fluid into the foreland basin and subsequently forced formation waters to be moved at higher flow rates through the up-dip portion of the study area. Maximum flow rates are estimated to be from 0.1 to 1 m/yr. Currently the Alberta basin is tectonically dormant; therefore, this mechanism is not active. However, it is possible that tectonic-induced flow occurred in the past when the basin was tectonically active (Oliver, 1986; Bachu, 1999; Machel and Cavell, 1999).

Hydrocarbon Generation

Generation of hydrocarbons can create overpressures that may drive fluid from the reservoir. This is caused by the phase change of solid, kerogen that fills the pore space, with fluid hydrocarbon and leads to volumetric expansion and generation of internal stresses (Spencer, 1987; Luo and Vasseur, 1996; Bekele, 2000). In order to generate these driving forces the reservoir must be confined by very low permeability aquitards to prevent the rapid dissipation of flow into the adjacent strata. Currently in the Alberta

basin, most of the hydrocarbon generation induced flow occurs in the southwest, near the thrust and fold belt, in deep Cretaceous strata (Cant, 1983; Bachu and Underschultz, 1995, Bekele *et al.*, 2002).

3.5 Chapter Summary

The hypothesised pathway for fluid flow through the study area can be summarised as follows. The Leduc reef provides the conduit for vertical flow travelling from the Cooking Lake aquifer into the Nisku Formation aquifer. This is made possible by fractures within the caprock sealing the reef. Fluids in the Nisku aquifer flow laterally updip along the aquifer and into the MGA at the subcrop. Above the reef, vertical flow occurs across the Nisku aquifer into the Wabamun aquitard. The fluid then travels across the Wabamun aquitard and finally enters the MGA. In the next chapter, this stratigraphy and hydrogeology will be applied in a numerical model of plume formation.

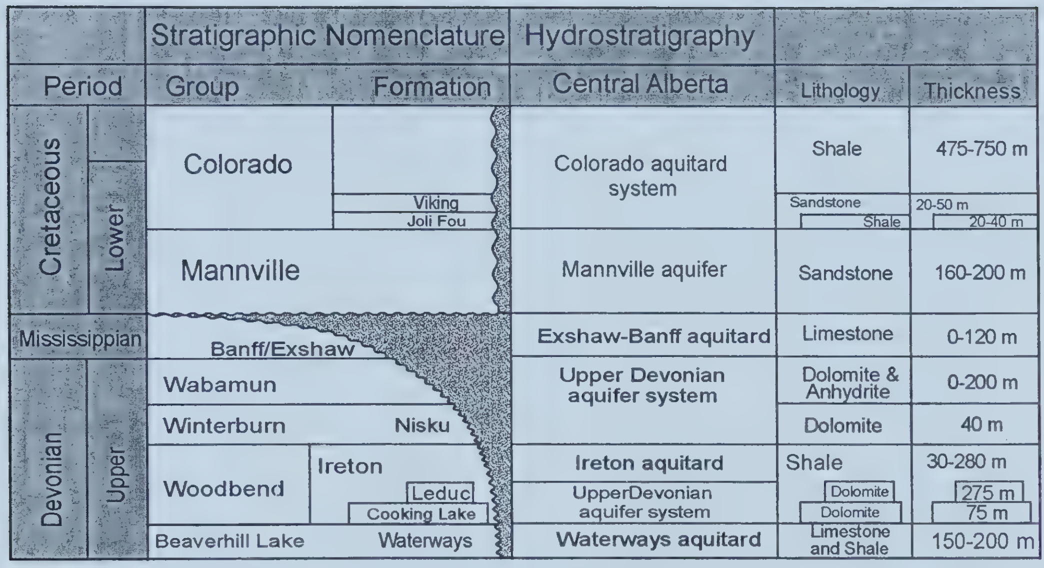

		Stratigraphic Nomenclature		Hydrostratigraphy		
Period		Group	Formation	Central Alberta	Lithology	Thickness
Cretaceous	Lower	Colorado		Colorado aquitard system	Shale	475-750 m
			Viking		Sandstone	20-50 m
			Joli Fou		Shale	20-40 m
		Mannville		Mannville aquifer	Sandstone	160-200 m
Mississippian		Banff/Exshaw		**Exshaw-Banff aquitard**	Limestone	0-120 m
Devonian	Upper	**Wabamun**		**Upper Devonian aquifer system**	Dolomite & Anhydrite	0-200 m
		Winterburn	**Nisku**		Dolomite	40 m
		Woodbend	**Ireton**	**Ireton aquitard**	Shale	30-280 m
			Leduc	UpperDevonian aquifer system	Dolomite	275 m
			Cooking Lake		Dolomite	75 m
		Beaverhill Lake	Waterways	**Waterways aquitard**	Limestone and Shale	150-200 m

Table 3.1 - Stratigraphic and equivalent hydrostratigraphic units for the study area with corresponding lithology and thickness.

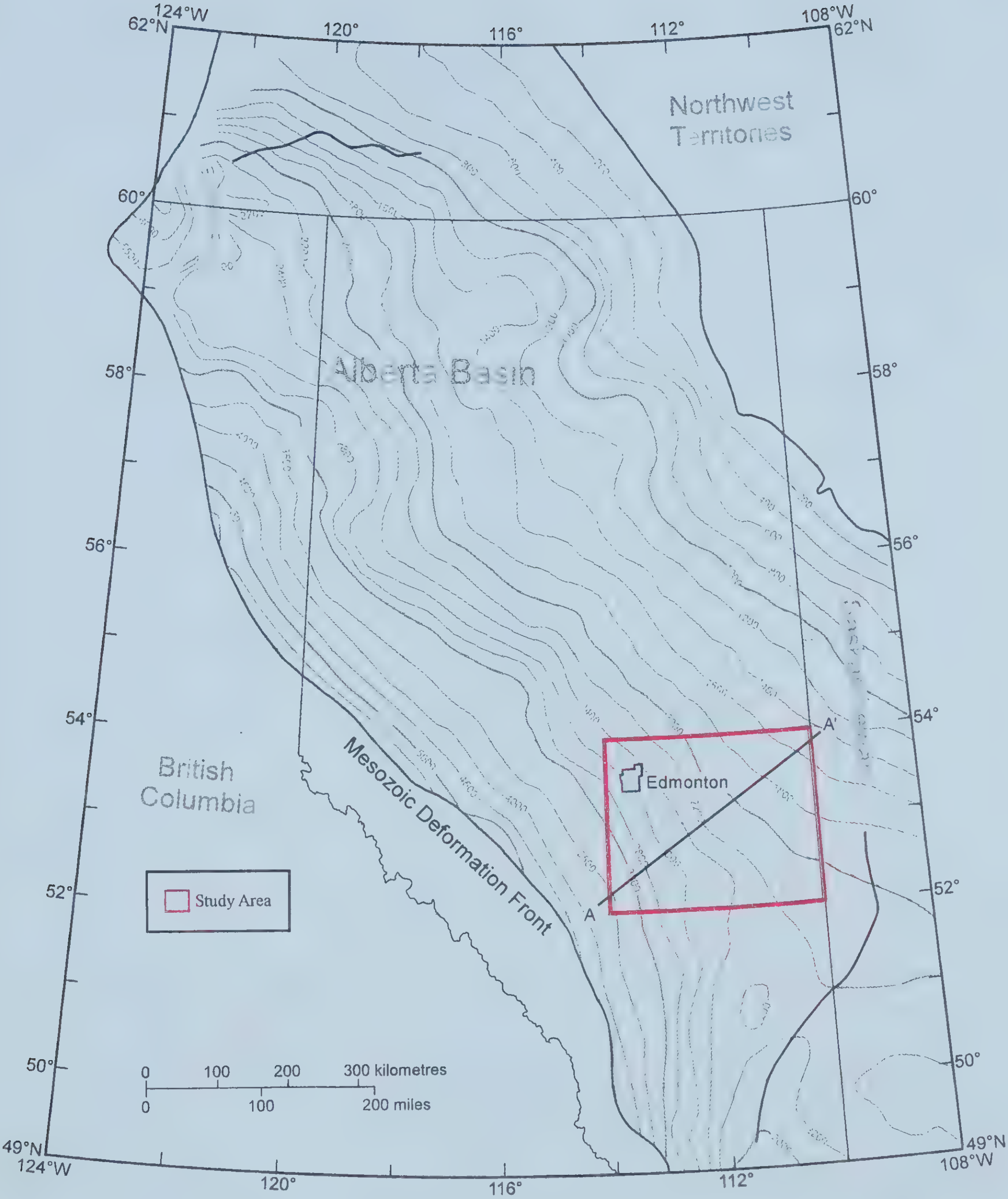

Figure 3.1 - Map of the Alberta basin showing the thickness of the Phanerozoic cover (Adapted from Mossop and Shetson, 1994). Note the shift in contour interval from 400 to 500 m near the disturbed belt. A - A' indicates the section used in the numerical model.

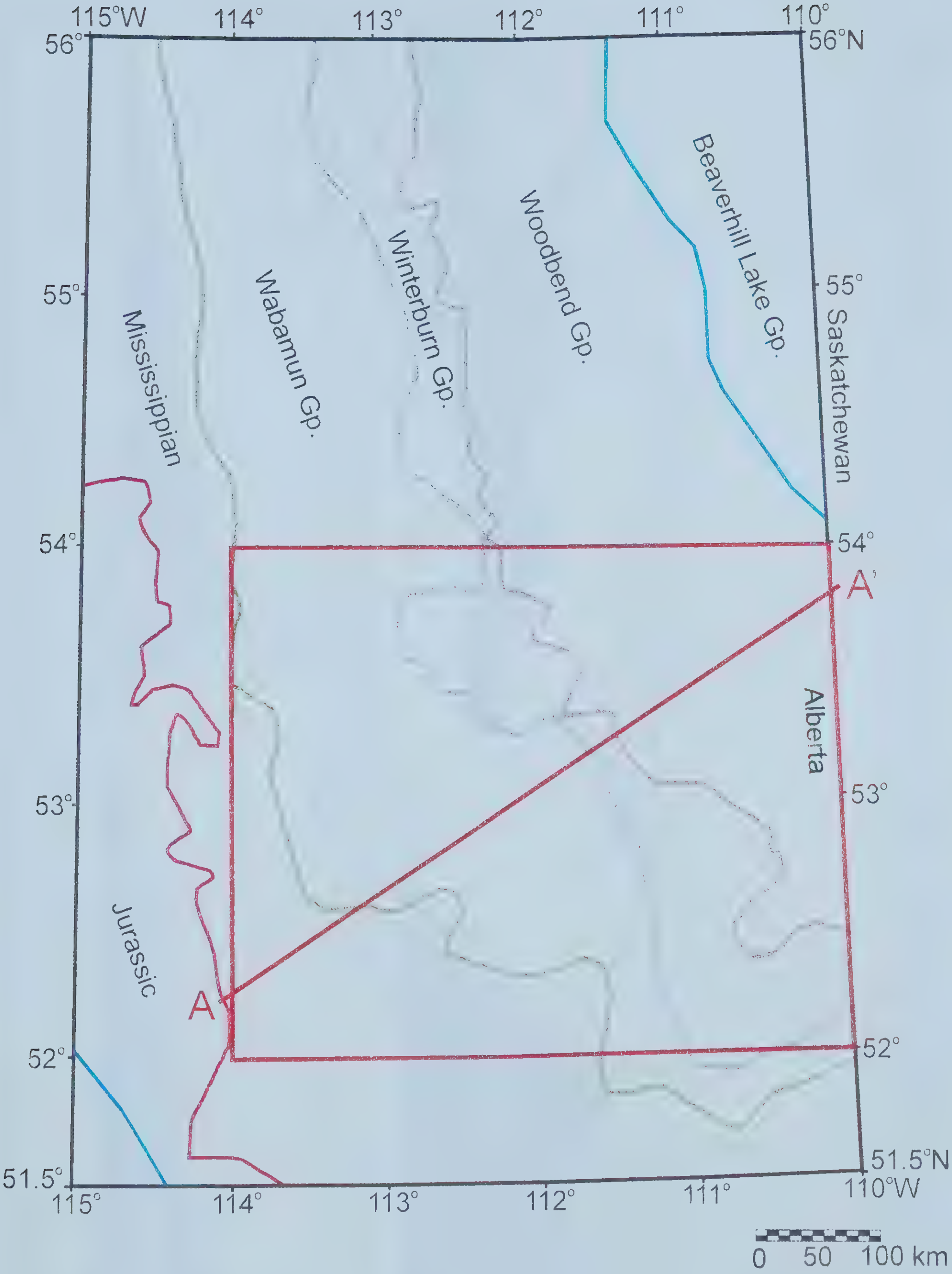

Figure 3.2 – Subcrop edges below the sub-cretaceous unconformity in the central part of the Alberta Basin (modified after Mossop and Shetson, 1994). A – A' indicates the cross section used in the numerical model.

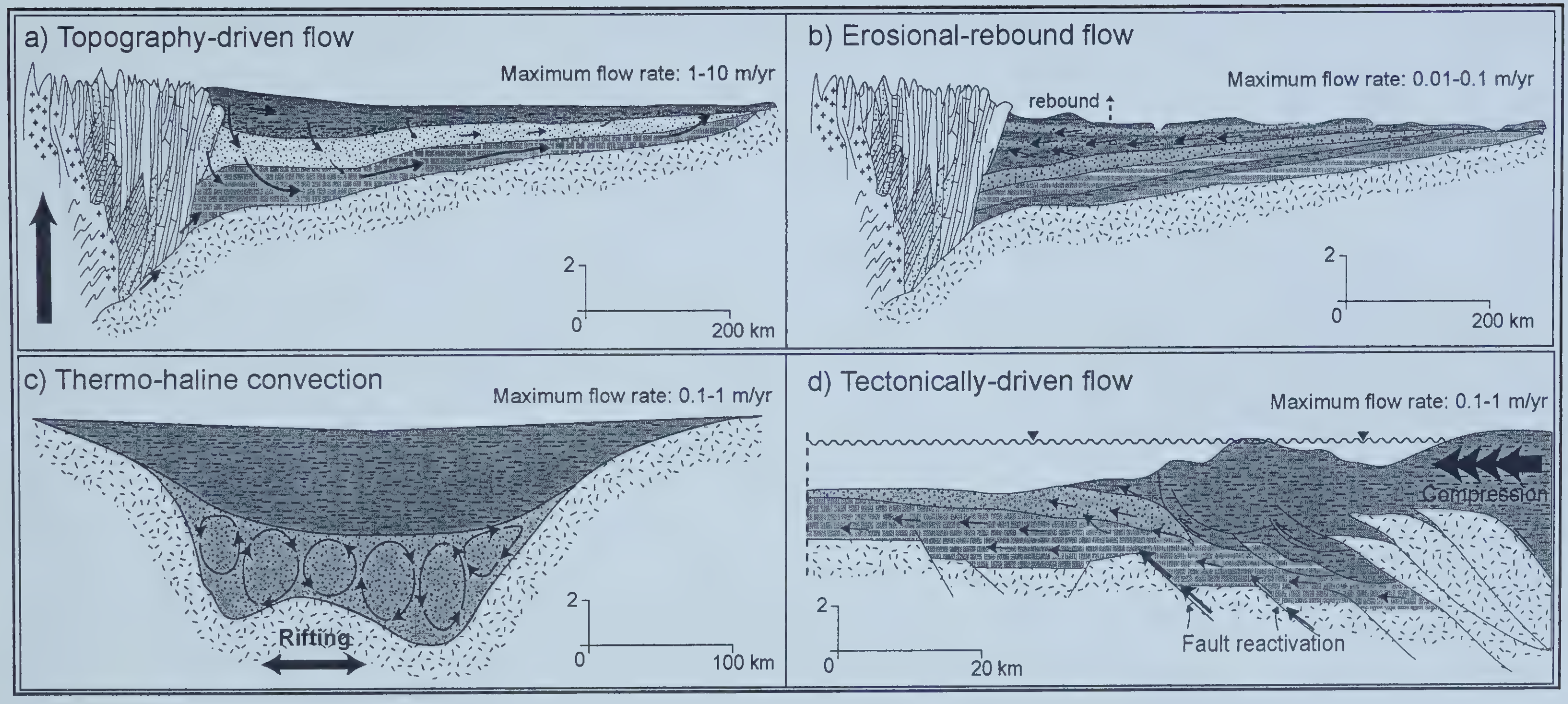

Figure 3.3 - Basinal flow regimes: a) Topography-driven flow due to tectonic rebound; b) Erosional-rebound flow; c) Thermo-haline convection during rifting; and d) Tectonically-driven flow during orogenic activity (modified after Garven,1995; Adams, 2001). Small vectors indicate direction of groundwater flow. Large arrows indicate basinal forces or stresses. Note scale changes for each case.

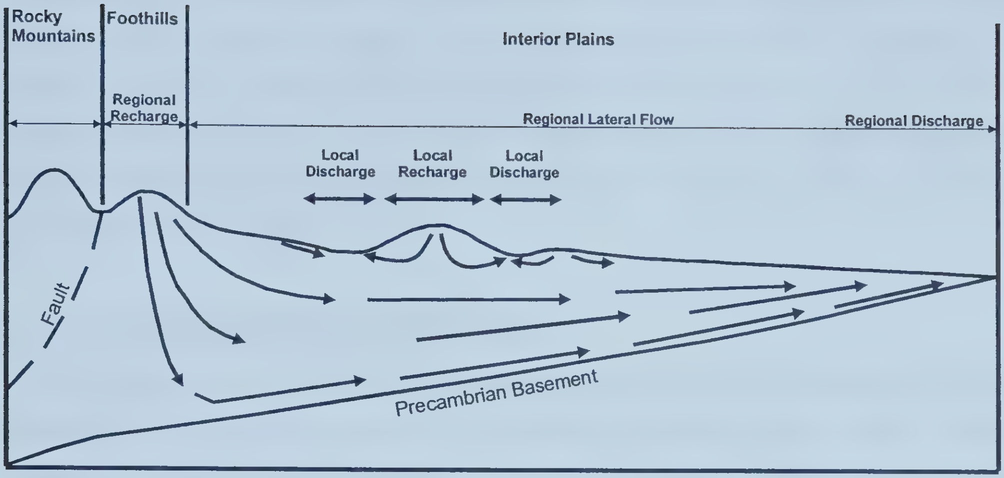

Figure 3.4 – Diagrammatic model of steady-state topographic-driven flow of formation waters in the Alberta basin (modified after Hitchon, 1984).

Chapter 4 Numerical Model and Approach

The objective of this chapter is to present the formulation of the numerical simulations. First, various numerical codes were evaluated based on their applicability to the problem. Once a code is chosen, a numerical model domain can be generated by designing the domain grid, applying the boundary conditions, and hydraulic parameters. Finally, various simulation approaches are described and the results from these are presented and discussed.

4.1 Numerical Model Evaluation

After evaluating the available finite-element, density-dependent numerical codes, it was determined that SUTRA (Saturated-Unsaturated TRAnsport) (Voss, 1984) best fit the criteria for this project (Table 4.1). The most important criterion was the ability to accurately simulate variable-density flow. SUTRA has been previously tested using standard density-driven flow benchmarks. These benchmarks include the Henry (1964) approximate analytic solution for steady–state saltwater intrusion and the Elder (1967) problem for complex natural convection where fluid flow is driven purely by fluid density differences. The decision to use this code was further supported by the numerous studies that have been published using this source code (eg., Lahm *et al.,* 1998; Simmons and Sharp, 2000). Many of the codes considered fit within the criteria; however, but the final decision was made based on the public availability of the source code and the corresponding graphical user interface (Voss, 1997).

4.2 The SUTRA Model

The SUTRA model is a 2-D density-dependant groundwater flow and solute transport code developed by Voss (1984). SUTRA employs a two-dimensional hybrid finite-element and integrated finite-difference method to approximate the governing equations that describe the two interdependent processes that are simulated: (1) density-dependent saturated ground water flow and either (2a) transport of a solute in the groundwater, or (2b) transport of thermal energy in the ground water and solid matrix of the aquifer. The following section summarizes the mathematical basis of the SUTRA model simulations (Voss, 1984).

SUTRA simulations are based on a hybridization of finite element and integrated finite-difference methods employed in the structure of the method of weighed residuals. Finite element approximations are used only for terms in the balancing of equations which describe fluxes of fluid mass and solute mass or energy. All other non-flux terms are approximated with finite element version of the integrated finite difference method. The advantage of this hybrid method is that it uses the geometric flexibility of finite-element simulations while taking advantage of finite-difference efficiency.

4.2.1 Fluid Mass Balance

The SUTRA flow simulation is a fluid mass balance which keeps track of the fluid mass contained at every point in the simulated groundwater system as it changes with time due to flow or density changes (Voss, 1984). SUTRA expresses the fluid mass balance as:

$$-\nabla \cdot (n_e \rho v) + Q_p = \frac{\partial (n_e \rho)}{\partial t} \tag{8}$$

v = fluid velocity (L/T)
P = fluid pressure (M/L^2)
k = intrinsic permeability (L^2)
n_e = effective porosity
ρ = fluid density (M/L^3)
g = magnitude of gravitational acceleration (L/T^2)
Q_p = fluid mass source [$M/(L^3T)$]

The term on the left side is the total change in fluid mass contained in the void space with time. This balances with the changes in average fluid velocity and fluid mass source on the right side of the equation.

Equation 8 needs to be expanded to represent each mechanism, in terms of the primary variables, pressure and concentration. The time derivative has been expanded in the following equation:

$$\frac{\partial (n_e \rho)}{\partial t} = (\rho S_{OP} + n_e \rho)\frac{\partial P}{\partial t} + \left(n_e \frac{\partial \rho}{\partial C}\right)\frac{\partial C}{\partial t} \tag{9}$$

S_{op} = specific pressure storativity $[M/(L^*s^2)]^{-1}$

Employing Darcy's law for the average fluid velocity in the previous equation (9), the form of the fluid mass balance implemented in SUTRA is:

$$\left(\rho S_{op} + n_e\rho\right)\frac{\partial P}{\partial t} + \left(n_e\frac{\partial\rho}{\partial C}\right)\frac{\partial C}{\partial t} - \nabla\left[\left(\frac{k\rho}{\mu}\right)\left(\nabla P - \rho g\right)\right] = Q_P \tag{10}$$

4.2.2 Subsurface Solute Transport Mechanisms

SUTRA solute transport simulation accounts for a single species mass stored in fluid solution as solute (Voss, 1984). The solute mass is transported through the porous medium by flow of groundwater (advection) and by molecular diffusion and dispersion. The mechanism for approximating the mixing process is called solute dispersion. This additional transport mechanism approximates the effects of solute advection and mixing of irregular flows which are not accounted for by solute advected by the average velocity. For a single species stored in solution the solute mass balance equation may be expressed as:

$$\frac{\partial(n_e C)}{\partial t} = -\nabla(n_e\rho v C) + \nabla\left[n_e\rho(D_m\underline{\underline{I}} + \underline{\underline{D}})\cdot\nabla C\right] + n_e\rho\Gamma_w + Q_P C^* \tag{11}$$

D_m = apparent molecular diffusivity of solute in solution in a porous medium including tortuosity effects (L^2/T)

I = identity tensor (1)

D = dispersion tensor (L^2/T)

Γ_w = solute mass source in fluid due to production reaction (M_s/M)

C^* = solute concentration of fluid sources (M_s/M)

The first term, on the right hand side of the equation, which includes the fluid velocity, v, represents average advection of solute mass into or out of the local volume. The second term involving molecular diffusivity, D_m, and dispersivity, D, expresses the contribution of solute diffusion and dispersion to the local changes in solute mass. The third term which includes the solute mass production rate per unit mass of fluid, Γ_w, expresses the contribution to dissolved species mass of chemical, biological or radioactive reactions in fluid. The last term, $Q_P C^*$, accounts for dissolved species of

mass added by fluid sources with concentrations, C*. The processes described by the last two terms are not applicable to this study.

SUTRA solves the governing equations of 'conservation of mass of fluid' and 'conservation of mass of salt' and computes flow velocities using Darcy's Law. SUTRA couples the equations 10 and 11 and these terms are then used to calculate the fluid mass balance and solute mass balance equations. The iterations continue with the solution of the concentration field used to compute the density distribution.

4.3 Numerical Model Parameters

This section discusses both the framework of the model, and the variables applied to that framework. The grid design and discretization remained constant throughout all simulations, as well as, non-spatial parameters such as fluid and soil compressibility. Variables that were modified included: boundary conditions and spatial parameters such as permeability.

4.3.1 Numerical Model Grid

Grid design is the foundation of any numerical model (Anderson and Woessner, 1991). Numerous problems can stem from bad grid design, such as oscillations and other grid artifacts (Holzbecher, 1998). Due to the importance of the grid design the following sections discuss the discretization of the grid and the steps taken to ensure grid accuracy.

Grid Discretization

Grid design is a key element in the numerical modelling process. In this study, the grid is a finite-element, two-dimensional cross-section, fishnet mesh consisting of quadrilateral elements. A fishnet mesh was created by superblocks (large adjacent quadrilaterals) each subdivided into a specific number of quadrilateral finite elements (Voss and Souza, 1987). This type of mesh may be considered similar to a deformed finite-difference grid. Each of these superblocks was filled by the fishnet mesh based on the information describing the number of quadrilaterals chosen for the X and Y direction. The model domain is 330 km long and varies in thickness, from 1200 m in the west to 300 m in the east (Figure 4.1). The mesh is made up of 22410 nodes and 21942 quadrilateral elements, with dimensions ranging from 800 m by 20 m to 1000 m by 5 m.

Grid Accuracy

The discretization of a numerical grid has a considerable effect on the stability of a numerical model (Anderson and Woessner, 1991). A more accurate and stable solution will be obtained with a very fine grid, but the computational (CPU) time may be extensive. A careful balance between nodal spacing and CPU time is essential in creating an accurate, yet efficient, simulation (Voss, 1984). There are certain accepted guidelines to follow when creating a grid to ensure a reasonable level of numerical stability. Most of these apply to linear problems and there are no guarantees for non-linear cases. The three principles of grid accuracy for transport simulations are: aspect ratio, Peclet number and Courant number. Violation of the following criteria can lead to oscillations and smearing of the results. If these values are within acceptable ranges then instabilities related to the grid should be minimized.

Aspect ratio defines the relationship between the horizontal and vertical dimensions of an element and the relative magnitude of hydraulic conductivity. The ideal ratio of these dimensions is 1:1, but a value of 10:1 is acceptable on some large-scale domains (Anderson and Woessner, 1991). For a regional-scale model, a 10:1 aspect ratio is difficult to achieve. Regional-scale models have a tendency to be long in the horizontal direction and thin in the vertical.

An aspect ratio of 4:1, in the area of interest is considered an acceptable value and was subsequently analysed for its effect further in this section. In the outer limits of the model, where flow is along the larger element dimension (i.e., horizontal flow along elements that are 800 metres long) the aspect ratio of approximately 20:1 was deemed sufficient (pers. comm. Mendoza, 2001).

The main criterion to ensure accuracy and stability of the numerical mesh is the **Peclet number** (Holzbecher, 1998). The Peclet number is calculated using the following equation:

$$\mathrm{Pe} = \frac{\Delta l}{\alpha} \tag{12}$$

Δl = characteristic nodal spacing

α = dispersivity

Ideally, the Peclet number should be less than or equal to 2 (Holzbecher, 1998). Values up to 10 have been shown to provide acceptable solutions (Huyakorn and Pinder, 1983).

For these models, Pe was calculated with the Δl from the grid (800 metres to 850 metres). The α longitudinal dispersivity is 100 metres throughout. The calculated Peclet number for this grid was found to range from 8 to 8.5 and therefore should be within an acceptable range.

The **Courant number** is used to address stability problems by verify the acceptability of the time discretization in a solute transport simulation (Holzbecher, 1998). Violation of this criterion leads to oscillations within the model domain (Holzbecher, 1998). The Courant criterion defines the time it takes for the solute to move the distance Δl. The time step can then be assigned as less than or equal to this period of time. According to Voss (1984), a general guideline is that relatively sharp solute fronts require time discretization which allows them to move only a fraction of an element per time step. The Courant number is as follows:

$$C = v\frac{\Delta t}{\Delta l} \tag{13}$$

Δl = characteristic nodal spacing

v = velocity

Δt = time step length

Along the flow path of the brine plume, evaluation of the model's base-case simulation shows that the Courant number remains below 1.0 (Table 4.2). Therefore, the relationship between the time step length and grid spacing should not have led to instability in the modelling results. This assertion has to be modified when fluid density is taken into account, since the solution is not linear. As a general rule, for density dependant simulations a Courant number of less than 0.1 is considered more reasonable. The results showed that the areas within the model that have Courant numbers of less than 1.0 but more than 0.1 produce minor numerical oscillations. It was determined that these oscillations are unimportant due to their position upstream from the sources of concentration. Downstream from the high concentration sources, in the areas of interest, the oscillations are not present because Courant numbers are significantly less than 0.1.

Improving the Peclet and Courant numbers was investigated as part of the study. A base-case simulation was run in order to determine if a finer grid mesh would generate more accurate results. The refined domain consisted of approximately twice the number of nodes in the horizontal direction (Table 4.3). Since the nodal length was divided in half and the other parameters stay constant the Peclet number and aspect ratio were also reduced by half (Table 4.3).

The results from this grid comparison test yielded a minor variation between the simulations. In addition, the small up-stream oscillations present in the base-case simulation are not present in the refined-grid simulation. It was stated earlier in this section that the upstream oscillations are of small consequence. Due to the lack of effect and the substantial increase in CPU time, from 27 to 325 hours, the refined grid was determined to be an inefficient use of time. This small improvement was not considered significant enough to outweigh the detriment of the extra 298 hours of CPU time necessary to run the refined-grid simulation. Therefore, the coarser grid was used in the remainder of the simulations.

4.3.2 Boundary Conditions

The boundary conditions control the movement of fluid through the domain either by impeding flow (no-flow boundaries), allowing fluid into the system, or removing fluid from the system. The study area flow system is bounded by low permeability aquitards, the shale of the Beaverhill Lake Group below the section and the thick Colorado Group shale act as barriers to flow above and below the cross section. These boundaries are implemented in the numerical model as no-flow upper and lower boundary conditions. In the model domain, these boundaries prevent the movement of fluid and solute through the top and bottom of the model domain.

Numerous combinations of lateral boundary conditions were tested before a final configuration was achieved, illustrated in Figure 4.2. On the western domain boundary, the boundary conditions consist of specified pressures and concentration boundary. For individual simulations, discussed later, the pressure distribution was altered to reproduce various average hydraulic head gradients. The value for the specified outflux boundary, on the east side of the domain, was determined by varying the flux value until the

required distribution of hydraulic head across the domain was observed in the models. The source of the pressure distribution will be discussed further along in this chapter.

4.3.3 Non-Spatial Parameters

Non-spatial parameters include all hydraulic parameters that are not a function of their spatial location and therefore remain constant throughout the model domain. The non-spatial parameters that need to be specified in SUTRA are as follows, fluid compressibility, solid matrix compressibility, diffusivity, fluid viscosity, solid grain density, the coefficient of fluid density change, and permeability anisotropy.

Fluid compressibility of water, β, is a function of both pressure and temperature. It ranges from $4x10^{-10}$ to $1x10^{-9}$ Pa^{-1}, as temperature and pressure increase from surface conditions to approximately 300°C and 100 MPa (Lachenbruch, 1980). For this simulation, a value of $4.5x10^{-10}$ Pa^{-1} was used for formation water compressibility. The compressibility of the solid matrix is affected by the compression of the solid grains and changes in pore space. Measured values range from $1x10^{-7}$ to $1x10^{-9}$ Pa^{-1} for clays and $1x10^{-9}$ to $1x10^{-8}$ Pa^{-1} for sandstones (Shi and Wang, 1986). SUTRA is not designed to have solid matrix compressibility vary in space. A value of $1x10^{-9}$ Pa^{-1} was chosen for the numerical model.

Diffusivity for solute transport represents molecular diffusivity of solute for geological media set at $1x10^{-10}$ m^2s^{-1} (Ingebritsen and Sanford, 1998).

Viscosity directly expresses the ease of fluid flow. Fluid viscosity is somewhat affected by pressure and concentration but is primarily a function of temperature. Since temperature effects are not taken into account for these simulations the viscosity was taken to be constant at $1x10^{-3}$ kg $m^{-1} \cdot s^{-1}$ (measured at 20°C) (Voss, 1984).

Fluid density is primarily a function of temperature and concentration. The approximate density models employed by SUTRA are first order Taylor expansions about a base density (Voss, 1984). For solute transport:

$$\rho = \rho(C) \cong \rho_0 + \frac{\partial \rho}{\partial C}(C - C_0) \qquad (14)$$

ρ_0 = base fluid density at $C=C_0$ (M/L^3)

C_0 = base fluid solute concentration (M/M)

C = solute concentration (M/M)

$\gamma = \frac{\partial \rho}{\partial C}$ = constant value of density change with concentration (M/L^3)

4.3.4 Spatial Parameters

Model parameters for porosity, permeability, (Table 4.5) have been compiled from existing hydrogeological literature (Bachu *et al.,* 1989b; Hitchon, 1989a; Hitchon, 1989b; Bachu and Underschultz, 1993). The values listed were determined to be the most representative of the regional hydraulic parameters. A sensitivity analysis will address the choice of these parameters and their impact on the results (Chapter 6).

The dispersivity expresses the contribution of irregular flow and mixing, which is not attributed to average solute advection (Voss, 1984). SUTRA allows the values of dispersivity be defined for each formation. Therefore, it was necessary to determine an appropriate value for each. There are no measured values for dispersivity on the regional scale (kilometres) (Gelhar, 1986). The values that are given for this scale range from 10 to 200 metres for longitudinal dispersivity (Figure 4.3). A value of 100 metres was chosen as the base longitudinal dispersivity and 10 metres for transverse dispersivity. Horizontal transverse dispersivities are at least an order of magnitude smaller than longitudinal values (Gelhar, 1986).

Table 4.5 shows the hydraulic parameters used in the numerical model. The values for regional-scale permeability were chosen from the published values of equivalent formations. A primary source of data used in this project was the Alberta Research Council (ARC) Bulletins (no. 58-60) (Bachu, 1989; Hitchon *et al.,* 1989a; Hitchon, 1989b). Cooking Lake Formation permeabilities are from a study of the regional-scale hydrogeology in northern Alberta (Bachu and Underschultz, 1993). Adjustments were made to the deeper portion of the platform carbonate to account for funnelling into the Leduc Formation reefs (discussed later). Mannville and Viking aquifer parameters are from Bachu *et al.,* (1989) from the analysis of regional parameters in the Cold Lake Area, Alberta. Joli Fou, Banff and Ireton aquitards permeability values are taken from

Hitchon *et al.* (1989), who report on the hydrogeological regime in the Phanerozoic succession, Cold Lake Area, Alberta. The Joli Fou (Hitchon *et al.*, 1989b) and Banff aquitard values are from Drill Stem Test (DST) and the Ireton value comes from literature (Bachu *et al.*, 1989b). The Nisku Formation values are from Bachu *et al.*, (1989).

Some values have been modified from the literature due to numerical constraints. From the literature, the permeability for the Ireton aquitard was determined to be 1×10^{-20} m^2. This value was 6 orders of magnitude less than the formations adjacent to it, created numerical instability in the model. The value used for Ireton aquitard permeability was modified to 1×10^{-18} m^2 to produce a stable solution. No values were found for the Wabamun aquitard in this study area. Due to the component of anhydrite and dolostone in the Wabamun, the assumption was made that the formation permeability was of the same order of magnitude as the Ireton aquitard.

4.4 Temporal Discretization

All transient simulations were run with 7000 time steps to cover a simulation time of 5 million years. The initial time step length was 100 years, increasing to 1000 years as the simulation progressed using a time step multiplier of 1.1.

4.5 Initial Conditions

Pressure and concentration distributions throughout the domain are defined as initial conditions at the beginning of the simulations. For the pressure field, the initial conditions were generated from the results of the steady-state simulations of flow. The initial concentration conditions for concentrations were set at 35 g/L throughout the domain. Therefore, the basin was essentially filled with seawater until transport moved the solute throughout the entire domain. In the transient simulation, sources of salt were placed in the lower aquifers to introduce solute to the system and therefore reproduce the salinity distribution. In the Cooking Lake aquifer, the source had a concentration of 200 g/L and in the Nisku aquifer the source concentration was 120 g/L (Figure 4.2). The concentrations are based on typical concentrations found in these aquifers.

4.6 Simulation Approach

Implementation of the conceptual model into a numerical simulation requires considerable time and effort. This numerical analysis considers topography-driven fluid flow due to the complicated nature of modelling various other driving forces and the increased likelihood that this was the active driving force. The objective of the following simulations was to determine the suitability of different topographic gradients as the driving force behind plume migration. The modelling approach was to select a topographic profile, assume instantaneous uplift, and apply a uniform hydraulic head gradient across the domain for duration of the simulations. The salinity profiles generated by the numerical model were then compared to present day distributions to evaluate the suitability of a particular paleo-topographic gradient.

Initially, it was necessary to determine if density-dependant flow played a significant role in the brine transport in this cross-section. These simulation results illustrate that the effects of density need to be taken into account. Once this was resolved, simulations using varying hydraulic head gradients were run to establish the gradient required to produce the observed salinity profile in the MGA. The results from the following simulations are discussed in Chapter 5.

4.6.1 Importance of Density Effects

It was previously established (Chapter 3) that ignoring the effects of density could lead to erroneous results when the DFR values are above 0.5. Bachu (1995) showed that the DFR values in the Wabamun Formation in the study area are greater than 0.5. A study of the regional-scale hydrogeology in the study area (Anfort *et al.*, 2001) also showed that DFR is greater than 0.5 in the westernmost portions of the Wabamun and Banff formations. Therefore density effects should be taken into account. Ignoring the density effects will most likely predict the solute plume to move more quickly since downdip buoyancy forces will not impede it. The comparison was made between a density-dependant and a non-density-dependant simulation to visually determine the density effects.

Ideally, the only difference between these simulations would be the calculation of density effects. However, this is not possible using SUTRA. Therefore, different boundary conditions had to be used, depending on whether density effects were taken into account (Table 4.6). Density dependant simulations use specified-pressure boundary

conditions and non-density dependant simulations use specified-head boundary conditions. Also, the flux boundary conditions are assigned different units. The density-dependant simulations units of flux are (mass of solute)/time and for non-density dependant simulations the units are in volume/time (Voss, 1984). The final difference is that permeability is used in the density dependant case and for the non-density dependant case hydraulic conductivity is used (Table 4.7). Conversions between these parameters were made carefully to insure that these differences are minor and it can be assumed that these simulations are essentially identical with the exception of solving for density.

4.6.2 Today's Gradient

The driving force generated by today's topography-driven flow gradient within this cross-section is limited due to low relief (Mossop and Shetson, 1994). Hitchon (1984) determined that barriers within the stratigraphic section of the Western Canadian Sedimentary Basin currently prevent direct meteoric recharge from the surface to the Upper Devonian flow system because of the presence of: (a) strong intervening aquitards, (b) overpressured zones and tight rocks in the Cretaceous strata in the deep basin and (c) higher concentration, higher density water in deep aquifers. Also, erosional rebound in the Cretaceous aquifers and aquitards creates a "sink" effect that would contain any recharge reaching these rocks (Corbet and Bethke, 1992). Over time, the potential for strong meteoric influx diminished as the overburden was eroded and currently there is not a significant driving force (Hitchon, 1984). Nonetheless, simulations were run using today's topographic gradient to allow for comparison between the magnitudes of hydraulic gradient. Also, the barrier effects that currently impede flow in the basin are ignored. Figure 4.4 shows a cross-section of today's topography in the study area with an average hydraulic gradient of 0.001. These simulations confirm the necessity of using paleo-topographic gradients to reproduce the observed salinity distribution.

4.6.3 Choosing the Paleo-topographic Gradient

The physical setting of the Mannville Group aquifer in southern Alberta has changed significantly through time. The Alberta basin has evolved from a foreland basin setting with little local relief, through a period of maximum burial at the end of the Laramide Orogeny and a period of uplift, to the present setting of a large tectonically dormant

plateau (Cody and Hutcheon, 1994). Corresponding to these changes, the nature of topography-driven flow must have also changed. During marginal marine deposition, the topographic relief was non-existent and therefore, unable to drive meteoric waters to displace the connate waters. However, post-Laramide uplift of the WCSB triggered a topography-driven hydrodynamic system capable of transporting large volumes of groundwater across a foreland platform (Garven, 1989).

The amount of uplift and subsequent erosion of the WCSB is a controversial subject on which many studies have been performed (Hacquebard, 1977; Beamount, 1981; Nurkowski, 1984; 1985; England and Bustin, 1986a; Osadetz *et al.,* 1990; Bustin, 1991). There are two main methods for calculating the amount of overburden removed by erosion using organic maturity: (1) use of lateral variation in maturity as determined by moisture content of coals (Nurkowski, 1984) and (2) extrapolation of vertical vitrinite reflectance gradients (England and Bustin, 1986; Osadetz *et al.,* 1990).

The modelling approach was to select a paleo-topographic profile and determine the corresponding hydraulic gradient for the duration of those simulations. Simulated salinity profiles were then compared to present day distributions to study the suitability of a particular paleo-topographic gradient. Three separate cases were considered to evaluate the resulting flowpaths and migration rates.

4.6.4 Bustin's Paleo-topography

England and Bustin (1986a) and Osadetz *et al.,* (1990) utilized a plot of vitrinite reflectance vs. depth to predict the thickness of eroded sediments, extrapolated the maturity gradients above the present surface to a zero maturity level and postulated that the amount of overburden removed from the basin axis is in the order of 5 km (England and Bustin, 1986). Over the entire basin, the results show a progressive west to east decrease in thickness of eroded overburden (3500 metres in the west to approximately 1500 metres in the east) (Figure 4.5).

Bustin's representation of the eroded sediments yields an average hydraulic gradient of 0.01 (Figure 4.6). For the simulations, a specified head value of 5000 metres on the west boundary and on the east, an outflux boundary corresponding to a head value of 1500 metres were assigned.

4.6.5 Nurkowski's Paleo-topography

Nurkowski (1985) published a theoretical model to account for the relationship between coal seam rank and its original depth of burial. Maximum depths were reconstructed on the basis of established relationships between equilibrium moisture loss and depth of coal seam burial (Figure 4.7). This model explains that the variations in coal rank in the plains area are a result of varying amounts of overburden that existed when the coal reached its current maturity. Nurkowski also determined that removal of the calculated overburden was plausible. Regional post-Jurassic erosional rates of 46 mm/1000 years were calculated for the Mississippian drainage basin (Menard, 1961). These values match Nurkowski's rates of 33-63 mm/1000 years based on 30 million years of erosion (from Oligocene to present).

Nurkowski's reconstructed overburden cross-section has a paleo-hydraulic gradient of 0.004 (Figure 4.8). Thus, a simulation was constructed with a specified pressure boundary corresponding to a head value of 2650 m, the outflux boundary corresponded to a head value of 1400 metres.

4.6.6 Base Case Paleo-topographic Gradient

For the base case, the minimum hydraulic gradient needed to drive flow updip under present day conditions was calculated using impelling force, Fe (see chapter 2, equation 3). Following the Driving Force Ratio (DFR) approach (Davies, 1987; Bachu, 1995a), the impelling force needed to drive dense brine updip was calculated using the slope of the regional aquifer of 0.002 and the maximum plume density of 1100 $kg \cdot m^{-3}$ (corresponding to 140 g/L TDS). From this calculation, it was determined that the model needs a hydraulic gradient >0.002. Published estimates of paleo-topographies (discussed above) provide a range of topographic gradients ranging from 0.004 to 0.01. Thus, a base case gradient of 0.007 was selected to represent the median between these published cases. The west boundary of the cross-section was given a fixed head of 3300 metres. On the east boundary, a head of 1000 metres was chosen.

4.7 Chapter Summary

This chapter discussed the design of the numerical simulation from the code evaluation, model design, model parameters, and temporal discretization. These are the building blocks of the numerical simulation and subsequently, the results of the various scenarios applied to this model will be discussed in the following chapter.

CODE	Developer	Dimensions	Grid Type	Public Domain	GUI available
SUTRA	Voss and Souza (1987)	2D	FD/FE	yes	yes
MOCDENSE	Sanford and Konikow (1985)	2D	FD	yes	no
HST3D	Kipp (1987)	3D	FD	no	yes
FEMWATER	Yeh *et al.*, (1987)	3D	FE	no	yes
RIFT2D	Person *et al.*, (in review)	2D	FE	no	no

Table 4.1 – Various variable density numerical codes.

Formation	Node Number	Velocity (m/s)	Length (m)	Time Step (s)	Courant #
Nisku	331	5.1×10^{-11}	800	3.2×10^{10}	2×10^{-3}
Nisku	3802	1.0×10^{-12}	800	3.2×10^{10}	4×10^{-5}
Ireton	1016	1.3×10^{-11}	800	3.2×10^{10}	1×10^{-3}
Cooking Lake	1616	1.8×10^{-08}	800	3.2×10^{10}	7×10^{-1}
Cooking Lake	1539	1.1×10^{-10}	800	3.2×10^{10}	4×10^{-3}

Table 4.2 – A sample of results from the Courant number evaluation of a base-case simulation.

Grid Parameters	Base Grid	Refined Grid
x direction nodal spacing	800-1000m	400-500m
y direction nodal spacing	20-25m	20-25m
Number of Nodes	21528	43004
Number of Elements	21063	42126
Aspect Ratio	4*	2*
Peclet Number	8 to 8.5	4
Courant Number	0.71**	0.071**
Approximate CPU time	27 hours	325 hours

Table 4.3 - Comparison between a coarse grid and a refined grid.

* Aspect Ratio varies throughout the model, the value here represents the largest value

** The Courant number varies throughout the model, the value here represents the largest value

Non-Spatial Model Parameters	Value	Units	Source
Fluid Compressibility	4.5×10^{-10}	Pa^{-1}	1
Solid Matrix Compressibility	1×10^{-10}	Pa^{-1}	4
Effective Molecular Diffusivity	1×10^{-10}	m^2s^{-1}	6
Fluid Dynamic Viscosity	1×10^{-3}	$kg\ m^{-1}s^{-1}$	2
Gravity	9.81	$m\ s^{-2}$	-
Density of Solid Grains	2600	$kg\ m^{-3}$	5
Coefficient Fluid Density Change	700	$kg\ m^{-3}$	2
Longitudinal Dispersivity (α_L)	100	m	3
Transverse Dispersivity (α_T)	10	m	3
Anisotropy Ratio (k_x/k_y)	10:1		-

Table 4.4 – Non-Spatial Model Parameters.

([1]Lachenbruch, 1980; [2]Voss, 1984; [3]Gelhar, 1986; [4]Shi and Wang, 1986; [5]Fetter, 1994; [6]Ingebritsen and Sanford, 1998)

Stratigraphic Unit	Porosity	Horizontal Permeability (m^2)	Vertical Permeability (m^2)	Source
West Cooking Lake East Cooking Lake	0.26 0.26	2×10^{-13} 2×10^{-15}	2×10^{-14} 2×10^{-16}	1
Leduc	0.30	1×10^{-12}	1×10^{-14}	5
Ireton Conduit	0.30	1×10^{-14}	1×10^{-14}	-
Ireton	0.12	1×10^{-18}	1×10^{-19}	2
Nisku	0.24	2×10^{-14}	2×10^{-15}	2
Wabamun	0.12	5×10^{-17}	5×10^{-18}	-
Banff	0.12	5×10^{-17}	5×10^{-18}	4
Mannville	0.24	4×10^{-14}	4×10^{-15}	3
Joli Fou	0.12	2×10^{-17}	2×10^{-18}	4
Viking	0.26	4×10^{-14}	4×10^{-15}	3

Table 4.5 – Aquifer Spatial Model Parameters.

([1]Bachu and Underschultz, 1993; [2]Bachu *et al.*, 1989; [3]Hitchon *et al.*, 1989a; [4]Hitchon *et al.*, 1989b; [5]Hugo, 1990)

Boundary Condition	Density Dependant Case	Non-density Dependant Case
Specified Flux	-0.0245 kg/s	$-6.4x10^{-5}$ m^3/s
Specified Pressure	$4x10^{7}$ $kg/m*s^2$	
Specified Head		3200 m

Table 4.6 – Boundary conditions used in the density dependent and non-density dependent cases.

	Density Dependant Case		Non-density Dependant Case	
Hydrostratigraphic Unit	**Horizontal Permeability (m^2)**	**Vertical Permeability (m^2)**	**Horizontal Hydraulic Conductivity (m/s)**	**Vertical Hydraulic Conductivity (m/s)**
Cooking Lake Updip from reef	$2x10^{-13}$ $2x10^{-15}$	$2x10^{-14}$ $2x10^{-16}$	$2x10^{-6}$ $4x10^{-8}$	$2x10^{-7}$ $4x10^{-9}$
Leduc	$1x10^{-13}$	$1x10^{-14}$	$1x10^{-6}$	$1x10^{-7}$
Ireton Conduit	$1x10^{-14}$	$1x10^{-14}$	$1x10^{-7}$	$1x10^{-8}$
Ireton	$1x10^{-18}$	$1x10^{-19}$	$1x10^{-11}$	$1x10^{-12}$
Nisku	$2x10^{-14}$	$2x10^{-15}$	$2x10^{-7}$	$2x10^{-8}$
Wabamun	$5x10^{-17}$	$5x10^{-18}$	$5x10^{-10}$	$5x10^{-11}$
Banff	$5x10^{-17}$	$5x10^{-18}$	$5x10^{-10}$	$5x10^{-11}$
Mannville Group Aquifer	$4x10^{-14}$	$4x10^{-15}$	$4x10^{-8}$	$4x10^{-9}$
Joli Fou	$2x10^{-17}$	$2x10^{-18}$	$2x10^{-10}$	$2x10^{-11}$
Viking	$4x10^{-14}$	$4x10^{-15}$	$4x10^{-7}$	$4x10^{-8}$

Table 4.7 – Hydraulic parameters used in the density dependent and non-density dependent cases (conversions are equivalent for air at 15 °C and normal pressure, $\mu = 1.8 \times 10^{-5}$ Pa·s and $\rho = 1.25$ kg·m^{-3}).

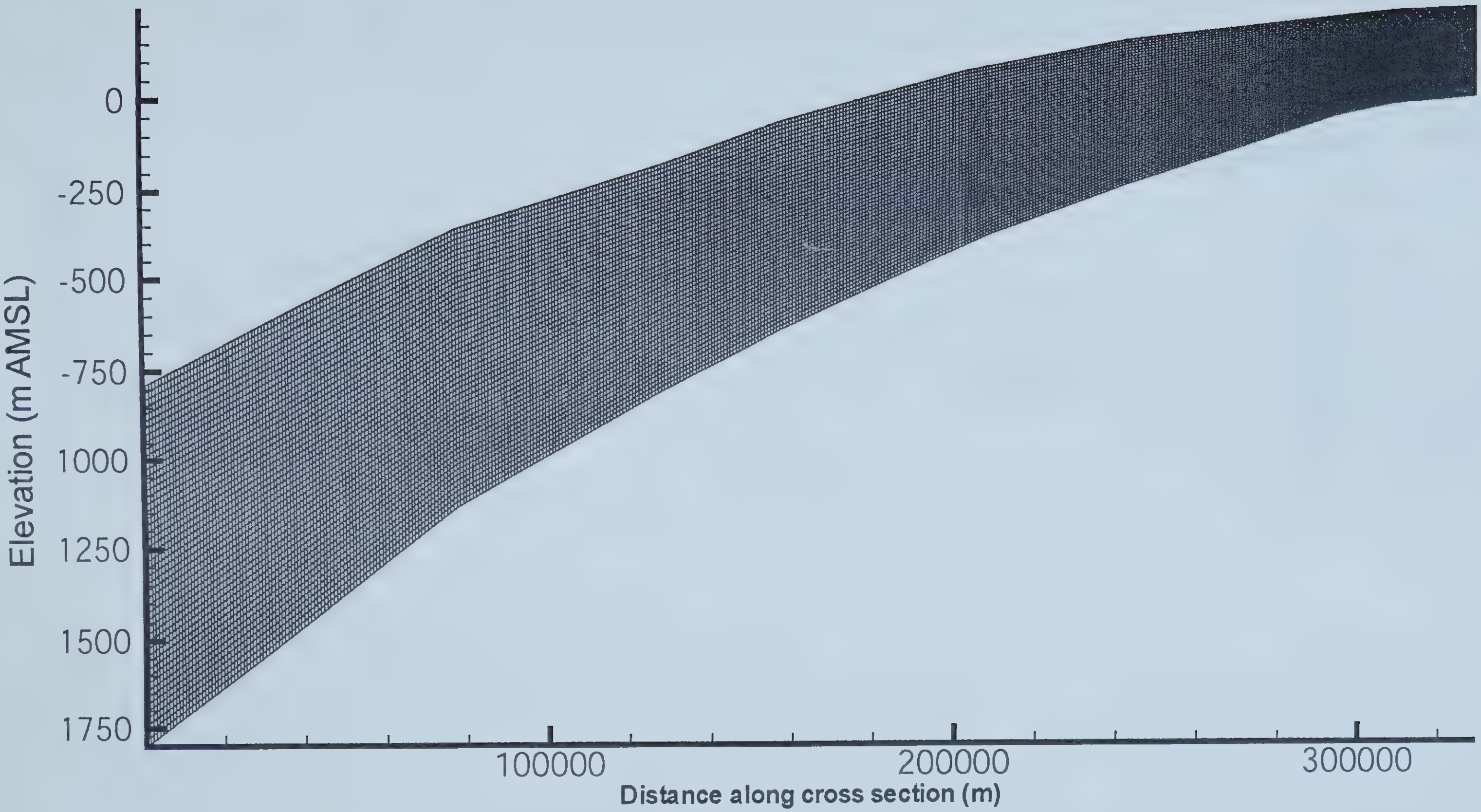

Figure 4.1 - Numerical Model Grid containing 22410 nodes and 21942 quardrilateral elements. 87x vertical exxageration.

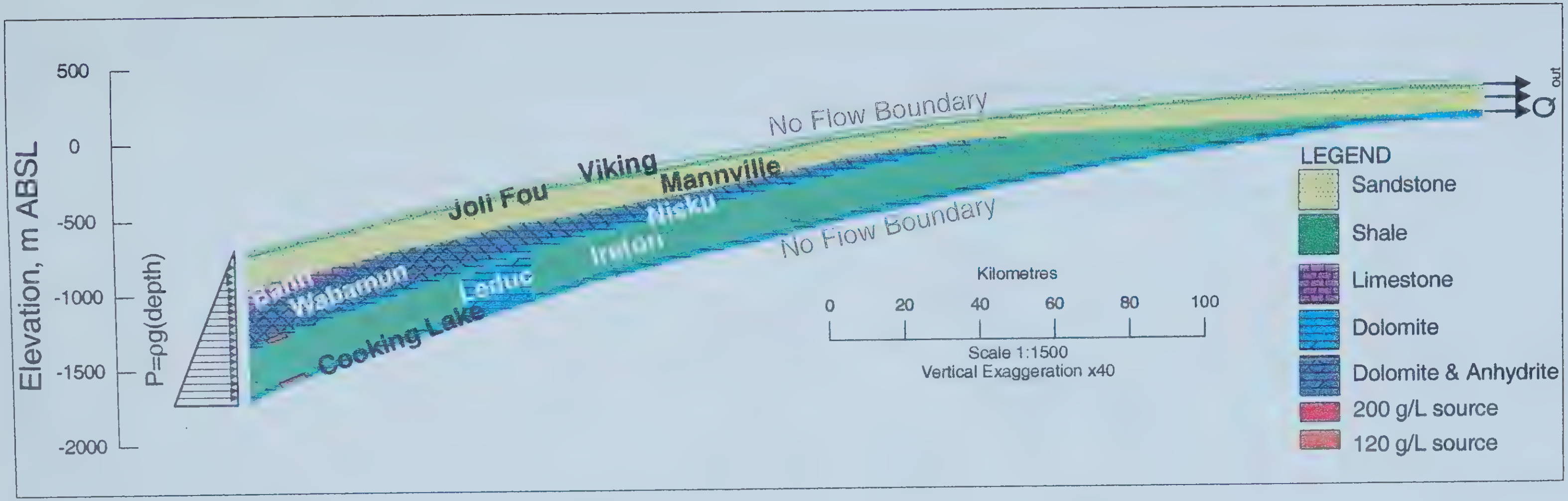

Figure 4.2 - The conceptual model used for the numerical simulation. A specified pressure boundary condition is applied on the left and on the right a specified flux boundary condition is applied.

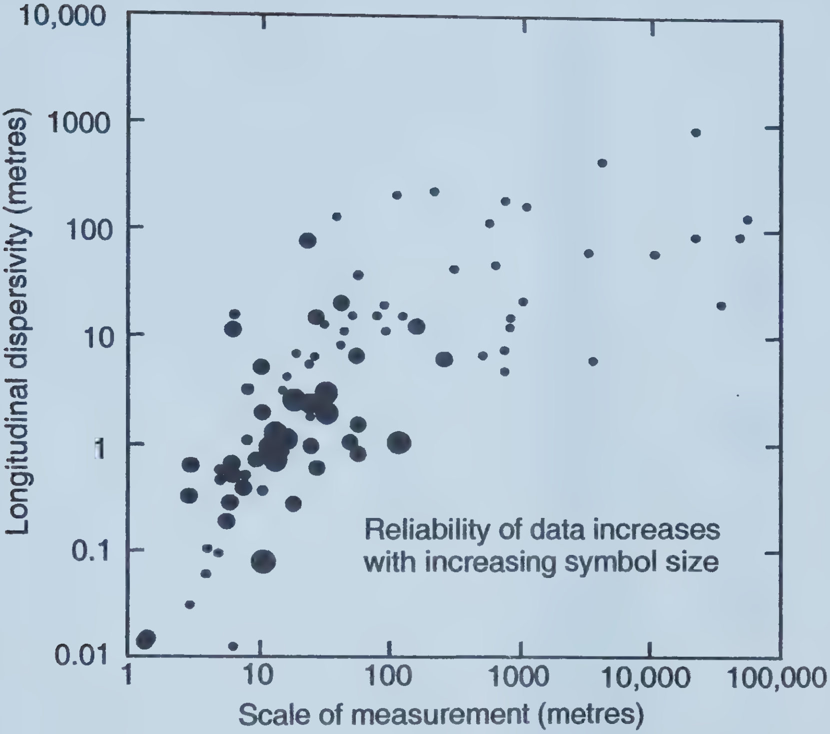

Figure 4.3 - Longitudinal dispersivity versus scale with data classified by reliability (modified after Gelhar, 1986).

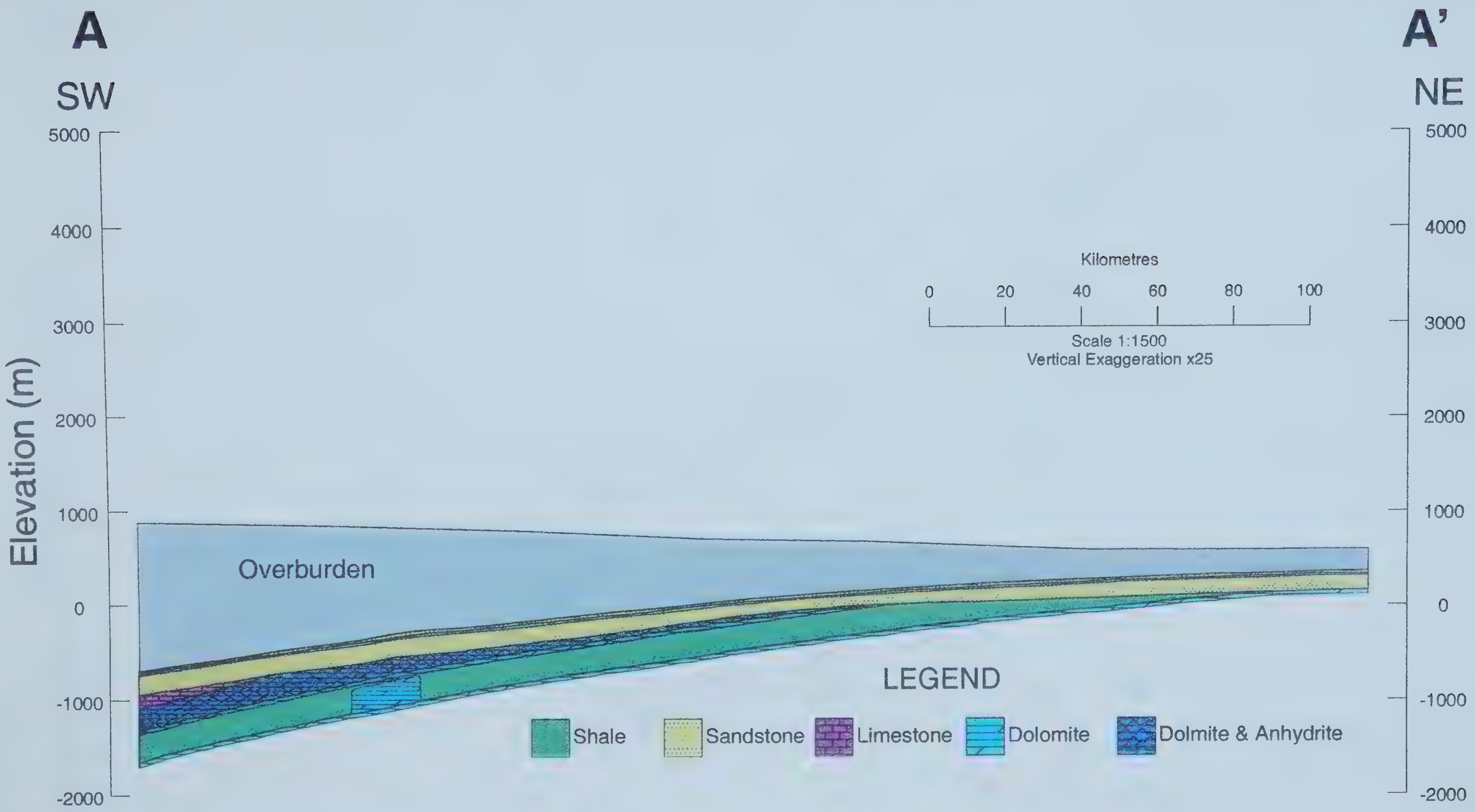

Figure 4.4 - Schematic of present day topography above the study area, hydraulic gradient 0.001.

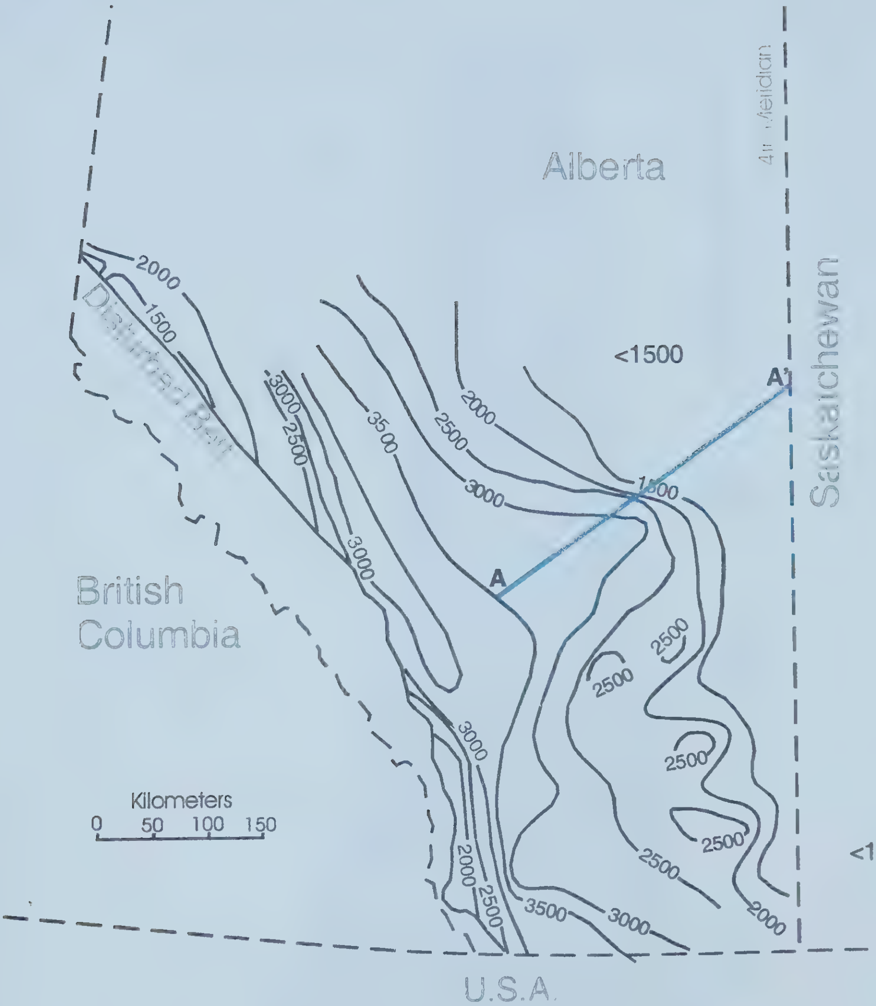

Figure 4.5 - Reconstructed thickness of overburden (eroded section) in the WCSB (Modified from Bustin, 1991).

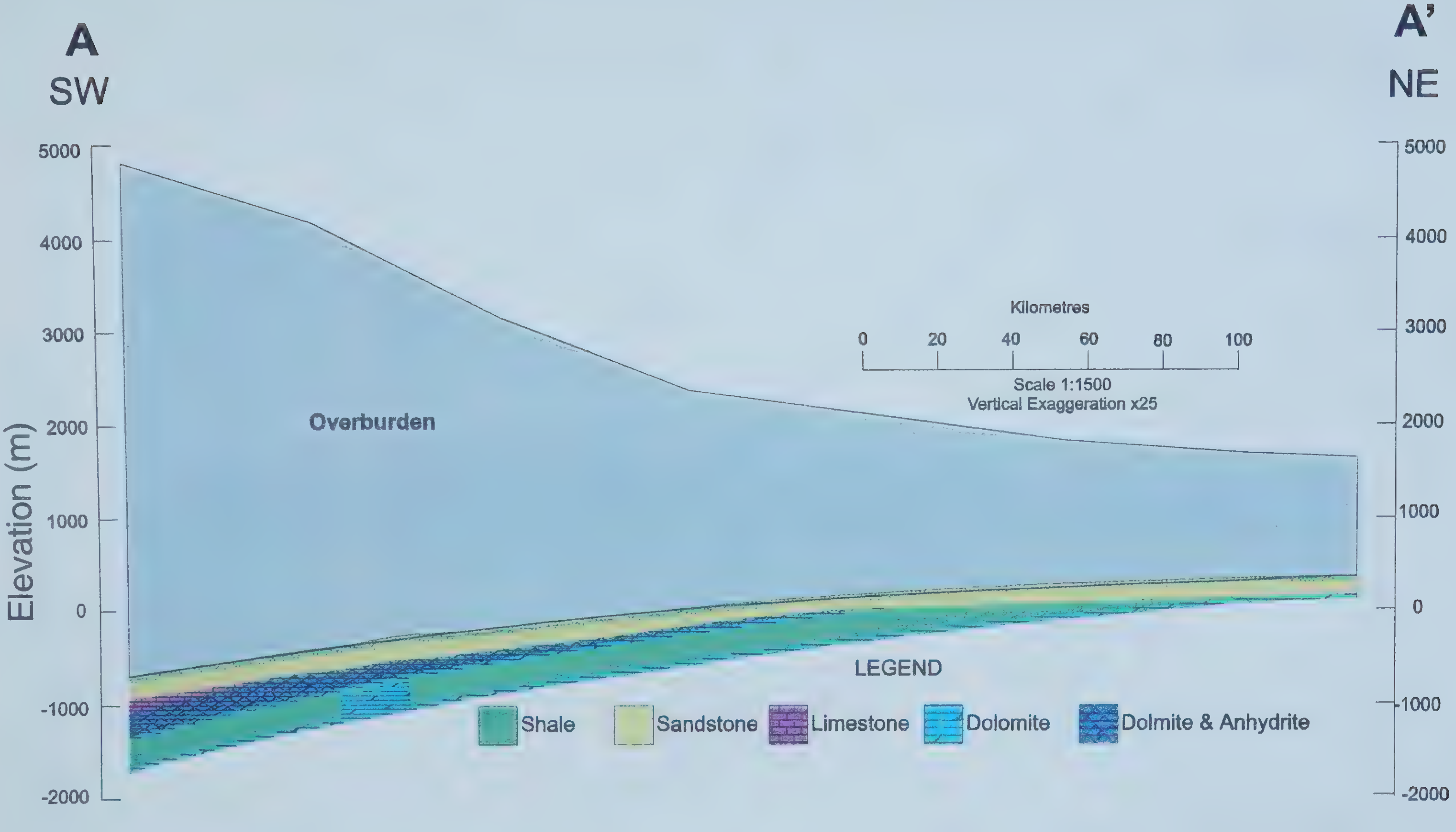

Figure 4.6 - Schematic of Bustin’s paleo-topography above the study area, paleo hydraulic gradient 0.001.

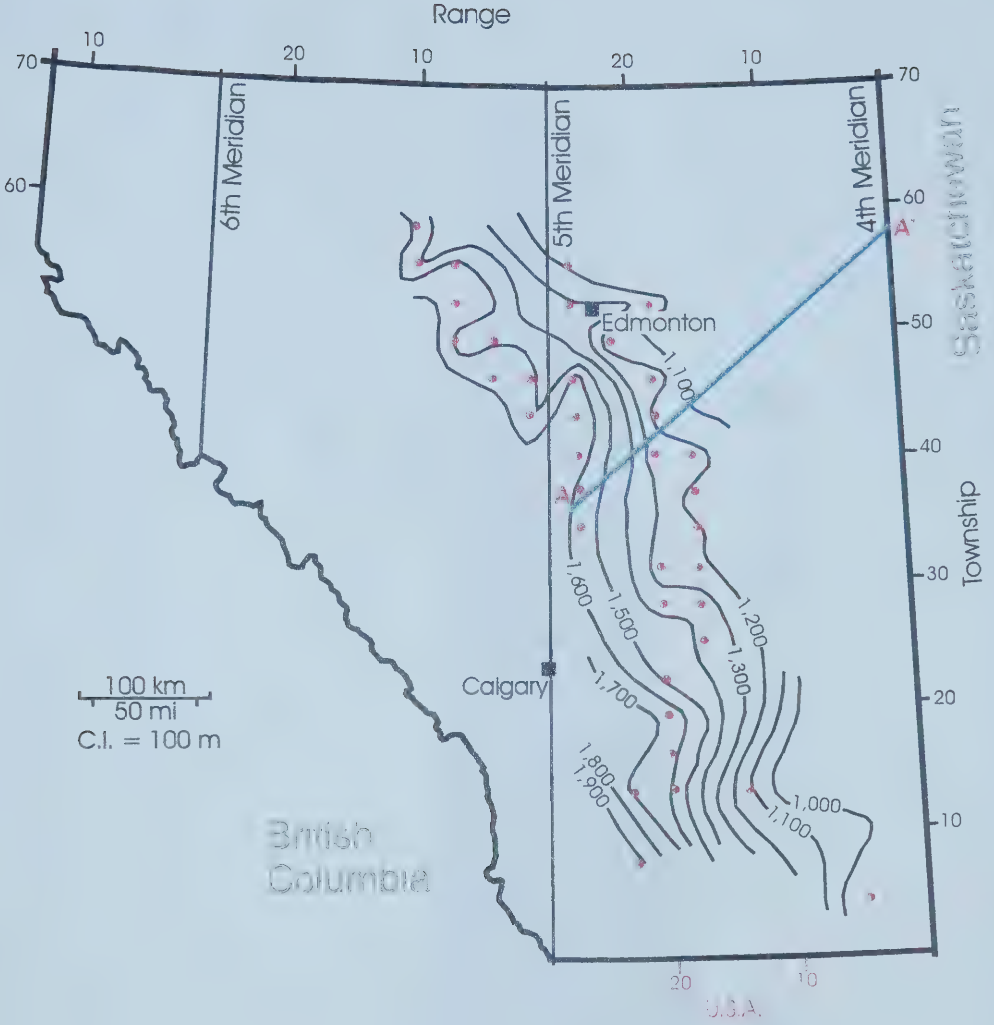

Figure 4.7 - Thickness of removed sediments from plains area of Alberta (Modified from Nurkowski, 1984)

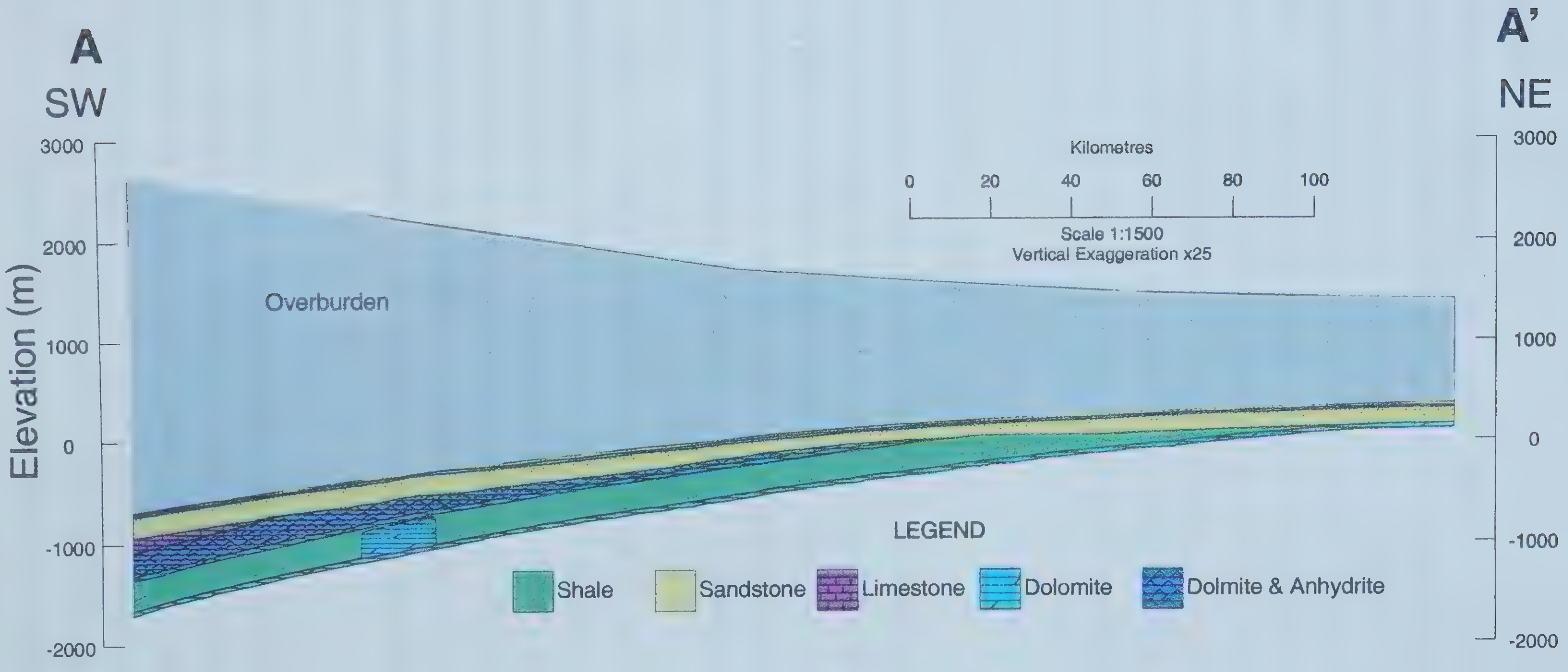

Figure 4.8 - Schematic of Nurkowski’s paleo-topography above the study area, paleo hydraulic gradient of 0.004.

Chapter 5 Results

Previous chapters have established: (a) the existence of the brine plume in the MGA, (b) the origin and pathway of the plume, (c) the importance of variable density effects on fluid flow, as well as, (d) the geology and hydrogeology of the study area. These concepts were combined in the preceding chapter to create the conceptual model and simulation scenarios. This chapter discusses the results of the simulations and the chapter organization is shown (Figure 5.1). Initially, the impact of density effects are addressed. This is followed by the results of the simulations using present day and paleo-topographic gradients as the hydraulic driving force for fluid flow. The chapter concludes with a discussion of the gradient which produces the best representation of the brine plume observed today.

5.1 Mapping of the Brine Plume

Previous studies mapped only a portion of the brine plume in the MGA. Thus, it was necessary to delineate the brine plume in the MGA so that the low salinity boundaries of the groundwater model cross-section could be established. Therefore, a total dissolved solids (TDS) map of the MGA in the Alberta Basin was created to show the location of anomalously high TDS values within this study area (Figure 5.2) (Appendix A).

The background value of TDS within the MGA is approximately the salinity of seawater, 35 g/L. TDS values exceeding 140 g/L are found in the MGA directly above the Leduc reefs. Values lower than 35 g/L are found in the southern portion of the MGA and indicate meteoric recharge occurs from the south (Anfort *et al.*, 2001). The localized high salinity values have been established as a plume of Paleozoic formation waters based on evidence from geologic, geochemical and hydraulic data (Bachu, 1995a, b; Rostron and Tóth, 1997).

A second objective of creating the TDS map was to determine the most appropriate location for the 2D cross section. The criteria for selection of the orientation of the cross section was the presence of a full range of 'typical' MGA TDS values, as well as, intersection of the high TDS values. It was also considered important that the cross section included a portion of the Bashaw reef complex, since the previous literature indicated that the reef was a fundamental element to the plume emplacement.

5.2 Numerical Simulations

5.2.1 Results Criteria

The most representative or "best" case was identified by selecting a set of parameters that created a salinity distribution closely resembling the observed plume. The present day map of the dimensions and concentration of the observed brine plume (Figure 5.2) provides the criteria by which the topographic driven flow simulations are evaluated. Currently, the brine plume in the MGA has a maximum concentration of >140 g/L TDS. The plume has an elliptical shape, with a >130 g/L TDS plume of approximately 20,000 metres in length and a >80 g/L TDS of approximately 120,000 metres in length (Figure 5.2). These plume characteristics form the primary basis of comparison for the model. The brine concentration was also evaluated over time at an observation point located in the MGA, directly above the Leduc Formation reefs. This observation point was chosen based on the fact that the highest TDS concentrations are observed there.

5.2.2 Physical Pathway of Flow

The simulation results, in general, show a similar flowpath for each of the simulations. The plume originates in the Cooking Lake aquifer, ascends through the Leduc aquifer, across the Ireton aquitard conduit, and into the Nisku aquifer. The solute then travels updip along the aquifer and then vertically across the overlying Wabamun aquitard. The solute enters the MGA directly from both the Wabamun aquitard subcrop and eventually at the Nisku aquifer subcrop. Exceptions to the general case can occur; these cases are discussed in the sensitivity analysis.

5.2.3 Importance of Density Effects

The importance of including density effects when analyzing flow in sedimentary basins was discussed previously (Chapter 4). Thus, it was necessary to run two simulations to determine the impact of density: case (a) without density effects and case (b) with fully coupled density effects.

Initially, a comparison was made between the distributions of hydraulic head for each case after 500 years (1 time step) in order to determine if an equivalent hydraulic gradient could be produced for each simulation (Figure 5.4). The results show that the hydraulic head distributions are similar when a hydraulic gradient of 0.007 was specified.

The head contour maps differ only above the reef feature at the 3200 metre contour. Analysis of the differences found in the simulation results shows that only a very small variation is predicted (Figure 5.4c). The maximum difference of 40 metres (or 1.3%) is considered negligible and consequently ignored. Therefore, the models were assumed to be approximately equivalent and density effects on solute migration could then be evaluated.

The effects of density were illustrated by comparing the concentration distributions after 2.5 million years (Figure 5.5). On the periphery of the model domain, the solute distributions appear very similar. In general, the model ignoring density effects shows that after 2.5 million years a larger volume of high concentration solute (>160 g/L TDS) has entered the MGA (Figure 5.5a). In this case, a small plume of >160 g/L TDS solute is located in the lower portion of the MGA (Figure 5.5a). For the same time span in the density dependent case the >160 g/L TDS solute plume has not migrated from the Wabamun aquitard (Figure 5.5b). In addition, it appears that more solute is moving updip in the Cooking Lake aquifer in the 'density dependent' case. This comparison shows that by taking into account density effects, the fluid preferentially moves updip along the Cooking Lake aquifer rather than rising vertically through the Leduc reef. One possible cause of this phenomenon may be the density gradient found within the reef. Figure 5.5c illustrates the difference between the salinity distributions of the two models and shows that most of the variation occurs where the solute plume has entered the MGA at the Wabamun subcrop (eg., the 30 metre contour).

The effects of density will be slightly exaggerated with this particular code since the effects of temperature are not taken into account. The high temperatures that are found in the deep basin would have lowered the density of the dense plume creating a solute distribution somewhere between these two cases. Since SUTRA is unable to couple the effects of both temperature and density it was decided that using the density dependent solutions would lead to more accurate representations of the solute distribution. Therefore, in all of the following scenarios only density dependent simulations were run.

5.2.4 Present Day Topography

The salinity distribution assuming today's topography was investigated. A constant gradient of 0.001 was applied to the model domain and the simulation was allowed to

proceed for 30 million years. To achieve this, a specified-pressure boundary condition was applied to the westmost edge, corresponding to a hydraulic head value of 930 metre above mean sea level (mAMSL). This lead to the application of a specified-flux boundary condition corresponding to a head value of 600 metres (mAMSL) on the east edge of the model domain (Figure 5.6). The value of specified-flux was determined by trial and error to achieve the required hydraulic head value.

The simulation results predicted that today's shallow topographic relief would contribute little to a regional groundwater flow system. Simulation results show that today's gradient of 0.001 slowly migrates solute through the system (Figure 5.7). After 10 million years, the TDS concentration in the MGA is slightly higher than seawater, approximately 40 g/L (Figure 5.7a). A plume of 60 g/L TDS is approximately 80,000 metres long in the MGA after 20 million years. After 30 million years, the 60 g/L TDS contour is approximately 140,000 metres long. However, the 80 g/L TDS contour never enters the MGA in the 30 million years of simulation time (Figure 5.7c).

The inability of the present day flow system to create the observed brine plume can be seen by analysis of a plot of concentration versus time at the observation point (Figure 5.8). Concentrations in the MGA never exceed 80 g/L TDS over 30 million years of simulation. This is due to the high flux within the MGA that quickly dilutes the plume emerging from the Wabamun aquitard. This shows that during the last 30 million years of relative tectonic dormancy the plume would not have formed. The concentration at the observation point increases a small amount over 30 million years. The TDS concentration at the observation point reaches 40 g/L and 60 g/L, at 300,000 and 12 million years, respectively. Given the mapped distribution of TDS in the MGA, higher concentrations need to be reached, most likely by a stronger flow system. Therefore, it was necessary to examine past conditions in the basin when paleo-topographies were such that a significantly stronger topography-driven flow system existed.

5.2.5 Paleo-topography Results

The preceding results using present day topography suggested that a stronger topographic gradient would be required to emplace the saline plume observed in the MGA. The Laramide orogeny changed the landscape of the Cretaceous by increasing the topographic relief from west to east (Chapter 4). It is believed that this relief created

a strong topographic driving force propelling basinal fluids through the study area. Various published paleo-topographies were simulated to determine the best relationship between the paleo driving forces and today's salinity distribution (see Chapter 4). Differing topographies were simulated by varying the specified head boundary conditions and the subsequent differences in hydraulic gradient. The different initial hydraulic head distributions are outlined in Figure 5.9.

5.2.5.1 Bustin's Paleo-topography

As discussed in Chapter 4, Bustin's re-constructed sediment overburden created a paleo-topography with a hydraulic gradient of 0.01. Hydraulic head values of 4400 and 1600 mAMSL were specified at the west and east boundaries, respectively (Figure 5.9a). On the west boundary, a specified-pressure boundary condition produced the required head value. Specified flux values on the east boundary were varied until a corresponding head value of 1600 metres was attained.

A gradient of 0.01 produces a fairly strong driving force, moving fluid quickly through the cross section. After 1 million years of simulated time, the >120 g/L TDS brine plume is approximately 30,000 metres long and the >160 g/L TDS brine plume is approximately 8,000 metres long (Figure 5.10a). After 2.5 million years, the lower salinity water (<100 g/L) has been flushed out of the updip portion of the MGA (Figure 5.10b). The >160 g/L TDS brine plume is approximately 140,000 metres long and the >180 g/L brine begins to enters the lower portion of the MGA. After 5 million years, the majority of the updip portion of MGA is filled with a brine TDS concentration >160 g/L. At the Cooking Lake aquifer subcrop the lower concentrations are entering the MGA from below. At this time, the 200 g/L TDS brine is still contained within the Wabamun aquitard.

5.2.5.2 Nurkowski's Paleo-topography

The paleo-hydraulic gradient derived from Nurkowski's paleo-topography is approximately 0.004. This gradient was applied to the model domain by a specified-pressure boundary condition on the westmost edge corresponding to 2600 metres head value. The specified flux boundary on the east side controlled the rate of fluid leaving the domain and was varied until a corresponding head value of 1400 metres was attained (Figure 5.9b).

The TDS distribution achieved using Nurkowski's hydraulic gradient of 0.004 is significantly different from the previously discussed cases. After 1 million years of simulated time, the >140 g/L TDS solute has travelled updip from the source and halfway into the reef (Figure 5.11a). After 2.5 million years, the simulation results show that the >140 g/L TDS solute has moved completely through the reef, partially updip in the Nisku aquifer and nearly through the Wabamun aquitard (Figure 5.11b). After 5 million years the >120 g/L TDS plume is approximately 27,000 metres in length with a small amount of 140 g/L TDS solute entering the MGA. The majority of the >140 g/L TDS solute is swept away by the lower concentration formation fluid in the MGA. This scenario creates a large plume of mid-range concentration rather than a small plume of high concentration.

5.2.5.3 Paleo-topographic Flow Discussion

The paleo-topographic simulations show a range of concentration distributions in the MGA. A comparison of concentration versus time for each of the paleo-hydraulic gradients at the observation point, allows for the evaluation of these driving forces with respect to the target maximum concentration (Figure 5.12).

The maximum simulated hydraulic gradient of 0.01 created a significant driving force and transported a substantial amount of brine into the MGA. This gradient creates a relatively quick increase in TDS concentrations, from 40 to 120 g/L in only 500,000 years (Figure 5.12). The high concentration solute of >160 g/L enters the MGA after 1 million years (Figure 5.12). The salinity then levels off between 180 and 190 g/L TDS for the remaining 4 million years of simulation time. This high salinity concentration indicates that a gradient of 0.01 creates a stronger driving force than is required for this flow system. Given the observed salinity distribution, this driving force could have only acted for a very short period of time since it would have filled the MGA with a >190 g/L TDS brine concentration.

The effects of the 0.004 hydraulic gradient are muted when compared to the previous case. At the observation point, the simulation of the lowest paleo-hydraulic gradient, 0.004, slowly increases concentration in the MGA over time reaching 80 g/L TDS after 1.5 million years (Figure 5.12). After 2.5 million years a concentration of 120 g/L TDS is reached. In this simulation, the high concentrations of the plume, above 140 g/L TDS,

reaches the observation point in the MGA some time after 5 million years (Figure 5.12). The observed slow increase in concentration creates a salinity distribution which is spread out within the MGA due to mixing of the ambient formation waters with the invading solute. The maximum concentration of approximately 140 g/L is below the target salinity values.

5.2.5.4 Base Case

These simulation results indicate that to re-create the desired salinity distribution a case should be run using an average of these paleo-hydraulic gradients (see chapter 4). Results from simulations using the mean value of 0.007 were used to better delineate the best fit of hydraulic gradients. The boundary conditions necessary to simulate this gradient were specified pressure and outflux boundaries, with corresponding heads of 3300 and 1000 metres, respectively (Figure 5.9c).

The simulated salinity distribution is shown in Figure 5.13. After 160,000 years the >140 g/L TDS solute enters the Leduc reef and makes its way into the Nisku aquifer after approximately 600,000 years. After 1 million years of simulation time, the >140 g/L TDS solute has moved updip along the Nisku aquifer and halfway into the Wabamun aquitard (Figure 5.13a). After 1.5 million years, the plume has entered the MGA. After 2 million years, the >140 g/L TDS plume is 11000 metres in length and >120 g/L TDS plume is 23,000 metres in length (Figure 5.13b). By 2.5 million years the >120 g/L TDS and >140 g/L TDS plumes were 24,000 metres and 65,000 metres in length, respectively (Figure 5.13c).

5.3 Discussion and Results Summary

The modeling results indicate that the physical pathway of the brine plume migrating into MGA is consistent with the postulated fluid flow patterns from previous studies (Rostron and Tóth, 1997, Anfort *et al.,* 2001). The solute originated in the Cooking Lake aquifer and ascended vertically through the Leduc aquifer. A conduit of highly permeable strata above the reef channeled the fluid into the overlying Nisku aquifer. The solute then traveled across the Wabamun aquitard and also entered the MGA at the Wabamun subcrop.

It was established in previous chapters (see Chapter 4) that it is necessary to take into account the effects of density in the study area, due to the salinity-induced density of the formation fluid. The simulation discussed in this chapter established the impact of density effects on the solute transport results. It was determined that by taking density effects into account the solute plume moves into the MGA at a slower rate due to the difficulty in transporting the dense fluid updip in the basin.

Results show that it is unlikely that today's topographic gradient produced the observed brine plume. The previous chapter discussed the limitation of today's gradient due to the available driving forces, as well as, barriers to regional flow. A simulation was run to confirm the inappropriateness of this low hydraulic gradient. The results of this simulation support the hypothesis that today's small topographic relief is insufficient to transport dense brines updip in the study area. The concentrations within the MGA never surpass 80 g/L in the 30 million years of simulation time (Figure 5.7), therefore stronger driving force is needed to emplace the dense plume in the MGA.

Simulations of the paleo flow system following the Laramide orogeny support the contention that a strong driving force would emplace the brine plume in the MGA. Previous research provides two representations of the paleo-topography. The modelled paleo-hydraulic gradients generated significantly different salinity distributions in the MGA. Figure 5.14 shows a comparison of concentration versus time for each of the hydraulic gradients at an observation point in the MGA, directly above the Wabamun aquitard subcrop. The highest gradient of 0.01 causes a relatively quick increase in salinity in the MGA and then fills the basin with >180 g/L TDS solute. The lowest gradient of 0.004 slowly increases concentration over time, reaching 140 g/L TDS after 5 million years. The median gradient of 0.007 reaches the target of 160 g/L after approximately 2.5 million years and then the salinity within the formation continues to increase to 170 g/L TDS after 30 million years.

The numerical model was highly sensitive to changes in gradients; a difference of 1 order of magnitude makes the difference between flooding the MGA with high salinity brine and having no salinity enter this formation. These results show that today's topography-driven gradient would be insufficient to create the observed salinity distribution, but a paleo-topography with an adequate amount of overburden could have

had sufficient driving force to emplace the brine plume in the MGA. From simulation results it is possible to replicate the target salinity profile in the Mannville Group aquifer by using topography-driven flow gradient of 0.007.

These simulation results indicate that the requirement for plume emplacement is a high driving forces over a short period of time. The observed plume has the appearance of a slug with strong concentration contrast over a short spatial distance. A hydraulic gradient of 0.007 would emplace the plume after 3 million years.

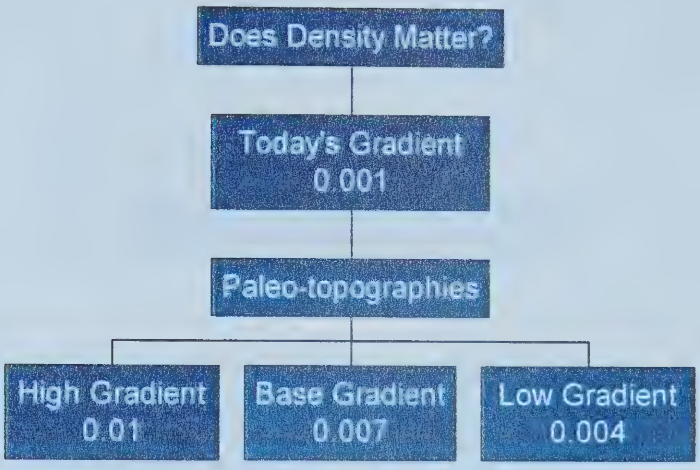

Figure 5.1 – Flow diagram of numerical simulation organization.

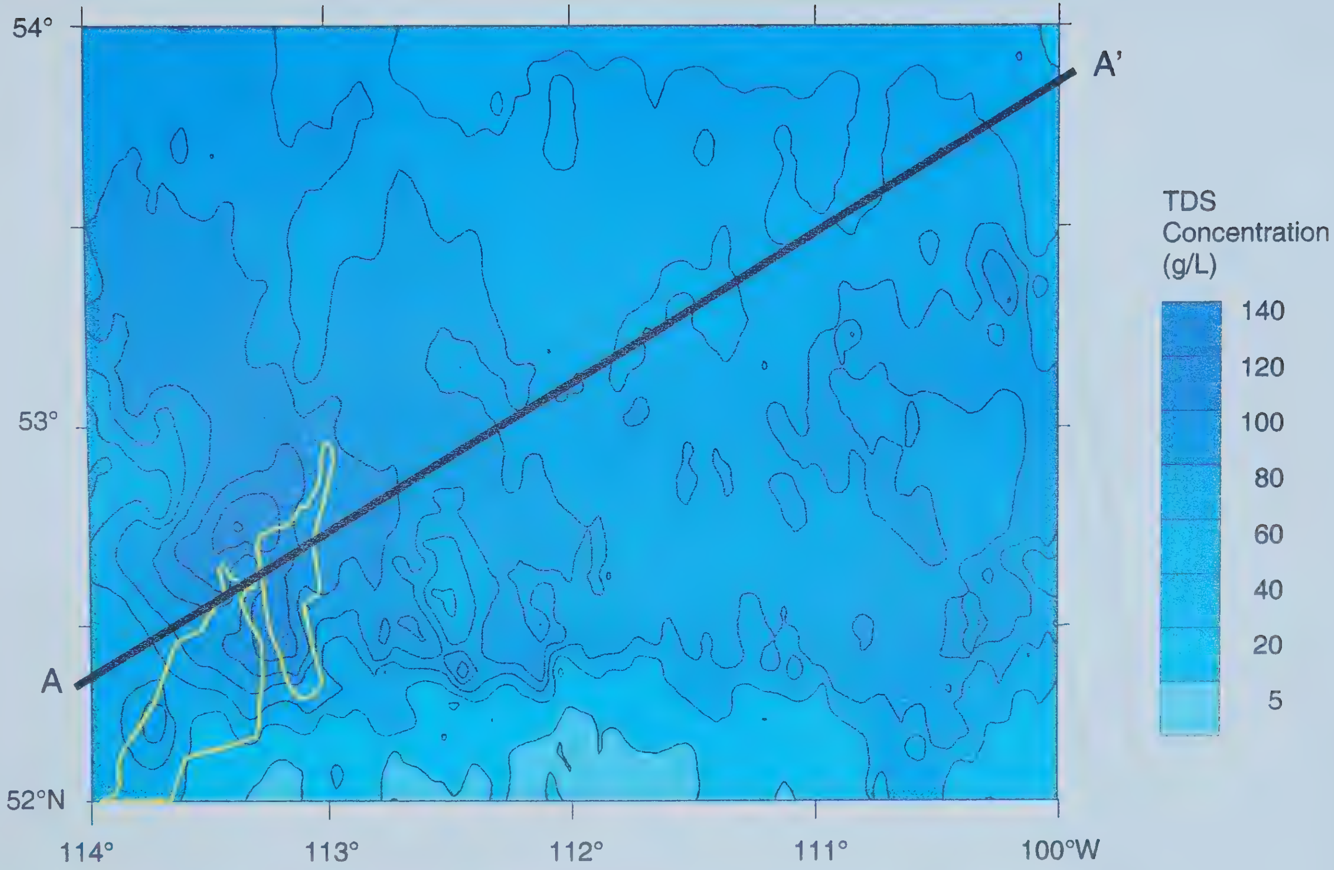

Figure 5.2 – Mapped distribution of total dissolved solids (TDS) in the Mannville Group Aquifer, south-central Alberta. Yellow outline indicates location of the Bashaw reef complex.

Figure 5.3 - Modelled cross section and location of observation point.

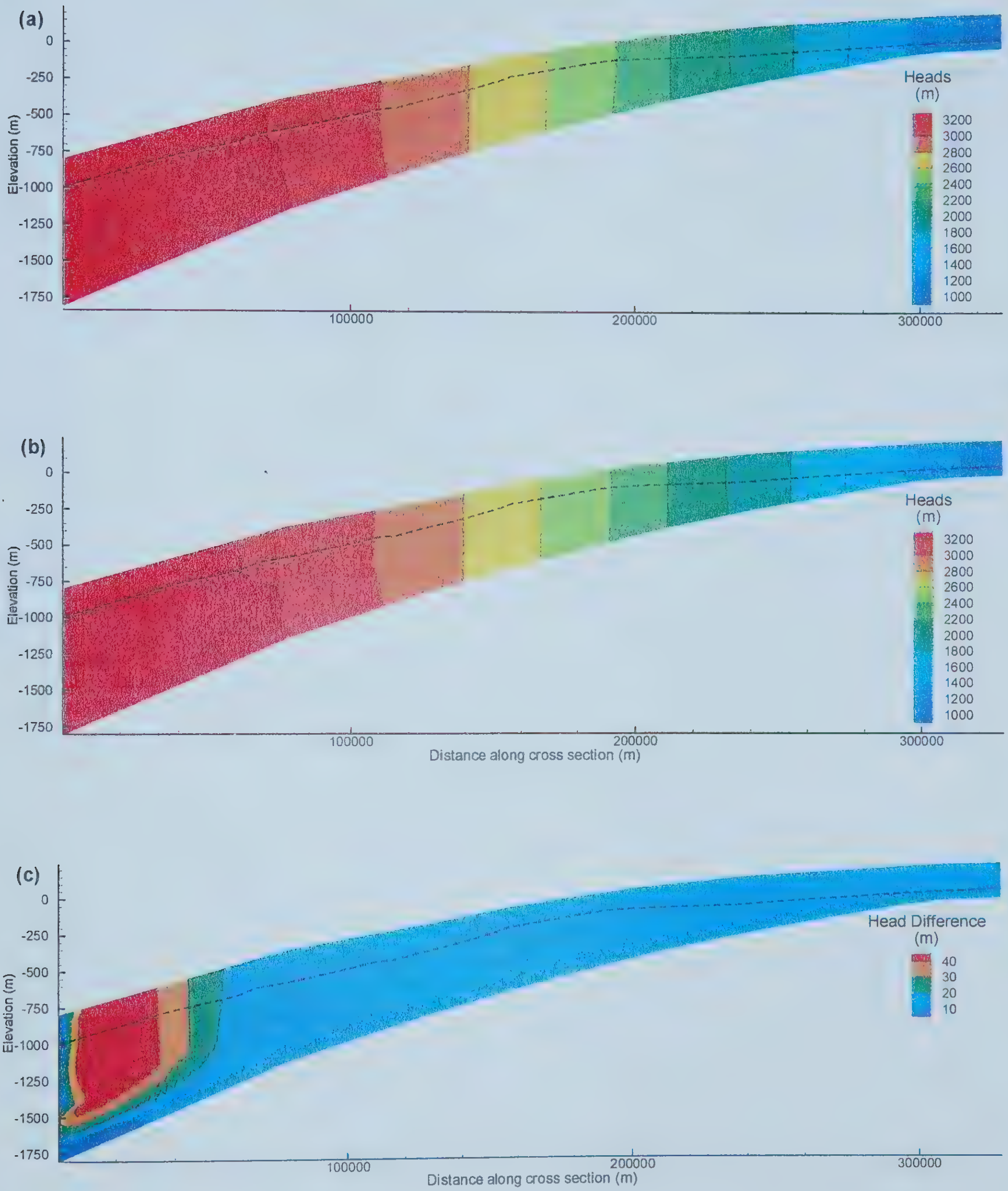

Figure 5.4 - Comparison of hydraulic head distributions after the first time step (500 years) between (a) non-density dependant and (b) density dependant cases. Contour interval of 200 m. (c) shows the difference between the cases with a contour interval of 10 m. Dashed line indicates the base of the MGA.

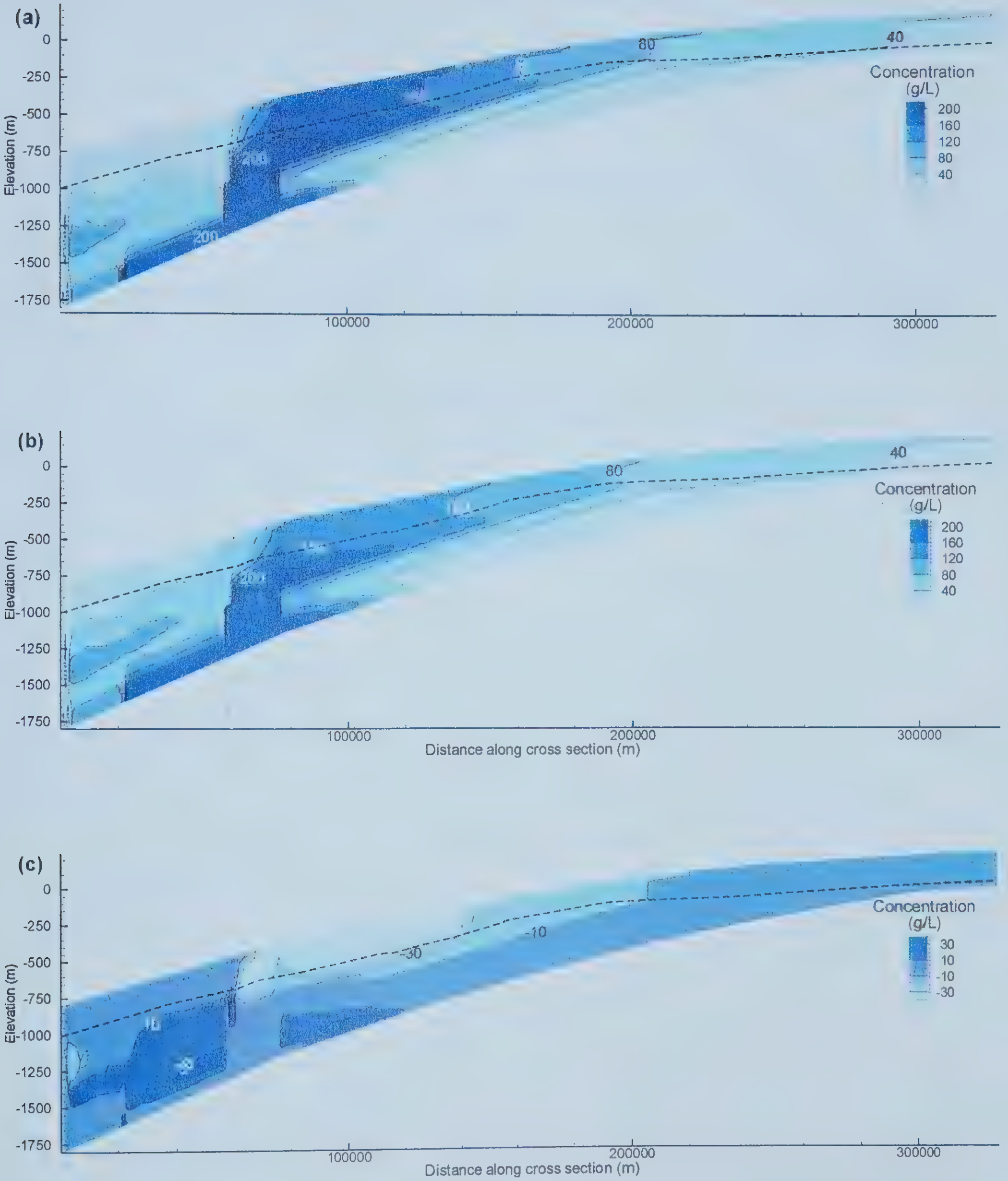

Figure 5.5 - Comparison of brine concentration distribution after 2.5 million years between (a) non-density dependent and (b) density dependent cases. Contour interval of 40 g/L. (c) shows the concentration differences between the cases. Contour interval of 10 g/L. Dashed line indicates base of the MGA.

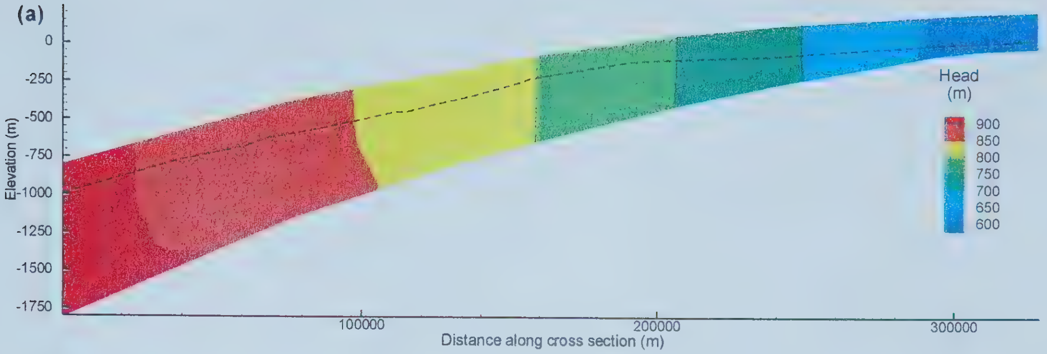

Figure 5.6 - Hydraulic head distribution results based on today's topographic gradient of 0.001. Contour interval of 200 m. Dashed line indicates base of the MGA.

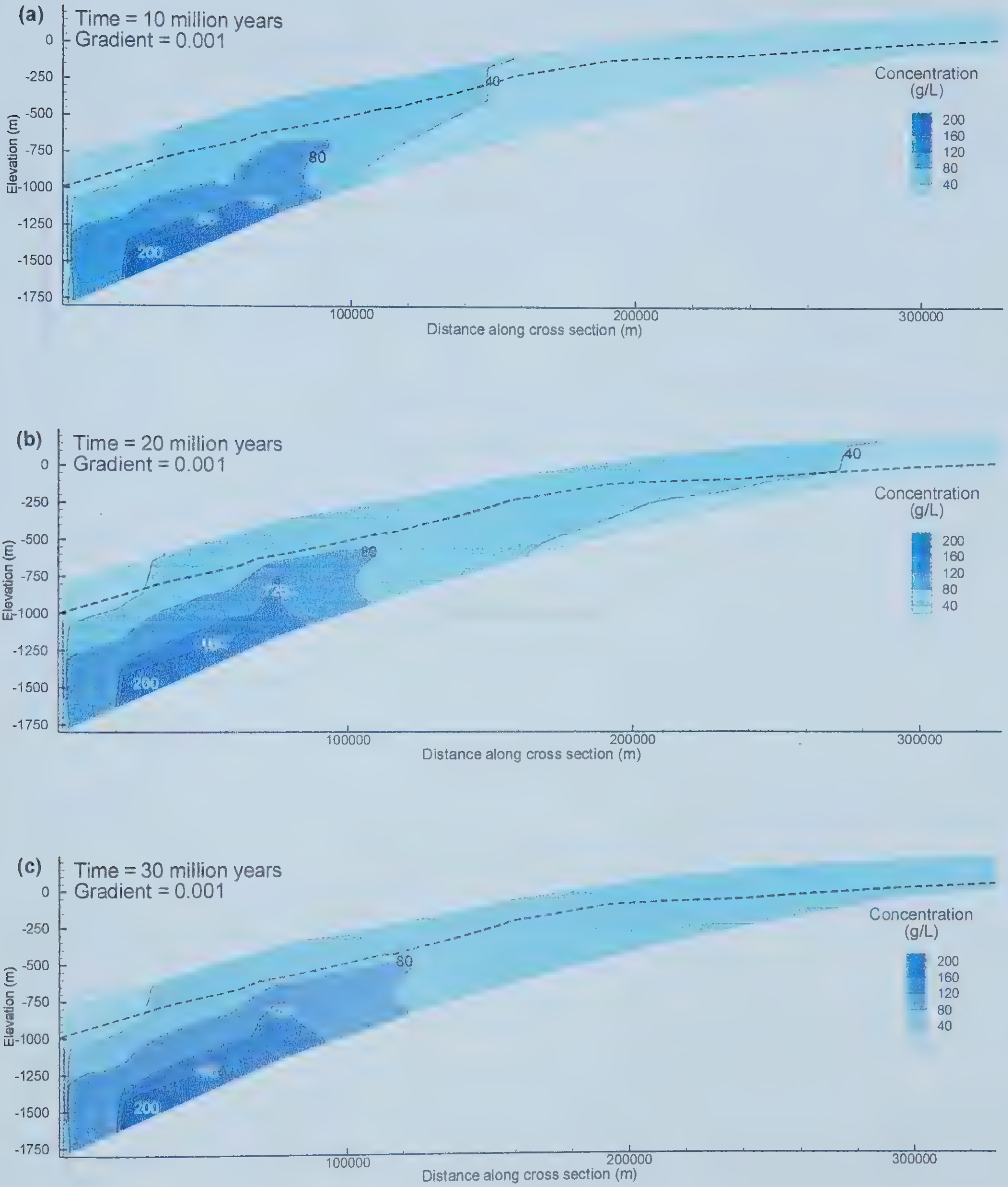

Figure 5.7 - Results of density dependent simulation using today's gradient of 0.001 after (a) 10 million, (b) 20 million, and (c) 30 million years. Contour interval of 40 g/L. Dashed line indicates base of the MGA.

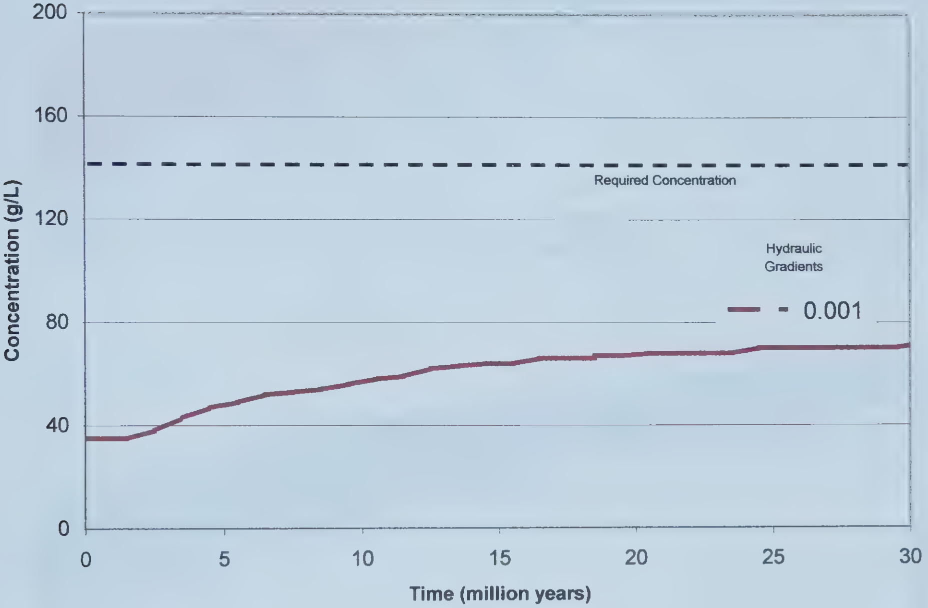

Figure 5.8 –Concentration versus time using today's hydraulic gradient of 0.001 at the observation point in the MGA.

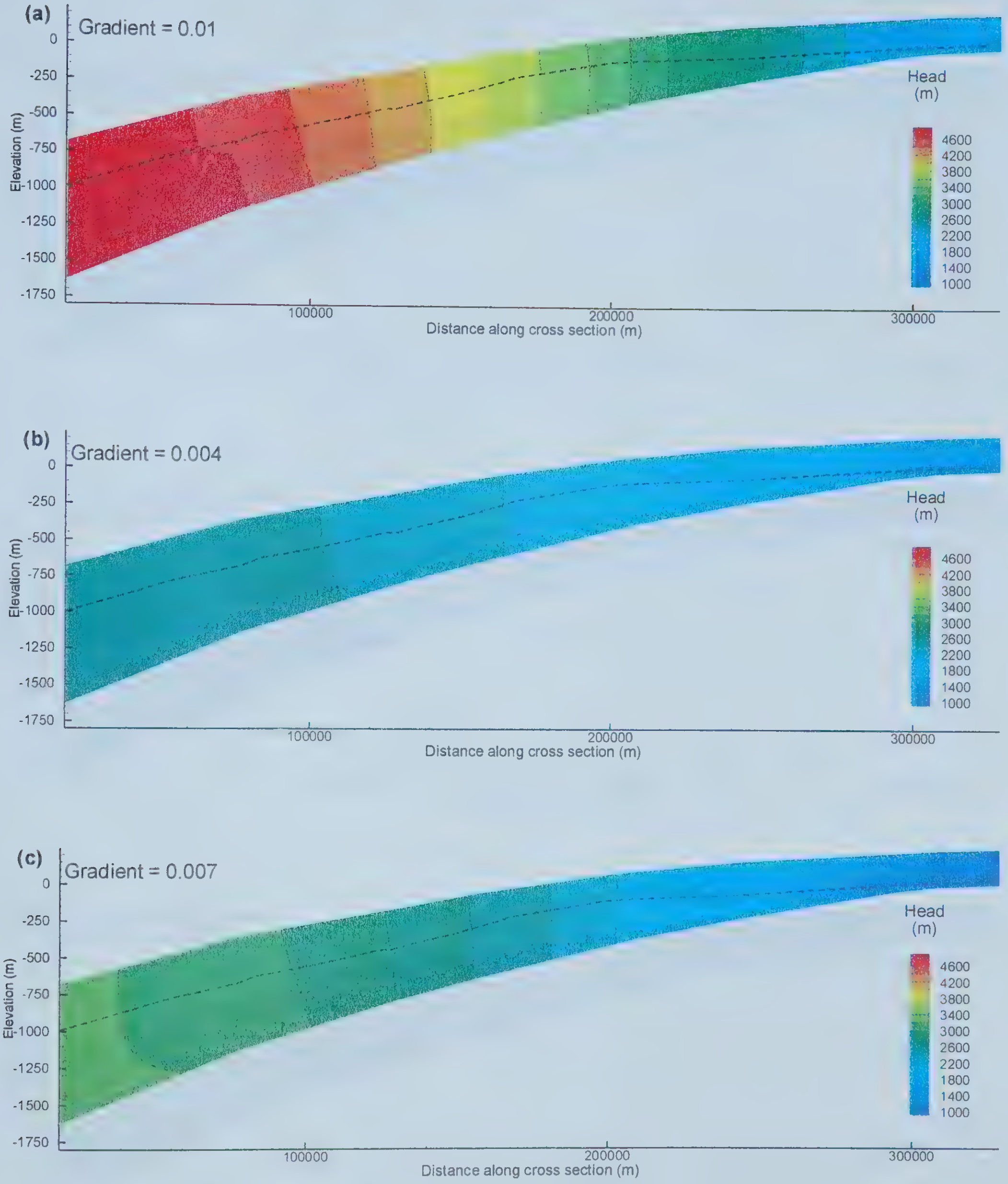

Figure 5.9 - Comparison between hydraulic head distribution based on variations in hydraulic gradients (a) 0.004, (b) 0.01, and (c) 0.007. Contour interval of 200 m. Dashed line indicates base of the MGA.

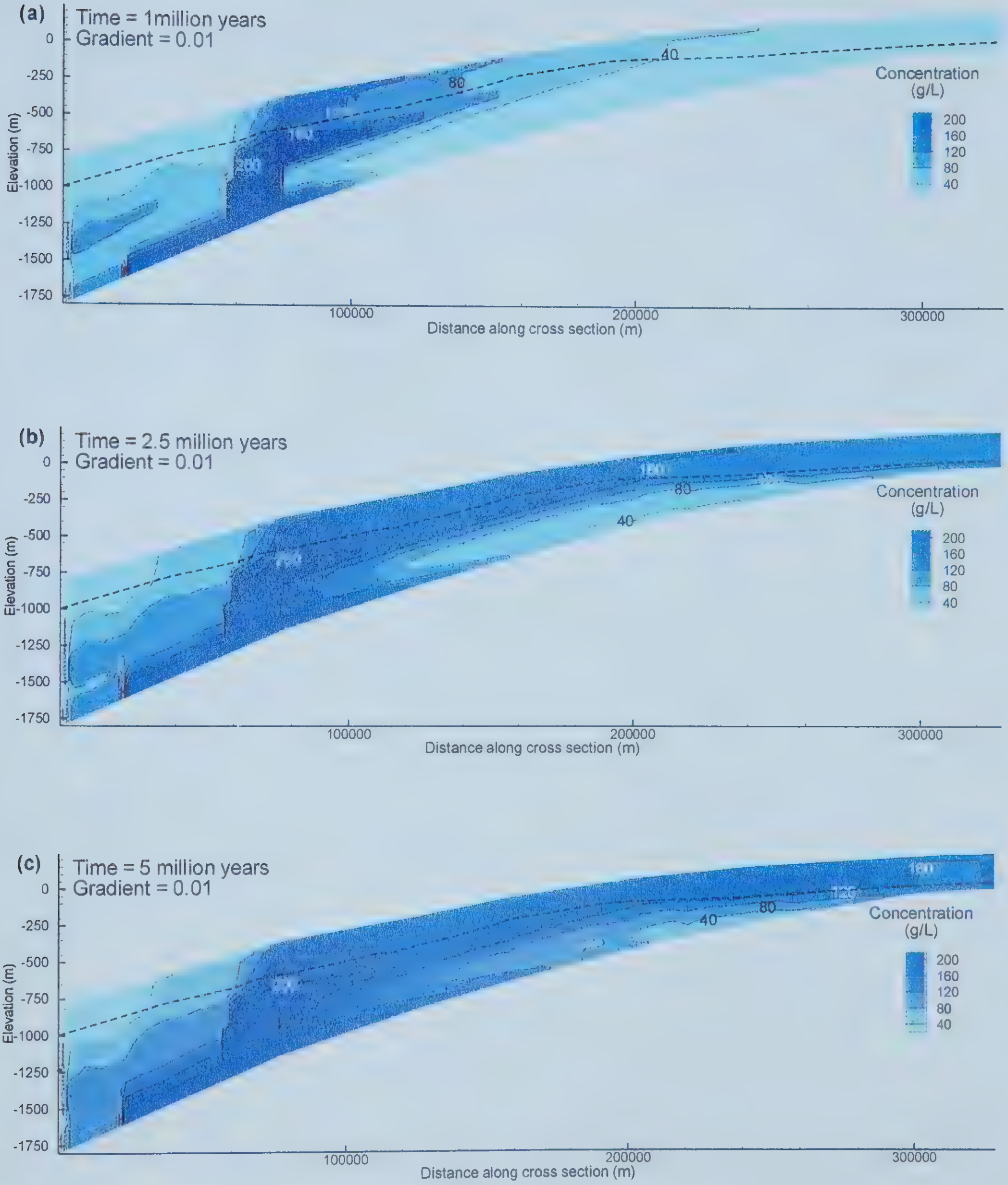

Figure 5.10 -Results of density dependent simulation with a hydraulic gradient of 0.01 after (a) 1 million, (b) 1.5 million, and (c) 2.5 million years. Contour interval of 40 g/L. Dashed line indicates base of the MGA.

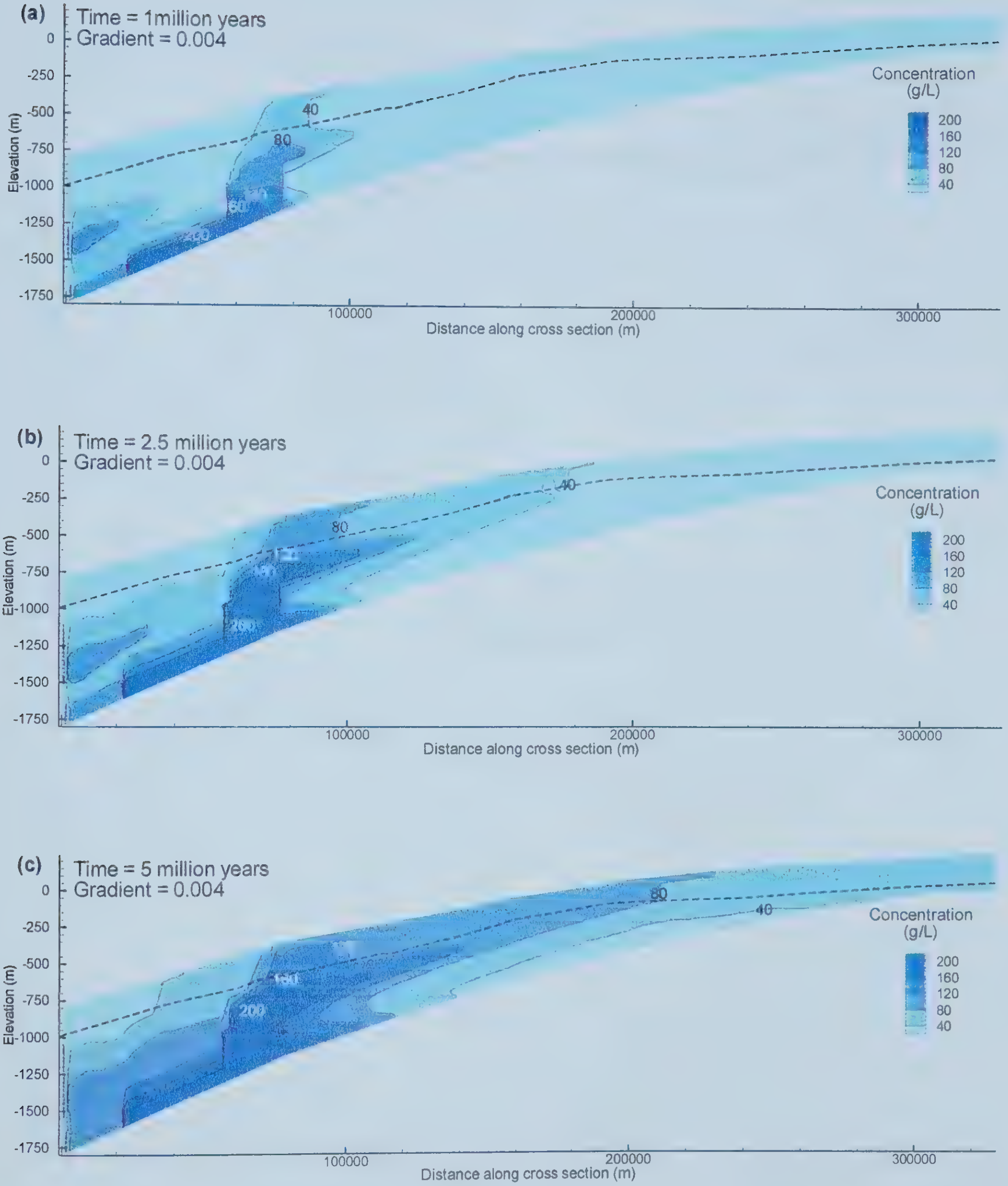

Figure 5.11 -Results of density dependent simulation with a hydraulic gradient of 0.004 after (a) 1 million, (b) 2.5 million, and (c) 5 million years. Contour interval of 40 g/L. Dashed line indicates base of the MGA.

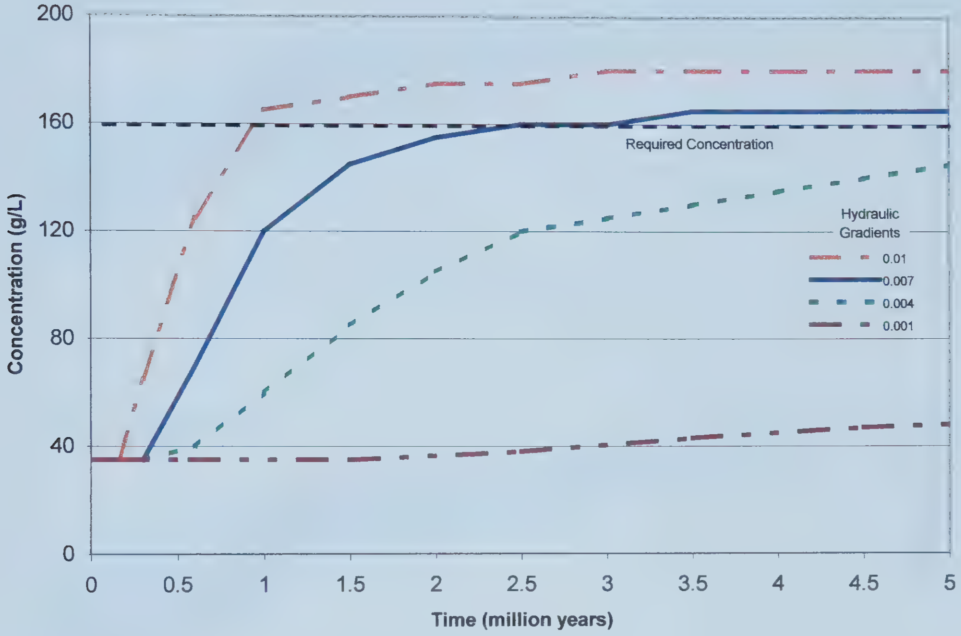

Figure 5.12 – Concentration versus time using paleo-topographic gradients at the observation point in the MGA.

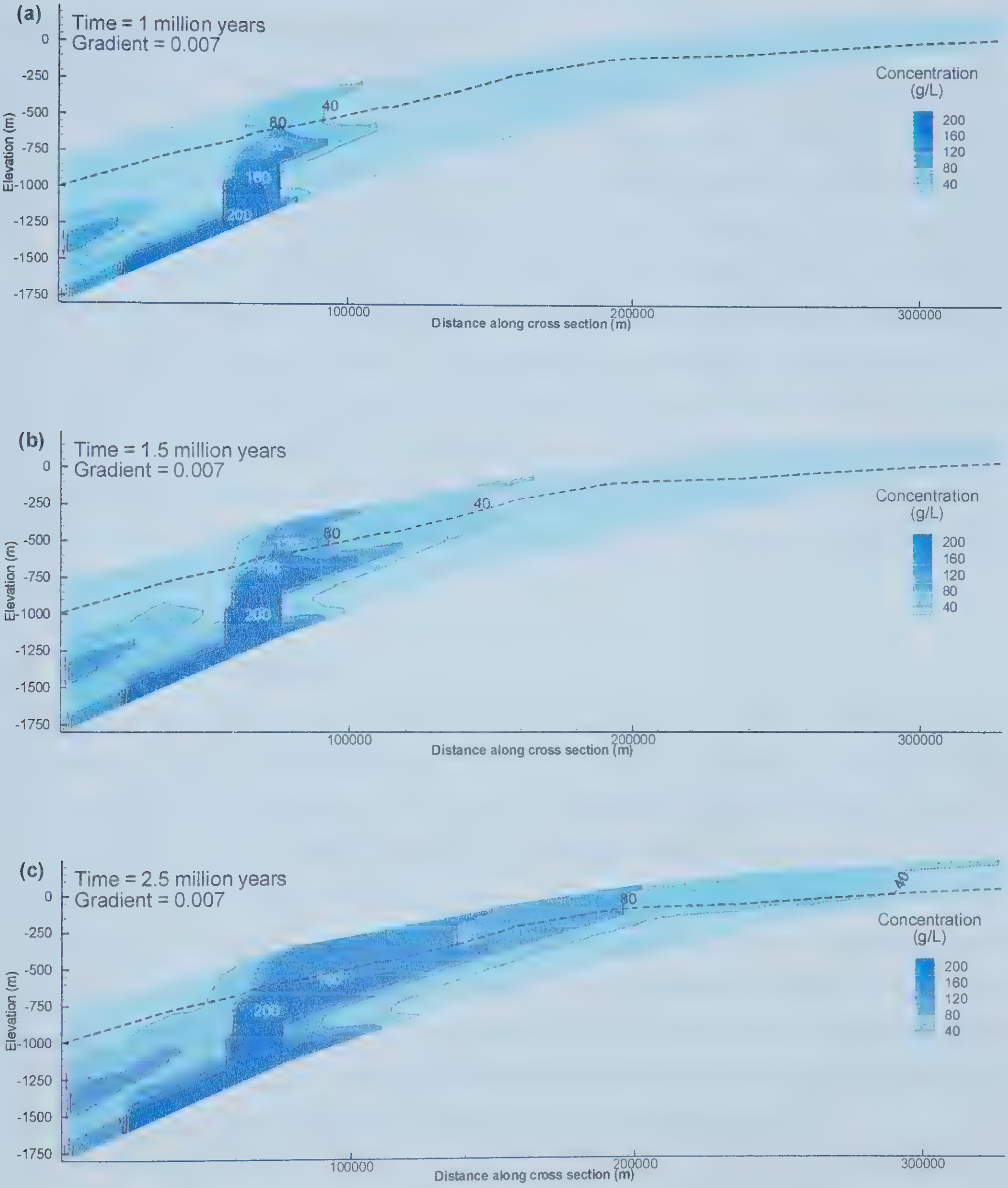

Figure 5.13 - Results of density dependent simulation with a hydraulic gradient of 0.007 after (a) 1 million, (b) 2.5 million, and (c) 5 million years. Contour interval of 40 g/L. Dashed line indicates base of the MGA.

Chapter 6 Sensitivity Analysis

It was determined in Chapter 5 that a paleo-topographic flow system provided the best representation of the observed plume and that the model is highly sensitive to changes in hydraulic gradient. There is a great deal of uncertainty associated with the paleo-hydraulic parameters due to the difficulty in quantifying these values on a regional scale. From previous studies (Nurkowski, 1984; Bustin, 1991), it was possible to estimate ranges of paleo-topographic hydraulic gradients, but for parameters such as permeability the present day values were used. Thus, a sensitivity analysis was used to determine how variations in these parameter values would influence the predicted flow system and salinity distribution. The parameters analyzed were those that are thought to have the greatest influence on the flow system: vertical gradient, permeability, and anisotropy. Table 6.1 lists the simulations that were run in the sensitivity analysis, highlighting the parameters that were varied.

6.1 Vertical Gradient

The results in Chapter 5 were based on a conceptual model in which a vertical gradient was not applied to the model domain. Vertical gradients in the basin could potentially have been created by tectonically induced fluxes originating deep in the basin producing the so-called “squeegee effect” (Machel and Cavell, 1999). It is possible that the expulsions of fluids due to tectonic activity could push fluid vertically, as well as horizontally, and therefore the effects of such a case were examined. Previous studies have shown that today’s measured pressure profile indicates upward vertical flow. Therefore, a 100 metre hydraulic head difference was added to the west boundary of the base case model to create a 0.05 vertical gradient and assist in the upward movement of solute. No change was made to the right hand side boundary condition.

This simulation showed the addition of a vertical gradient on the boundary made a significant change to the distribution of solute in the MGA. After 1 million years of simulated time the 120 g/L TDS solute plume is present in the MGA (Figure 6.1a). After 2.5 million years the >160 g/L TDS solute plume is approximately 70,000 metres long with a maximum concentration of approximately 180 g/L TDS (Figure 6.1b). After 5 million years the >160 g/L TDS plume is approximately 220,000 metres long (Figure 6.1c)

When these results are compared with the results from the base case (Figure 6.2), it is clear that higher concentration solute enters the MGA when a vertical gradient is applied. In the vertical gradient case the maximum concentration at the observation point is slightly less than 200 g/L and in the base case it is only 160 g/L. Also, the solute enters the MGA at a faster rate (e.g., 150 g/L TDS at the observation point after approximately 2 million years with the base case and in 1 million years with a vertical gradient).

A conclusion that may be taken from these results is that the vertical gradient changes the solute concentration in the MGA, as well as the rate in which it is emplaced in the aquifer. The vertical gradient also causes more solute movement across the Ireton and Wabamun aquitards at the western boundary. Vertical gradients in the system are possible, but unlikely because of the distance the study area is away from the deformation front where the fluid expulsion would occur. Deformation from tectonic stresses should occur less than 50 km from deformation front (Ge and Garven, 1994). In addition, the low salinity concentrations currently observed at the west boundary does not support the idea that there was vertical flow across these formations (Figure 5.2). Thus, the numerical model is sensitive to vertical gradient, but these effects are not likely important due to their proximity to the model boundary.

6.2 Permeability

Analyzing the sensitivity of a model to changes in permeability is one of the keys to understanding uncertainty within the model. According to Darcy's Law (Chapter 2), fluid flow is primarily controlled by the hydraulic conductivity and hydraulic gradient. Hydraulic conductivity is related to permeability by taking into account density and viscosity (Chapter 4). The sensitivity of the model to hydraulic gradients was shown previously. Therefore, the importance of permeability, as the other major control to fluid flow must also be addressed.

Determining the paleo-hydraulic parameters is beyond the scope of this thesis and therefore present day parameters were used. Present values are reasonable since maximum burial was achieved simultaneously with the onset of maximum hydraulic gradients. However, this sensitivity analysis considers the possibility that the hydraulic

parameters might have changed due to continuing compaction of the strata which could have decreased the permeability. An increase in permeability might have resulted from 60 million years of erosion.

This sensitivity analysis allows for the examination of the temporal variation of permeability in time. The permeabilities of the primary aquifers and aquitards were varied by one order of magnitude, higher and lower within ranges reported earlier. Important formations were defined as those that would make a significant impact to the flow system, such as the Ireton conduit, the Wabamun aquitard and the MGA. Initially, this section of the sensitivity analysis looks at the effects of the three individual formations. Then the effect of lowering the permeability of the aquitards in the system was examined.

6.2.1 Ireton Conduit

A sensitivity analysis was performed on the permeability of the Ireton conduit. This conduit allows solute to flow easily from the Leduc aquifer 'reef' structure into the Nisku aquifer (Figure 5.12). The conduit is hypothesized to exist based on the fractured nature and absences of the seal capping the Leduc reef (Hearn, 1996; Rostron and Tóth, 1997). Uncertainty arises due to the fact that it is only possible to speculate on when the fractures above the reef developed. It is possible that the fractures may not have existed to the same extent as they do presently. Therefore, the values of the permeability sensitivity analysis were varied between $1\text{x}10^{-18}$ m^2 (Ireton aquitard) to $1\text{x}10^{-16}$ m^2 (Nisku aquifer).

Varying the permeability of the Ireton conduit did not have a significant effect on the results (after 2.5 million years) (Figure 6.3). There is not a significant difference found between the Ireton conduit permeability base case ($1\text{x}10^{-14}$ m^2) and the lower Nisku permeability ($1\text{x}10^{-16}$ m^2) case. In both cases, after 2.5 million years the 160 g/L TDS solute is observed in the MGA (Figure 6.2a, b). A minor effect is encountered when the conduit permeability is lowered to that of the tight Ireton aquitard shale ($1\text{x}10^{-18}$ m^2) (Figure 6.2c). In this case the 160 g/L TDS solute does not reach the MGA. On the periphery of the models, there are no differences between the cases, but a small distinction is present in the MGA above the Leduc aquifer. After 2.5 million years the

160 g/L TDS solute has not travelled as far into the MGA using the lowest permeability ($1\text{x}10^{-18}$ m^2) for the conduit.

Overall, the model sensitivity to the uncertainty in the permeability of the Ireton conduit is insignificant (Figure 6.4). There is a slight decrease in the maximum concentration at the MGA observation point. The maximum concentration at 5 million years in the base case is 160 g/L and is approximately 155 g/L in the sensitivity cases. This unit appears to have an insufficient thickness to effect the flow system at the large spatial- and time-scales of these simulations. Therefore, the values used for the base case were determined to be sufficient to represent a wide range of potential permeabilities. Variation between the real permeability and the values used would not have a serious effect on the results of the model. Therefore, the value of permeability of the Ireton conduit used in the base case ($1\text{x}10^{-14}$ m^2) is acceptable.

6.2.2 Wabamun Aquitard

The Wabamun aquitard has a significant impact on the cross-formational flow though this system (e.g., Figure 5.12). The thick aquitard, which subcrops at the MGA, controls the rate and volume of solute moving into the MGA and thus the creation of the plume. Since there are no permeability measurements available from the aquitard, the permeabilities of the aquitard were varied approximately by one order of magnitude, above and below the base case permeability of $5\text{x}10^{-17}$ m^2 to address the uncertainty of this parameter.

The Wabamun aquitard permeability has a significant effect on the direction of solute movement in the model. Results from the base case, using a permeability of $5\text{x}10^{-17}$ m^2, after 2.5 million years, show a small amount of 160 g/L TDS water in the MGA (Figure 6.5a). When the model was run with a higher Wabamun aquitard permeability ($1\text{x}10^{-16}$ m^2) a 40,000 metre long plume of >160 g/L TDS water was observed in the MGA after 2.5 million years (Figure 6.5b). In the higher permeability case the high TDS water enters the MGA at the Wabamun subcrop. This flow path is the same as predicted in the base case. In comparison, the sensitivity model using a lower permeability of $1\text{x}10^{-18}$ m^2 results in a 140,000 metres long plume of >80 g/L TDS in the MGA after 2.5 million years (Figure 6.5c). In this case the solute moves into the MGA at the Nisku subcrop

and along the Wabamun subcrop where the Wabamun aquitard is thinnest, but not vertically above the Leduc reef.

A comparison of the effects of varying the Wabamun permeability on concentration over time at the observation point is shown in Figure 6.6. In the lower permeability case the concentration rises slowly over time to a maximum of 100 g/L TDS. The high permeability case follows the same flow path as the base case, but the concentrations at the observation point increase faster and the maximum concentration is higher (170 g/L).

Overall, variations in the permeability of the Wabamun aquitard appears to significantly affect the direction of solute movement in the system. In the base case, the solute moved both up-dip along the Nisku aquifer and through the Wabamun aquitard. With a higher permeability in the Wabamun aquitard solute preferentially flows vertically across the Wabamun aquitard into the MGA allowing more high concentration solute into the MGA. When the Wabamun aquitard permeability is lowered, the solute is forced updip along the Nisku aquifer causing the plume to be emplaced further updip in the MGA. Neither of these cases are supported by the map of TDS concentration in the MGA (Figure 5.2). The results indicate that the value used in the base case for permeability was appropriate to emplace the plume within the MGA.

6.2.3 Mannville Group Aquifer

Since the plume is presently located in the MGA, the hydraulic properties of the MGA will have the greatest effect on the plume's creation. The permeability of the MGA was varied by one order of magnitude to determine the amount of uncertainty associated with the value used in the base case. The base case permeability in the MGA is 4.0×10^{-15} m^2 therefore, the sensitivity studies run were a high permeability case using values of 4.0×10^{-14} m^2 and a low permeability case using values of 4.0×10^{-16} m^2.

After 2.5 million years, results from the base case show a small amount of 160 g/L TDS in the MGA (Figure 6.7a). When a higher permeability is used for the MGA results show a large plume of moderate concentration, > 80 g/L TDS in the MGA. This plume extends from above the reef to the east edge of the model (Figure 6.7b). The low permeability case was significantly different, with concentrations as high as 200 g/L TDS observed in the MGA after 2.5 million years (Figure 6.7c).

A comparison of the effects of varying the permeability of the MGA on concentrations over time at the observation point is shown in Figure 6.8. The sensitivity analysis shows that high permeabilities in the MGA (4.0×10^{-16} m^2) result in lower concentration of solute in the MGA than observed today. In contrast, the low permeability case predicts a quick rise to very high concentration of solute in the MGA. This can be explained by the fact that the low permeability in the aquifer creates a stagnant condition, preventing the dilution of the high concentration solute.

The rate of formation fluid travelling through the MGA acts to control the distribution of solute in the aquifer. Low concentration fluids moving slowly through the aquifer allows for the accumulation of high salinity water at the subcrop, resulting in the creation of a solute plume in the aquifer. Conversely, low concentration fluid travelling quickly through the aquifer would dilute and flush away the invading high concentration solute and redistribute it through the aquifer.

The results of the sensitivity analysis show that the base case permeability for the MGA (4×10^{-15} m^2) creates a distribution of solute that is the closest representation of the plume in the MGA. The base case permeability allows the high TDS solute to enter the MGA at a rate which allows the plume to form, but not flood, the aquifer with high TDS solute.

6.2.4 Aquitard Permeabilities

Aquitard permeabilities play an important role in constraining fluid flux and flow direction. Other studies of regional flow in the Alberta basin were considered when determining the best hydraulic parameters (Bachu and Underschultz, 1984; Bachu *et al.*, 1989; Hitchon et al, 1989a; Hitchon et al, 1989b; Hugo, 1990). For the most part the parameters are on the same order of magnitude as the ones used in the base case. The exceptions are the values used for the aquitards (Ireton and Joli Fou) which can be found in previous studies to be one to two orders of magnitude lower than those used in the base case (Hitchon et al, 1989a; b; Bekele, 1999). The base case permeability for these formations were chosen conservatively due to a concern that using lower permeabilities would lead to instability in the model. Therefore, the higher values were used for the base case. It

was determined that the low values of permeability in the aquitards should be considered as part of the sensitivity analysis (Table 6.2).

Lowering the permeabilities in the aquitards result in a much different distribution of solute in the MGA, compared to what is currently observed and what was modelled in the base case. The low permeability case shows that after 5 million years, the highest concentration observed in the MGA should be >80 g/L TDS (Figure 6.9 c). This solute entered the MGA from the Nisku aquifer subcrop and across the thinnest portion of the Wabamun subcrop. The solute does not move across the Wabamun aquitard above the reefs, as observed in the base case. In general, the lowering of the permeabilities of the aquitard did not create model instability but it is clear that a better solution was obtained using the base case permeabilities.

The permeabilities of the Ireton and Joli Fou aquitards have little effect on the distribution of the solute in the MGA; it is the permeability of the Wabamun aquitard that leads to the greatest uncertainty in model results. A comparison of the effects of the aquitards permeability on concentration over time at the observation point is shown in Figure 6.10. This figure shows that a lower aquitard permeability prevents the accumulation of the plume at the present location. The concentration slowly rises but barely exceeds 50 g/L TDS.

The low permeability sensitivity case showed the most significant effects. Lowering the aquitard permeabilities caused a large decrease in the maximum concentration at the Wabamun subcrop. It also changed the location of the maximum concentrations found in the MGA at the observation point to above the Nisku aquifer subcrop. The majority of the changes are due to decrease in the Wabamun aquitard. There are no previous studies to support that the permeability value used in the Wabamun aquitard in this sensitivity case and this is supported by the modeling results. Therefore, the aquitard values used in the base case are determined to be valid.

6.3 Anisotropy

For a formation to be isotropic the hydraulic conductivity must be independent of the direction of measurement. It is much more common that the hydraulic conductivity, or permeability, varies with the direction of measurement, or in other words, anisotropic.

Clay minerals within sedimentary rocks have the tendency to orient themselves horizontally, causing high hydraulic conductivity to occur along them. Anisotropy tends to be less pronounced within clastic formations but it is still observed (Fetter, 1994). Anisotropy also accounts for heterogeneties in the layers that couldn't be modelled (i.e. small scale heterogeneities show up as layers.)

The base case uses a moderate anisotropy of 10:1 (kx:kz) throughout the cross-section; the horizontal permeability is one order of magnitude greater than the vertical. Sensitivity cases were run to determine the effects of anisotropy on the model: case (1) isotropic 1:1 and case (2) a highly anisotropic 100:1. Also, a case (3) where the anisotropy varies between the different lithologies was run (Table 6.3). These anisotropy ratios were taken from a modelling study in the Alberta basin (Beleke, 1999).

A comparison between the base case and the isotropic case after 2.5 million years shows little significant differences (Figure 6.11). Both cases have a plume of >160 g/L TDS entering the MGA but the plume in the isotropic case is a slightly larger plume (Figure 6.11a, b). Also, in the isotropic case, there is increased vertical migration of fluid through the Ireton aquitard into the Nisku aquifer. In the case with high anisotropy, 100:1, the highest solute concentration in the MGA is >120 g/L TDS and it appears that the solute flow occurs preferentially horizontally through the system (Figure 6.11 c).

A comparison of the effects of the aquitard permeability on the concentration of the solute over time at the observation point is shown in Figure 6.12. The 1:1 case has a maximum concentration of approximately 195 g/L TDS after 5 million years. In comparison, the 100:1 case has a maximum concentration of approximately 150 g/L TDS.

A comparison between the base case and the varied anisotropy case did not produce a significant effect (Figure 6.13). After 2.5 million years, the solute distribution in the MGA is almost identical, with only minor variations. In the varied anisotropy case, the solute has travelled slightly farther in the MGA when compared to the distance travelled in the base case (Figure 6.13 b).

A comparison of the effects of the aquitard permeability on concentration over time at the observation point is shown in Figure 6.14. This figure illustrates that the varied anisotropy case produces a slightly higher concentration throughout the simulation.

Overall, the anisotropy used in the simulation controlled the salinity distribution in the MGA. The isotropic case allows for slightly more vertical solute movement due to higher permeabilities in the vertical orientation, resulting in higher concentrations into the MGA. In the 100:1 anisotropy case, the solute is horizontally funneled due to the low permeabilities in the vertical direction. The varied anisotropy case did not result in flow patterns varying significantly from the base case. The base case, 10:1 anisotropy, produced the most representative solute concentration in the MGA (Figure 6.12 and Figure 6.14).

6.4 Discussion and Summary

The results of the sensitivity analysis show that the parameters used in the base case model created the best representation of the plume.

The addition of an upward vertical hydraulic gradient along the west boundary increases the rate at which the solute is emplaced in the MGA, as well as the maximum concentration at the observation point. The result of the simulation supports the theory that the chance of this happening is remote, therefore vertical gradient did not need to be taken into account for the best case.

The sensitivity analysis showed that the distribution of solute in the MGA is effected by the permeabilities of a few key formations. The model was found not to be sensitive to the Ireton aquitard permeability, therefore the values used in the base case are acceptable. The results from varying the permeability of the MGA and Wabamun aquitard show that the values used in the base case create the most representative plume.

The effects of anisotropy sensitivity analysis were also significant. A high anisotropy caused funnelling of high salinity brine along the horizontal formations, which is not shown by the plume distribution in the MGA. Lower anisotropy caused a greater amount of vertical flow through the model domain, but the model was not very sensitive to this

effect. The varied anisotropy case was the least sensitive, creating a solute distribution very similar to the one seen today but with a slightly higher TDS concentration after 5 million years. The results from this portion of the sensitivity analysis also support the base case as being the most representative or best case.

Sensitivity Cases	Density	Vertical	Conduit	Wabuman	MGA	Ireton	Joli Fou	Anisotropy
		Gradient	Permeability	Permeability	Permeability	Permeability	Permeability	k_x/k_z
Base Case	Yes	None	$1x10^{-14}$	$5x10^{-17}$	$4x10^{-15}$	$1x10^{-18}$	$2x10^{-17}$	10:1
No Density Effects	**No**	None	$1x10^{-14}$	$5x10^{-17}$	$4x10^{-15}$	$1x10^{-18}$	$2x10^{-17}$	10:1
Gradient								
Vertical	Yes	**0.05**	$1x10^{-14}$	$5x10^{-17}$	$4x10^{-15}$	$1x10^{-18}$	$2x10^{-17}$	10:1
Permeability								
Low Ireton Conduit	Yes	None	$1x10^{-16}$	$5x10^{-17}$	$4x10^{-15}$	$1x10^{-18}$	$2x10^{-17}$	10:1
Lower Ireton Conduit	Yes	None	$1x10^{-18}$	$5x10^{-17}$	$4x10^{-15}$	$1x10^{-18}$	$2x10^{-17}$	10:1
High Wabamun	Yes	None	$1x10^{-14}$	$1x10^{-16}$	$4x10-^{15}$	$1x10^{-18}$	$2x10^{-17}$	10:1
Low Wabamun	Yes	None	$1x10^{-14}$	$1x10^{-18}$	$4x10^{-15}$	$1x10^{-18}$	$2x10^{-17}$	10:1
High Mannville	Yes	None	$1x10^{-14}$	$1x10^{-17}$	$4x10^{-16}$	$1x10^{-18}$	$2x10^{-17}$	10:1
Low Mannville	Yes	None	$1x10^{-14}$	$1x10^{-17}$	$4x10-^{14}$	$1x10^{-18}$	$2x10^{-17}$	10:1
Low Aquitard	Yes	None	$1x10^{-14}$	$1x10^{-19}$	$4x10^{-15}$	$1x10^{-20}$	$2x10^{-19}$	10:1
Anisoptropy								
1:1	Yes	None	$1x10^{-14}$	$5x10^{-17}$	$4x10^{-15}$	$1x10^{-18}$	$2x10^{-17}$	**1:1**
100:1	Yes	None	$1x10^{-14}$	$5x10^{-17}$	$4x10^{-15}$	$1x10^{-18}$	$2x10^{-17}$	**100:1**
Varied	Yes	None	$1x10^{-14}$	$5x10^{-17}$	$4x10^{-15}$	$1x10^{-18}$	$2x10^{-17}$	**varies**

Table 6.1 – Simulations run in the sensitivity analysis. The grey boxes indicate the varied parameter.

Aquitards	Horizontal Permeability (m^2)	Vertical Permeability (m^2)
Ireton	$1.0\text{x}10^{-20}$	$1.0\text{x}10^{-20}$
Wabamun	$1.0\text{x}10^{-19}$	$1.0\text{x}10^{-20}$
Joli Fou	$2.0\text{x}10^{-19}$	$2.0\text{x}10^{-20}$

Table 6.2 – Aquitard permeability for the low permeability sensitivity analysis

Lithology	Varied Anisotropy	Base Case Anisotropy
Sandstone	2.5:1	10:1
Shale	10:1	10:1
Carbonate	6:1	10:1

Table 6.3 – Varied Anisotropies from Beleke (1999). The MGA, and Viking aquifers equate to sandstone lithology. Joli Fou and Ireton aquitards equate to Shale lithology. Cooking Lake, Nisku Formation, Wabamun, and Banff formations equate to carbonate lithology.

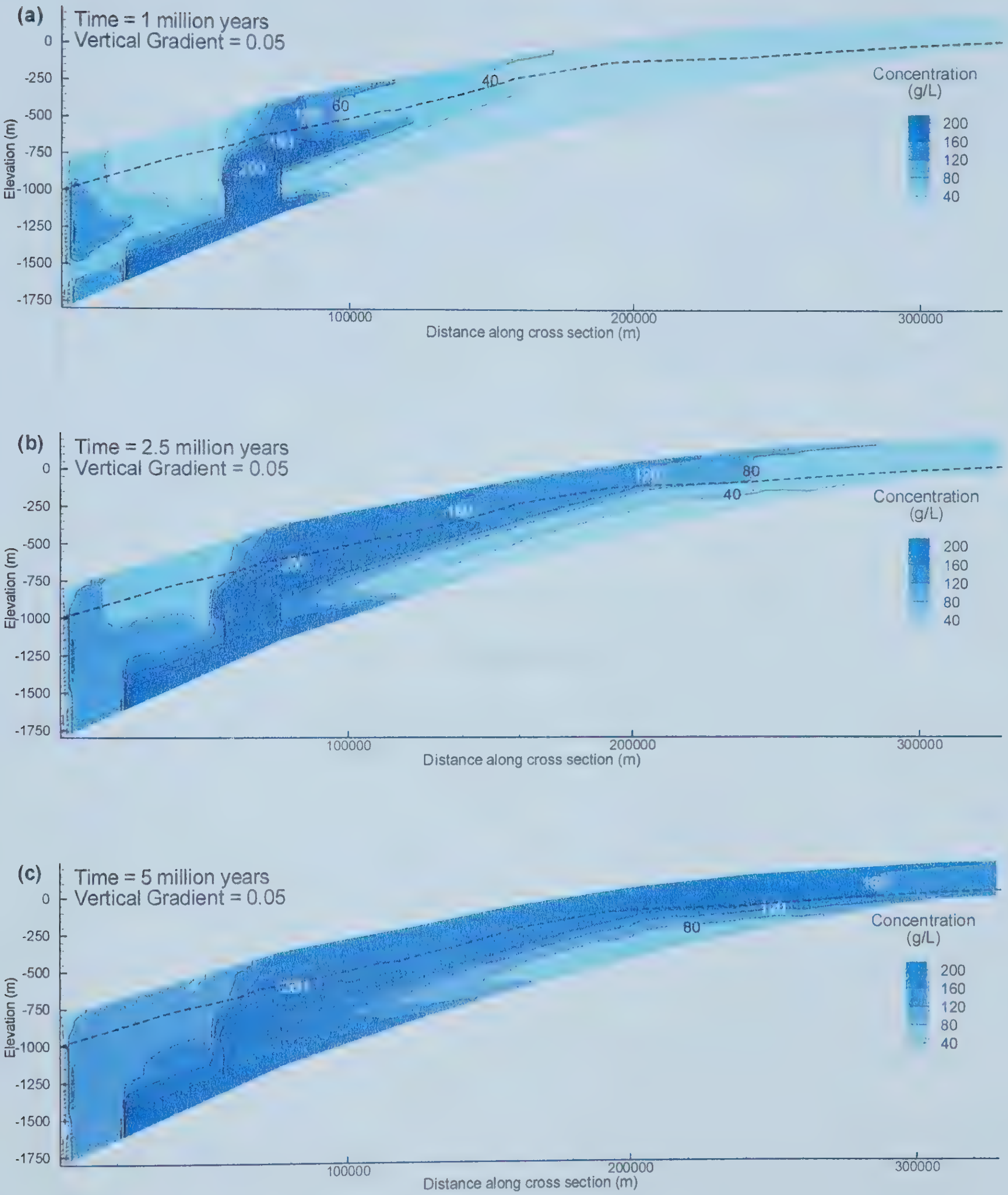

Figure 6.1 - Results of sensitivity analysis to determine the effects of a vertical gradient of 0.05 forcing water up the west boundary after (a) 1 million, (b) 2.5 million, and (c) 5 million years. Contour interval of 40 g/L. Dashed line indicates base of the MGA.

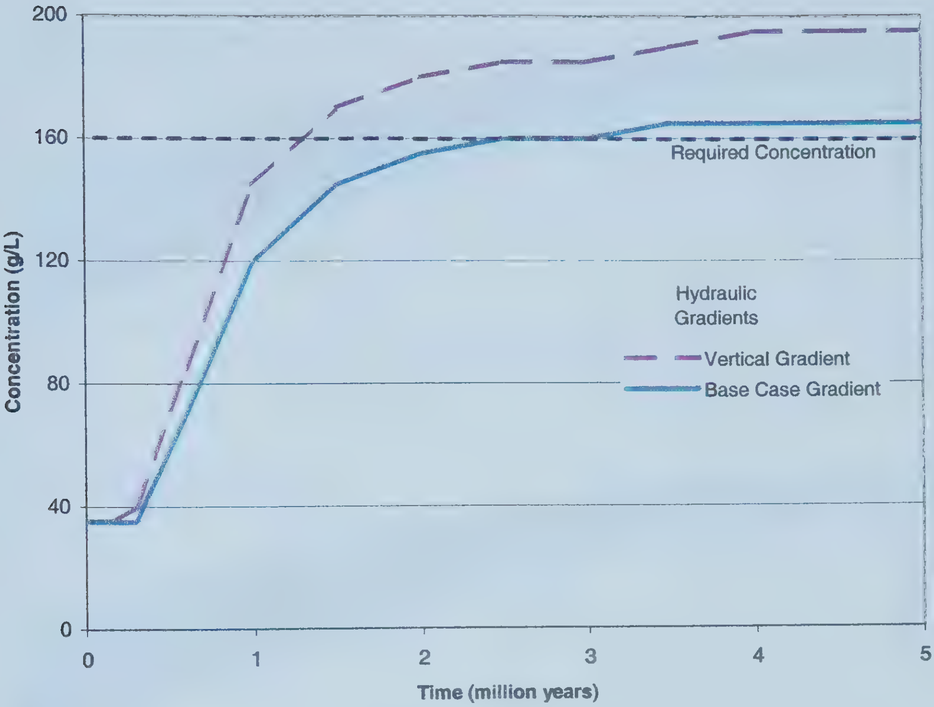

Figure 6.2 – Comparing the effect of vertical gradient on the concentration over time at an observation point in the MGA.

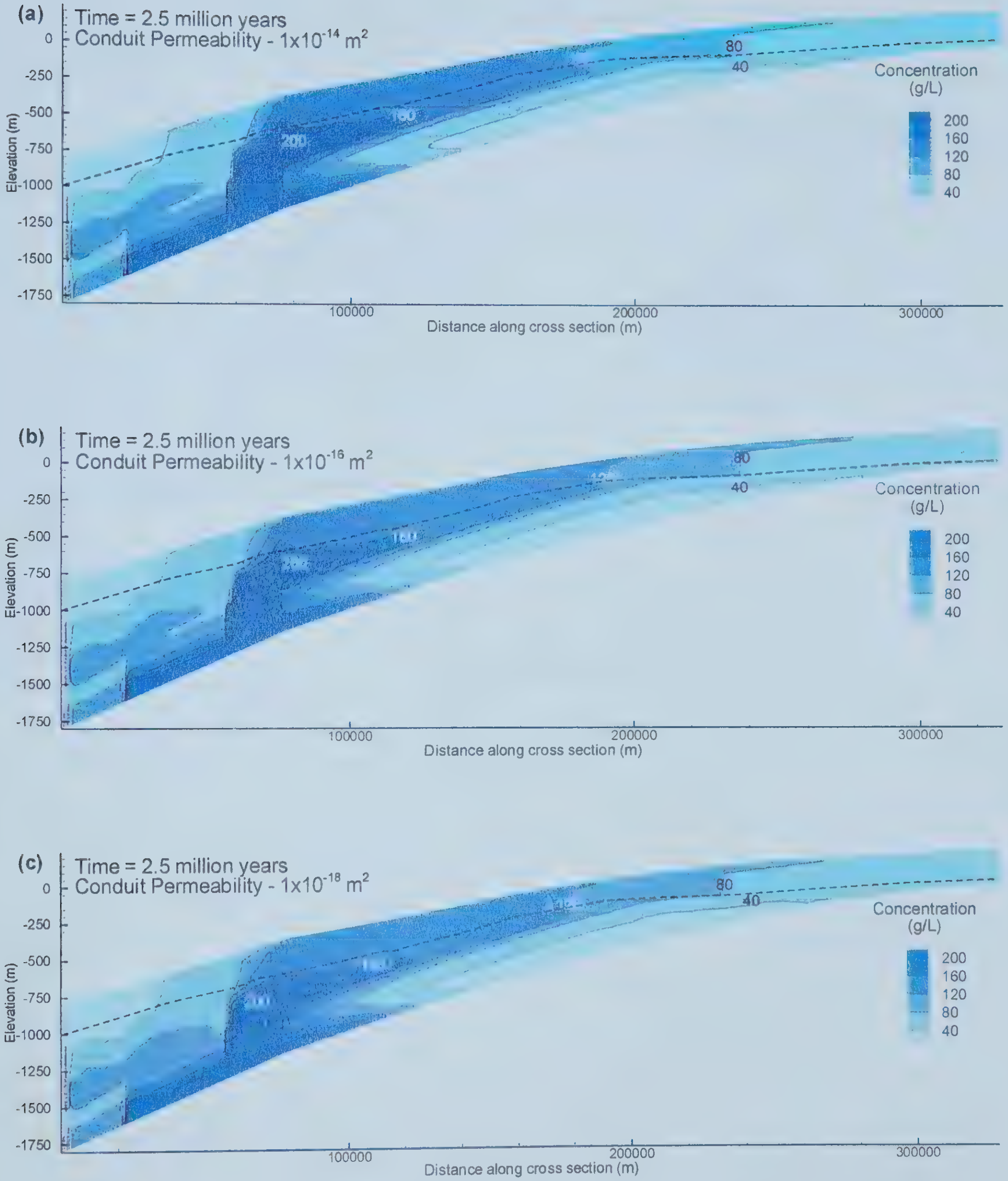

Figure 6.3 - Results of the sensitivity analysis to determine the effects of the Ireton aquitard conduit permeability (a) 1x10^{-14}, (b) 1x10^{-16}, and (c) 1x10^{-18} m^2. Contour interval of 40 g/L. Dashed line indicates base of the MGA.

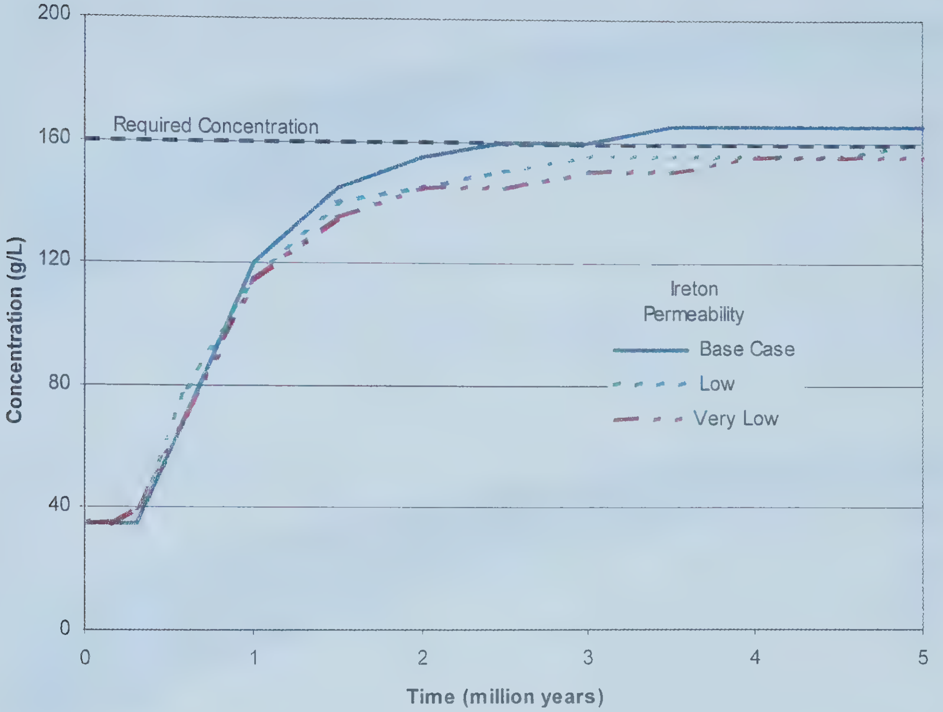

Figure 6.4 – Comparing the effect of the Ireton conduit permeability on the concentration over time at an observation point in the MGA.

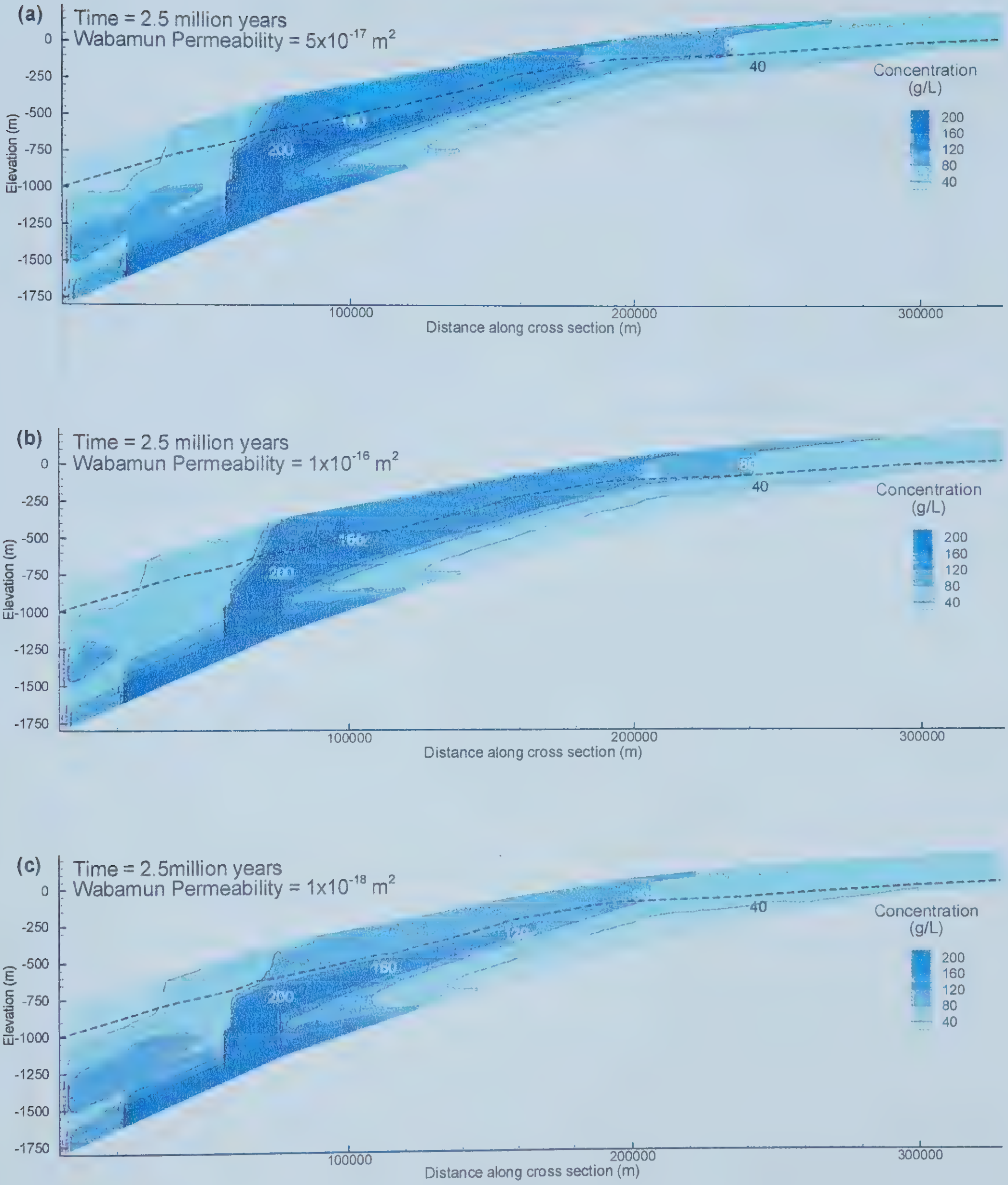

Figure 6.5 - Results of the sensitivity analysis to determine the effects of the Wabamun aquitard permeability (a) 1x10^{-17}, (b) 1x10^{-16}, and (c) 1x10^{-18} m^2. Contour interval of 40 g/L. Dashed line indicates base of the MGA.

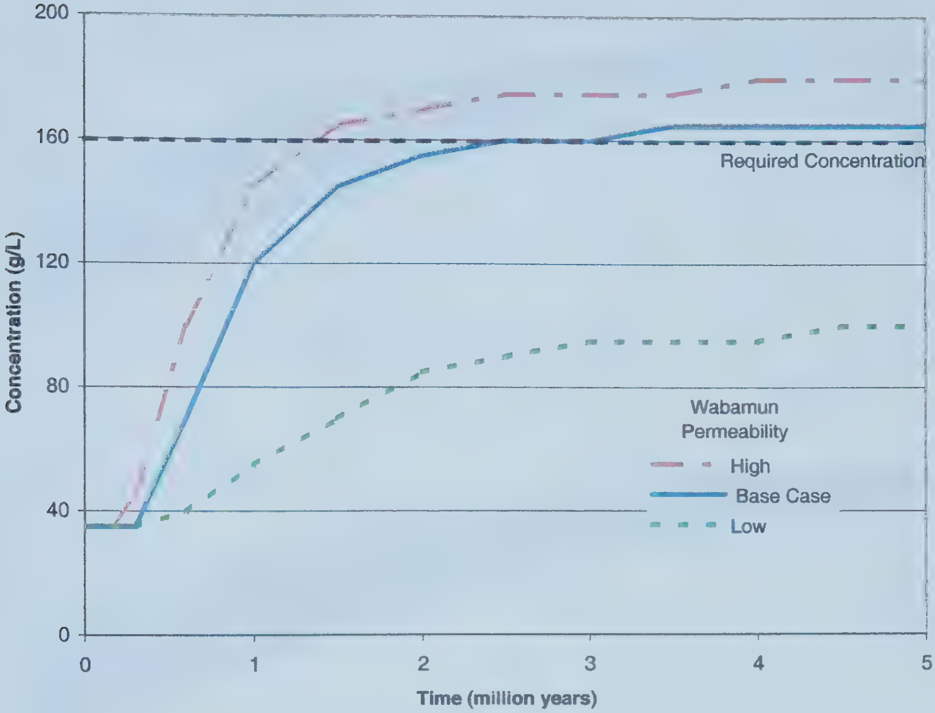

Figure 6.6 – Comparing the effect of the Wabamun permeability on the concentration over time at an observation point in the MGA

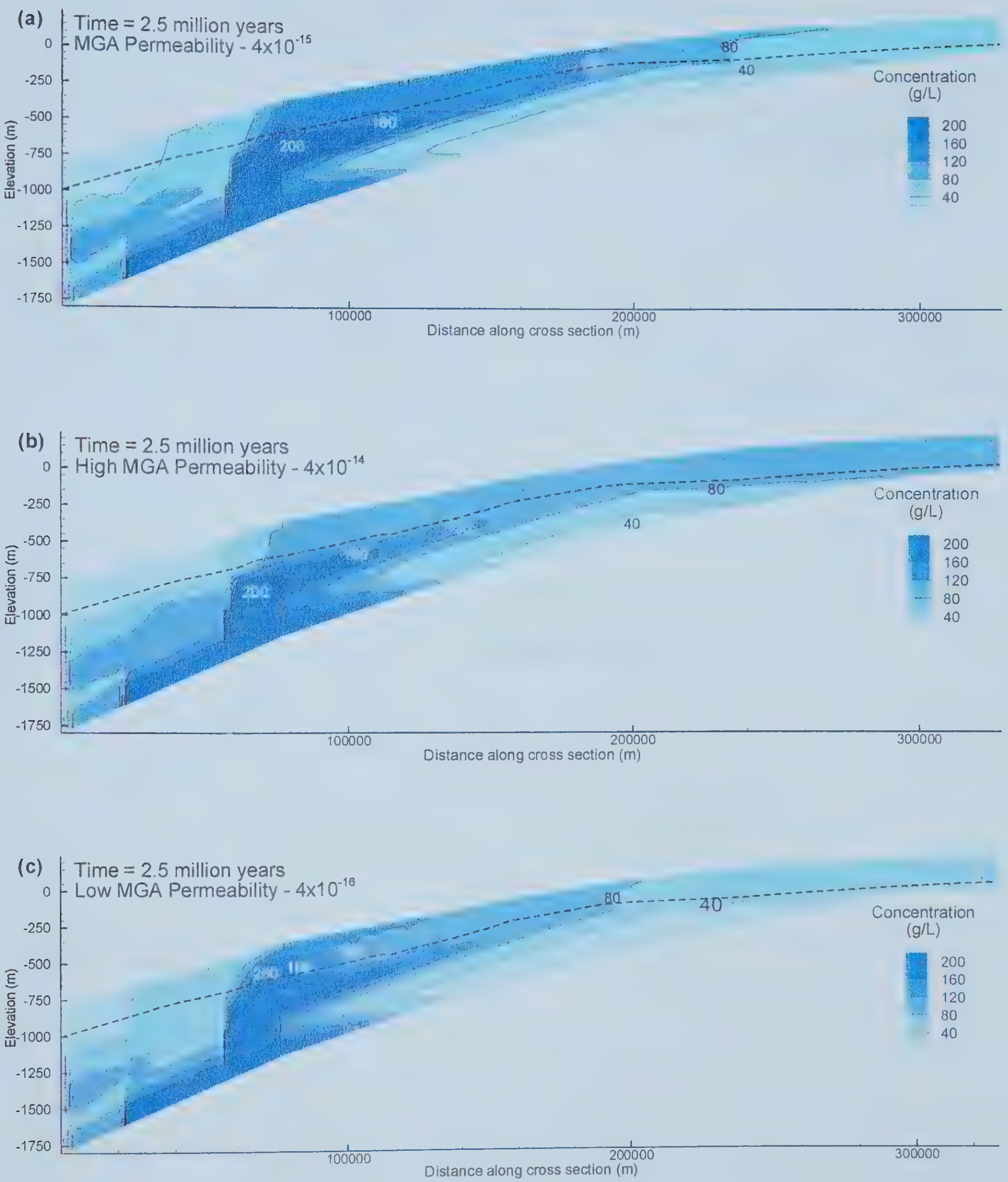

Figure 6.7 - Results of the sensitivity analysis to determine the effects of the Mannville Group aquifer permeability (a) $4x10^{-15}$, (b) $4x10^{-14}$, and (c) $4x10^{-16}$ m^2. Contour interval of 40 g/L. Dashed line indicates base of the MGA.

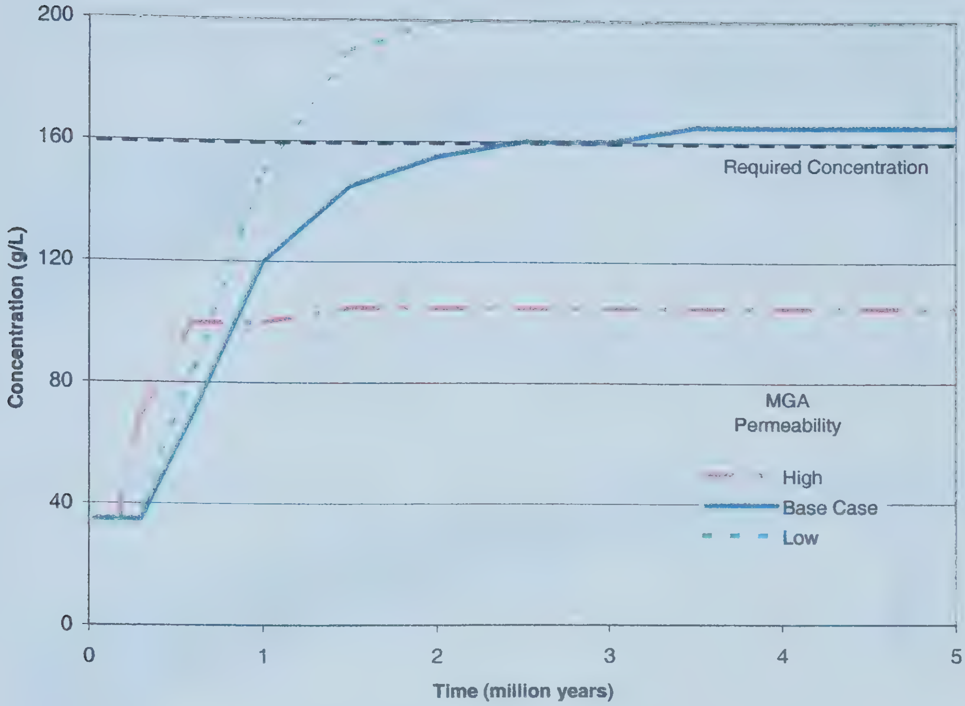

Figure 6.8 – Comparing the effect of the MGA permeability on the concentration over time at an observation point in the MGA

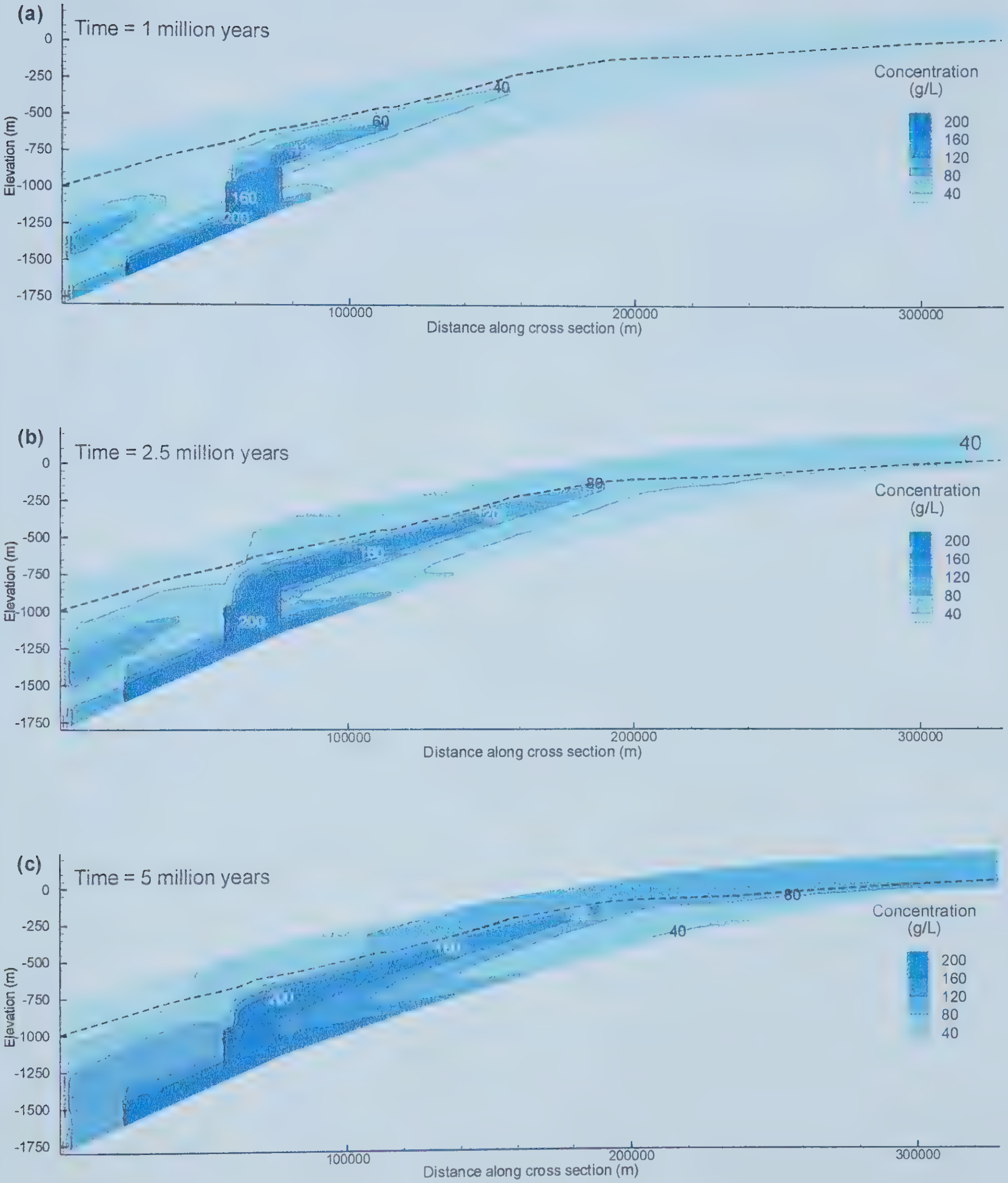

Figure 6.9 - Results of the sensitivity analysis to determine the effects of low aquitard permeability in the study area after (a) 1 million, (b) 2.5 million, and (c) 5 million. Contour interval of 40 g/L. Dashed line indicates base of the MGA.

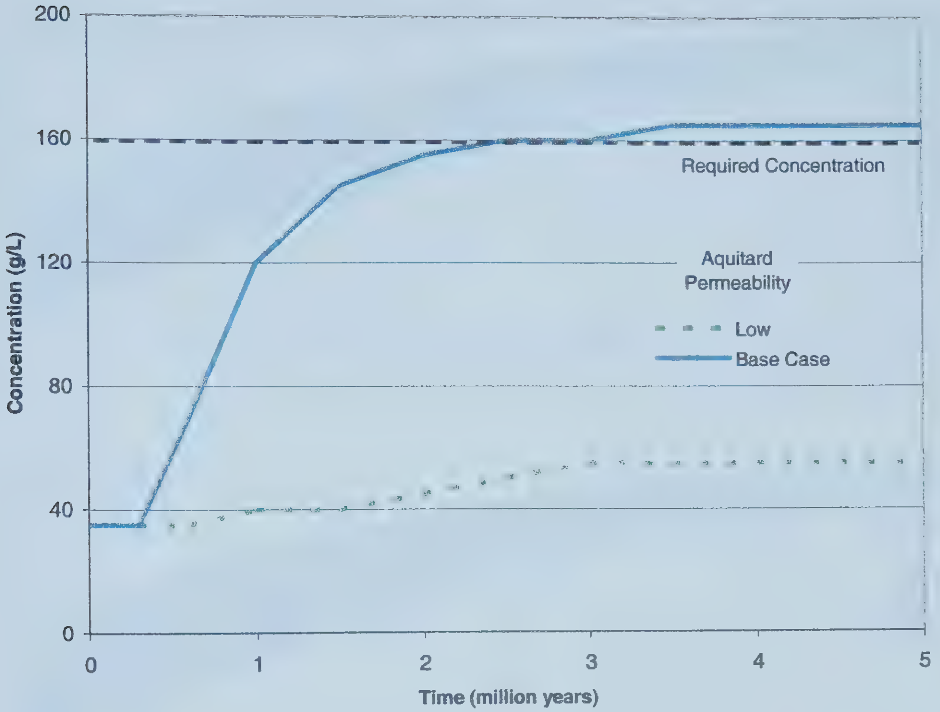

Figure 6.10 – Comparing the effect of the aquifer permeability on the concentration over time at an observation point in the MGA

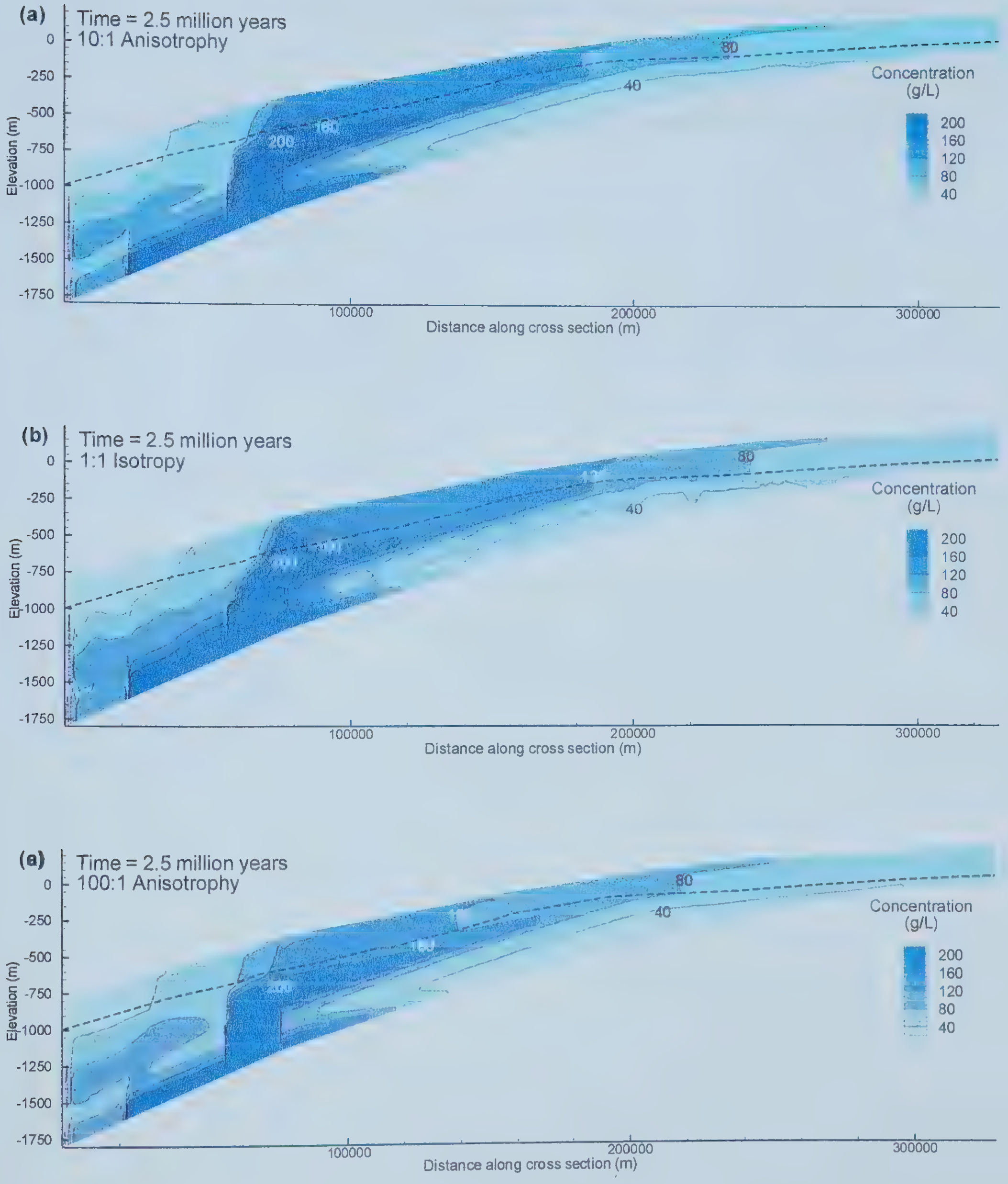

Figure 6.11 - Results of the sensitivity analysis to determine the effects of anisotropy (a) 10:1, (b) 1:1, and (c) 100:1. Contour interval of 40 g/L. Dashed line indicates base of the MGA.

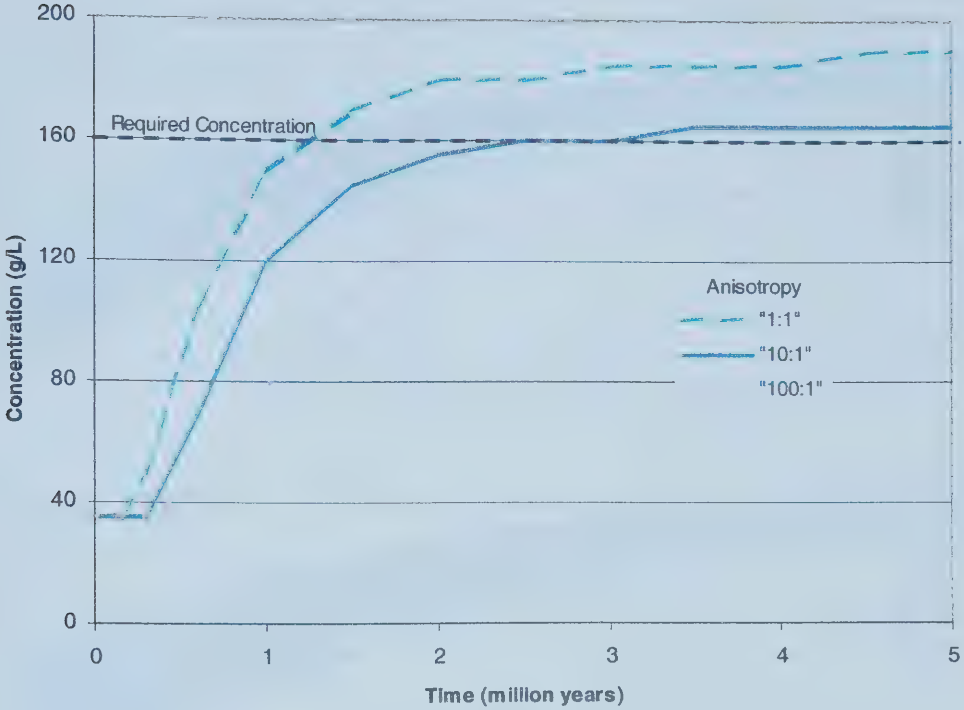

Figure 6.12 – Comparing the effect of anisotropy on the concentration over time at an observation point in the MGA

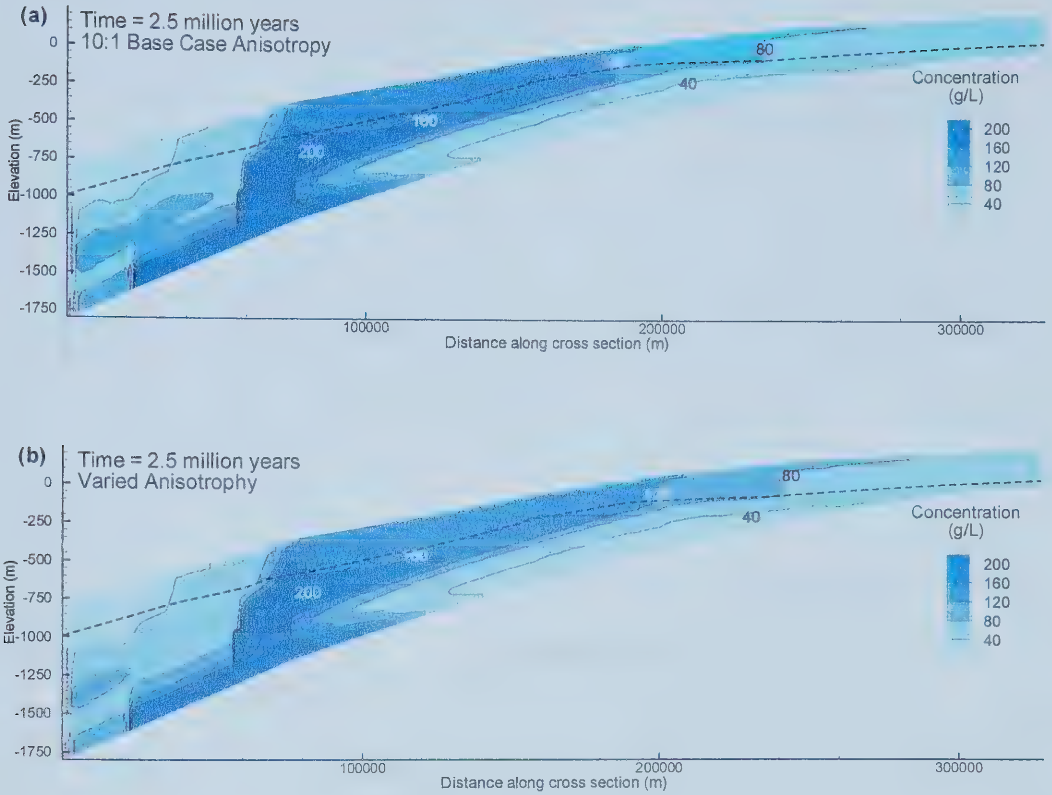

Figure 6.13 - Results of the sensitivity analysis to determine the effects of anisotropy (a) 10:1 and (b) varied anisotropy. Contour interval of 40 g/L. Dashed line indicates base of the MGA.

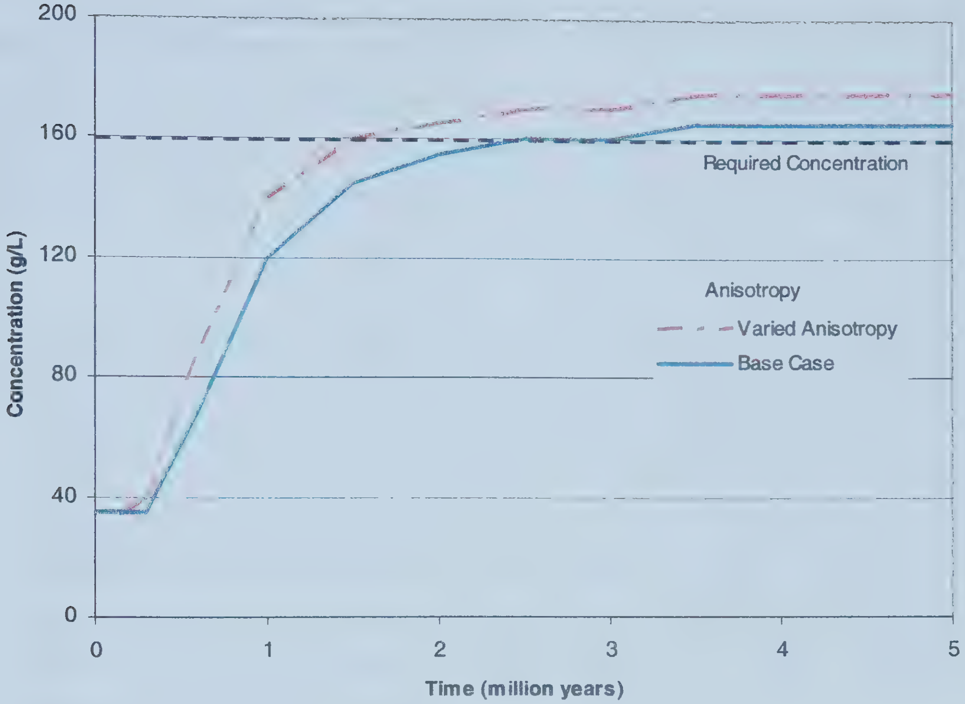

Figure 6.14 – Comparing the effect of varied anistropy on the concentration over time at an observation point in the MGA.

Chapter 7 Conclusions

Numerical simulations and field data analysis of density-dependent topography-driven fluid flow within the Alberta basin were used to investigate the migration and cross-formational flow behaviour of an anomalous brine plume found in the Mannville Group Aquifer.

1. The full extent of the brine plume in the MGA was delineated in the study area. The highest concentration of >140 g/L TDS is located slightly north of the Leduc Formation reef structure. The concentric contours of the high TDS plume are orientated in the south-west to north-east direction, following the structure of the dipping pre-Cretaceous strata in the basin. The >130 g/L TDS plume is estimated to be approximately 20,000 metres long. The >80 g/L TDS plume has an irregular shape, most likely resulting from mixing of the high concentration Devonian waters with the lower salinity MGA waters. The >80 g/L TDS plume is approximately 120,000 metres long.

2. Simulation results of the paleo fluid system support the predicted physical pathway of the brine migration (Rostron and Tóth, 1997). Previous studies used chemical similarities and hydraulic mapping to trace the plume in the MGA back to Devonian strata. Numerical simulations showed that brine originating in the Cooking Lake aquifer, and constrained by the geology and boundary conditions, would travel updip and then vertically ascend through the Leduc aquifer, and continue to travel vertically through/across the Nisku aquifer and the Wabamun aquitard, ultimately entering the MGA..

3. The present day topographic gradient produced a hydraulic gradient of 0.001 which was insufficient to emplace the observed brine plume in 30 million years, the amount of time in which the basin has been tectonically dormant. The simulation results show that after 30 million years the maximum concentration in the MGA never exceeded 80 g/L TDS.

4. The results using a paleo-hydraulic gradient of 0.01 (Bustin, 1991) did not fit the criteria of desired salinity distribution. At the observation point in the MGA a TDS concentration of 160 g/L is reached after 1 million years. Simulation results

indicated that a high TDS plume >180 g/L would have filled the MGA after 5 million years. As the highest of the simulated gradients, this scenario produced an unrealistic salinity distribution.

5. A paleo-hydraulic gradient of 0.004 (Nurkowski, 1984) was applied to the model domain, the resulting salinity distribution in the MGA was a large plume of low concentrations. The concentration at the observation point in the MGA slowly increased in the simulation. After 5 million years of simulation time the maximum concentration in the MGA were <160 g/L. This hydraulic gradient allowed the fluid within the MGA to dilute the upwelling higher TDS fluid, therefore preventing the desired salinity distribution. This gradient produced a large, low concentration plume which did not represent the plume observed today.

6. Best estimate of hydraulic gradient was found to be the average gradient of 0.007. The results from the paleo-hydraulic gradient simulation based on hypothesised gradients indicated that the model is very sensitive to changes in the hydraulic gradient. The high case of 0.01 fills the basin with very high TDS fluid and the low 0.004 case is unable to achieve the desired maximum concentration in the MGA.

7. The time scale for plume emplacement in the MGA was approximately 5 million years using a median hydraulic gradient of 0.007. A maximum concentration of >160 g/L TDS enters the MGA after 2.5 million years and then levels off. This simulation creates a condensed salinity distribution in the MGA, ranging from 35 g/L TDS downdip from the plume to the maximum of 160 g/L at the Wabamun aquitard subcrop and back to 40 g/L at the Ireton subcrop and is the best representation of the observed brine plume.

8. A sensitivity analysis performed on the base case allowed for the evaluation of various key simulation parameters, such as, vertical gradient, permeability, and anisotropy. This analysis showed that the parameters used in the base case are the most representative.

7.1 Recommendations

1. A 3D model might have provided additional insight into the problem but in terms of the paleo-flow system it is believed that the flow is occurring up the tilted strata of the Paleozoic therefore, the 2 dimensional model used was appropriate.

2. Further study into the anomalous brine plume should take into account both density and temperature.

References

Abercrombie, H.J., and Fullmer, E.G. 1992. Regional hydrogeology and fluid geochemistry of the Mannville Group, Western Canada Sedimentary Basin: Synthesis and reinterpretation. 7th international symposium on water-rock interaction, p.1101-1104.

Abercrombie, H.J., Cody, J.D., Hutcheon, I.E. and Myers, T.R. 1994. Fluid geochemistry of the Mannville Group, Alberta: Physical and chemical processes, implications for basin evolution. Programs, Expanded Abstracts, and Biographies, Canadian Society of Exploration Geophysicists and Canadian Society of Petroleum Geologists, 1994 Annual Conference, p. 307-308.

Alberta Energy and Utilities Board. 2001. Statistical Series 2001-98: Alberta's Reserves 2000 and supply/demand outlook 2001-2010. AEUB, Calgary AB.

Anderson, M.P. and Woessner, W.W. 1991. Applied Groundwater Modeling; Simulation of Flow and Advective Transport. Academic Press, Inc., 381p.

Anfort, S.J., Bachu, S., and Bentley, L.R. 2001. Regional-scale hydrogeology of the Upper Devonian-Lower Cretaceous sedimentary succession, south-central Alberta Basin, Canada. AAPG Bulletin, v. 85, no. 4, p. 637-660.

Bachu, S. 1985. Influence of lithology and fluid flow on the temperature distribution in a sedimentary basin: A case study from the Cold Lake area, Alberta, Canada. Techonophysics, v. 120, p. 257-284.

Bachu, S. 1995a. Flow of variable density formation water in deep sloping aquifers: review of methods of representation with case studies. Journal of Hydrology, v. 164, p. 19-38.

Bachu, S. 1995b. Synthesis and model of formation-water flow, Alberta Basin, Canada. AAPG Bulletin, v. 79, no. 8, p. 1159-1178.

Bachu, S. 1999. Flow systems in the Alberta Basin: Patterns, types and driving mechanisms. Bulletin of Canadian Petroleum Geology, v. 47, no. 4, p. 455-474.

Bachu, S., Sauveplane, C.M., Lytviak, A.T., and Hitchon, B. 1987. Analysis of Fluid and Heat Regimes in Sedimentary Basins: Techniques for Use with Large Data Bases. AAPG Bulletin, v. 71, no.7, p. 822-843.

Bachu, S., Perkins, E.H., Hitchon, B., Lytviak, A.T. and Underschultz, J.R. 1989. Evaluation of effects of deep waste injection in the Cold Lake area, Alberta. Alberta Research Council Bulletin 60, 57p.

Bachu, S. and Michael, K. 2002. Flow of variable-density formation water in deep sloping aquifers: minimizing the error in representation and analysis when using hydraulic head distributions. Journal of Hydrology, v. 259, p. 49-65.

Bachu, S. and Underschultz, J.R. 1993. Hydrogeology of formation waters, Northeastern Alberta Basin. AAPG Bulletin, v. 77, no. 10, p. 1745-1768.

Barson, D. 1993. The Hydrogeology Characterization of Oil Fields in North-Central Alberta for Exploration Purposes. PhD, Department of Geology, Edmonton, University of Alberta, 301p.

Barson, D., Rakhit, K., Myers, T., Powers, N., and Poletto, C. 1998. A new look at tilted oil/water contacts in the Williston Basin. In: Eighth International Williston Basin Symposium, J.E.

Christopher, C.F. Gilboy, D.F. Paterson and S.L. Bend (eds), Saskatchewan Geological Society Special Publication, no. 13, p. 226-228.

Beaumont, C. 1981. Foreland Basins. Geophysical Journal of the Royal Astronomical Society, v. 56, p. 291-329.

Beaumont, C., Quinlan, G.M., and Stockmal, G.S. 1993. The evolution of the Western Interior Basin: causes, consequences and unsolved problems. W.G.E. Caldwell and E.G. Kauffman (eds), Geological Association of Canada. Special Paper 39, p. 97-117.

Bekele, E.B., Person, M.A., Rostron, B.J., and Barnes, R. 2002. Modeling secondary oil migration with core-scale data: Viking Formation, Alberta Basin. AAPG Bulletin, v. 86, no. 1, p. 55-74.

Belitz, K., and Bredehoeft, J.D. 1988. Hydrodynamics of Denver Basin: explanation of subnormal fluid pressure. AAPG Bulletin, v. 72, no.11, p. 1334-1359.

Bethke, C.M. 1989. Modeling subsurface flow in sedimentary basins. Geologische Rundschau, v. 78, no.1, p. 129-154.

Bradley, J.S. 1975. Abnormal formation pressure. AAPG Bulletin, v. 59, no.6, p. 957-973.

Bustin, R.M. 1991. Organic maturity in the Western Canada Sedimentary Basin. International Journal of Coal Geology, v. 19, p. 319-358.

Caldwell, W.G.E. 1984. Early Cretaceous transgressions and regressions in the Southern Interior Plains. The Mesozoic of Middle North America. D. E. Stott and D. J. Glass (eds), Canadian Society of Petroleum Geologists. Memoir 9, p. 173-203.

Cant, D.J. 1983. Spirit River Formation: a stratigraphic-diagenetic gas trap in the deep basin of Alberta. AAPG Bulletin, v. 67, no. 4, p. 577-587.

Cathles, L. 1981. Fluid flow and hydrothermal ore deposits. Economic Geology, v. 75, p. 424-457.

Cody, J.D. and Hutcheon, I.E. 1994. Regional water and gas geochemistry of the Mannville Group and associated horizons, southern Alberta. Bulletin of Canadian Petroleum Geology, v. 42, no. 4, p. 449-464.

Corbet, T.F. and Bethke, C. M. 1992. Disequilibrium fluid pressures and groundwater flow in the Western Canada Sedimentary Basin. Journal of Geophysical Research, v. 97, no. 5, p. 7203-7217.

Creaney, S. and Allan, J. 1990. Hydrocarbon generation and migration in the Western Canada Sedimentary Basin. Classic Petroleum Provinces. J. Brooks, Geological Society Special Publication, v. 50, p. 189-202.

Davies, P.B. 1987. Modelling areal, variable density, groundwater flow using equivalent freshwater heads - analysis of potential significant errors. In: Proceedings of the NWWA-IGWMC Conference - Solving groundwater problems with models. National Water Well Association, Dublin Ohio, p. 888-903.

de Marsily, G. 1986. Quantitative hydrogeology. Academic Press Inc., San Diego, 440p.

DeWiest, R.J. 1965. Geohydrology. John Wiley and Sons Inc., New York, 366p.

Downey, M.W. 1984. Evaluating seals for hydrocarbon accumulations. AAPG Bulletin, v. 68 no.11, p. 1752-1763.

Elder, J.W. 1967. Transient convection in a porous medium. Journal Fluid Mechanics, v. 27, no. 3, p. 609-623.

Energy Resources Conservation Board. 1991. Alberta's reserves of crude oil, oil sands, gas, natural gas liquids and sulphur, at December 1991, Report ST-92-18. Energy Resources Conservation Board, Calgary.

England, T.D. and Bustin, R.M. 1986. Thermal maturation of the Western Canadian Sedimentary Basin south of the Red Deer River; Alberta plains. Bulletin of Canadian Petroleum Geology, v. 34, no. 1, p. 71-90.

Fetter, C.W. 1994. Applied Hydrogeology. Prentice Hall, Inc., New Jersey, 691 p.

Freeze, R.A. and Witherspoon, P.A. 1967. Theoretical analysis of regional groundwater fFlow 2) Effects of water-table configuration and subsurface permeability variation. Water Resources Research, v. 3, no. 2, p. 623-634.

Garven, G. 1985. The role of regional fluid flow in the genesis of the pine point deposit, Western Canada Sedimentary Basin. Economic Geology, v. **80,** p. 307-324.

Garven, G. 1989. A hydrogeologic model for the formation of the giant oil sands deposits of the Western Canada Sedimentary Basin. American Journal of Science, v. 289, no. 2, p. 105-166.

Garven, G. 1995. Continental-scale groundwater flow and geologic processes. Annual Reviews in Earth and Planetary Science, v. 23, p. 89-117.

Ge, S. and Garven, G. 1989. Tectonically induced transient groundwater flow in foreland basin: Origin and evolution of sedimentary basins and their energy and mineral deposits. R. A. Price (eds). Washington, D.C., American Geophysical Union. Monograph 48: p. 145-157.

Ge, S. and Garven. G. 1994. A theoretical model for thrust-induced deep groundwater expulsion with application to the Canadian Rocky Mountains. Journal of Geophysical Research, v. 99, no. B7, p. 13851-13868.

Gelhar, L.W. 1986. Stochastic subsurface hydrology from theory to applications. Water Resources Research, v. 22, no. 9, p. 135S-145S.

Hacquebard, P.A. 1977. Rank of coal as index of organic metamorphism for oil and gas in Alberta, Canada. AAPG Bulletin, v. 61, no. 5, p. 791.

Halbertsma, H.L. 1994. Devonian Wabamun Group of the Western Canada Sedimentary Basin. In: Geological Atlas of the Western Canada Sedimentary basin, G.D. Mossop and I. Shetson (eds.), Canadian Society of Petroleum Geologists and Alberta Research Council, p. 203-221.

Hanor, J.S. 1994. Origin of saline fluids in sedimentary basins. Geofluids: Origin, Migration and Evolution of Fluids in Sedimentary Basins, Parnell, J. (eds), Geological Society Special Publication No. 78, p. 151-174.

Hayes, T.S., LaRock, E.J., Gaines, J., Seger, C.M., Lasemi, Z., and Olive, W.W. 1992. Mapping lithologic criteria for mineral deposit potential using a subsurface lithologic database

interactive with ARC/INFO. In: USGS Open File Report 92-1: Mineral Resources of the Illinois Basin in the Context of Basin Evolution. p. 22-24.

Hearn, M.R. 1996. Stratigraphic and Diagenetic Controls on Aquitard Integrity and Hydrocarbon Entrapment, Bashaw Reef Complex, Alberta, Canada. MSc. thesis, University of Alberta, 134p.

Henry, H.R. 1964. Effects of dispersion of salt encroachment in coastal areas, In: Sea Water Coastal Aquifers, U.S. Geological Survey Water-Supply Paper 1613-C: p. C71-C84.

Hitchon, B. 1969a. Fluid flow in Western Canada Sedimentary Basin 1) Effects of topography. Water Resources Research, v. 5, no. 1, p. 186-195.

Hitchon, B. 1969b. Fluid flow in Western Canada Sedimentary Basin 2) Effects of geology. Water Resources Research, v. 5, no. 2, p. 460-469.

Hitchon, B. 1974. Application of geochemistry to the search for crude oil and natural gas. Introduction to exploration geochemistry. A.A. Levinson (eds). Calgary, Alberta, Applied Publishing Limited, v. 13, p. 509-554.

Hitchon, B. 1984. Geothermal gradients, hydrodynamics, and hydrocarbon occurances, Alberta, Canada. AAPG Bulletin, v. 68, no. 6, p. 713-743.

Hitchon, B., Sauveplane, C.M., Bachu, S., Koster, E.H.J. and Lytviak, A.T. 1989a. Hydrogeology of Swan Hills area, Alberta: Evaluation for deep water injection. Alberta Research Council_Bulletin 58. 79p.

Hitchon, B., Bachu, S., Sauveplan, C.M., Ing, A., Lytviak, A.T. and Underschultz, J.R. 1989b. Hydrogeology and geothermal regimes in the Phanerozoic succession, Cold Lake area, Alberta and Saskatchewan. Alberta Research Council Bulletin 59, 84p.

Hitchon, B., and Brulotte, M. 1994. Culling criteria for “standard” formation water anaylses, Applied Geochemistry, v. 9, p. 637-645.

Holzbecher, E. 1998. Modeling Density-Driven Flow in Porous Media: Principles, numerics, software. Springer-Verlag, Berlin, 286p.

Hubbert, M. K. 1953. Entrapment of petroleum under hydrodynamic conditions. AAPG Bulletin, v. 37, no. 8, p. 1954-2026.

Hugo, K.J. 1990. Mechanisms of groundwater flow associated with Leduc reefs. Bulletin of Canadian Petroleum Geology, v. 38, no. 2, p. 307-319.

Huyakorn, P.S., and Pinder, G.F. 1983. Computational Methods in Subsurface Flow, Academic Press Inc., New York, 473p.

Ingebritsen, S.E. and Sanford, W.E. 1998. Groundwater in geologic processes. Cambridge University Press, Cambridge, United Kingdom, 341p.

Jorgensen, D.G, Gogel, T., and Signor, D.C. Spring 1982. Determining of flow in aquifers containing variable density water. Ground Water Monitoring Review, p. 40-45.

Kipp, K.L. 1897. HST3D; a computer code for simulation of heat and solute transport in three-dimensional ground-water flow systems. Water-Resources Investigations. U.S. Geological Survey. 517p.

Kalkreuth, W. and McMechan, M. 1988. Burial history and thermal maturity, Rocky Mountain front ranges, foothills and forelnad, east-central British Columbia and adjacent Alberta, Canada. American Association of Petroleum Geologists Bulletin, v. 72, no. 11, p. 1395-1410.

Lachenbruch, A.H. 1985. Regional thermal structure in the Western U.S. In: American Geophysical Union, 1980 fall meeting, Eos, Transactions, American Geophysical Union. v. 61, no. 46, p. 1144-1145.

Lahm, T. D., Blair, E.S., and VanderKwaak, J. 1998. Role of salinity-derived variable-density flow in the displacement of brine from a shallow, regional extensive aquifer. Water Resources Research, v. 34, no. 6, p. 1469-1480.

Leckie, D.A., Bhattacharya, J.P., Bloch, J., Gilboy, C.F. and Norris, B. 1994. Creteceous Colorado/Alberta Group of Western Canadian Sedimentary Basin. Geological Atlas of Western Canada Sedimentary Basin, G. D. Mossop and I. Shetsen (eds.), Canadian Society of Petroleum Geologists and Alberta Research Council, p. 335-353.

Luo, X. and Vasseur, G. 1996. Geopressuring mechanism of organic matter cracking: Numerical modeling. AAPG Bulletin, v. 80, no. 6, p. 856-874.

Luscynski, N.J. 1961. Head flow of groundwater of variable density. Journal of Geophysical Research, v. 66, no. 12, p. 4247-4255.

Machel, H.G. and Cavell, P.A. 1999. Low-flux, tectonically-induced squeegee fluid flow hot flash into the Rocky Mountain Foreland Basin. Bulletin of Canadian Petroleum Geology, v. 47, no. 4, p. 510-533.

Menard, H.W. 1961. Some rates of regional erosion. Journal of Geology, v. 69, no. 2, p. 154-161.

Mossop, G.D. and Shetsen., I. (compilers), 1994. Geological Atlas of Western Canada Sedimentary Basin. Canadian Society of Petroleum Geologists and Alberta Research Council, 510p.

Moore, P.F. 1988. Devonian Geohistory of the Western Interior of Canada. Devonian of the World. N. J. McMillan, A. F. Embry and D. J. Glass (eds). Canadian Society of Petroleum Geologists, Calgary, v. 1, p. 67-83.

Nurkowski, J.R. 1984. Coal quality, coal rank variation and its relation to reconstructed overburden, Upper Cretaceous and Tertiary Plains Coal, Alberta, Canada. AAPG Bulletin, v. 68, no. 3, p. 285-295.

Nurkowski, J.R. 1985. Coal quality and rank variation within Upper Cretaceous and Tertiary sediments, Alberta plains region. Earth Science Report 85-1: Alberta Research Council, 38p.

Oliver, J. 1986. Fluids expelled tectonically from orogenic belts: Their role in hydrocarbon migration and other geologic phenomena. Geology, v. 14, p. 99-102.

Osadetz, K.G., Goodarzi, F., Snowdon, L.R., Brooks, P.W., and Fayerman, S. 1990. Winnipegosis pinnacle reef play in Williston basin, Saskatchewan and North Dakota: oil compositions and effects of oil-based drilling muds on exploration geochemistry. Current Research Part D, Geological Survey of Canada Paper 90-1D. p. 153-163.

Parks, K.P. and Tóth, J. 1995. Field evidence for erosion-induced underpressuring in Upper Cretaceous and Tertiary strata, west central Alberta, Canada. Bulletin of Canadian Petroleum Geology, v. 43, no. 3, p. 281-292.

Paul, D. 1994. Hydrogeology of the Devonian Rimbey-Meadowbrook reef trend of central Alberta, MSc. thesis, University of Alberta. 162p.

Person, M., Neuzil, C., Dahlstrom, D., Mailloux, B., Wieck, J., Toupin, D., Eadington, P., Wheelock, S., Bekele, E., and Swenson J. in review. RIFT2D: A finite element model for simulating two-dimensional fluid, heat, and solute mass transport in evolving sedimentary basins, US Geological Survey Water Resources Investigation, *Water Resources Investigations Report*.

Porter, J.W., Price, R.A., and McCrossan, R.G. 1982. The Western Canada Sedimentary Basin. Phil. Transaction of the Royal Society of London, A 305, p.169-192.

Riediger, C. L., Fowler, M.G., Showdon, L.R., MacDonald, R., and Sherwin, M.D. 1999. Origin and alteration of Lower Cretaceous Mannville Group Oils from the Provost oil field, east central Alberta, Canada. Bulletin of Canadian Petroleum Geology, v. 47, no. 1, p. 43-62.

Reinson, G.E., Warters, W.J., Cox, J. and Price, P.R. 1994. Cretaceous Viking Formation of the Western Canada Sedimentary Basin. In: Geological Atlas of Western Canada Sedimentary Basin, G.D. Mossop and I. Shetsen (eds.), Canadian Society of Petroleum Geologists and Alberta Research Council, p. 353-363.

Richards, B.C., Barclay, J.E., Bryan, D., Hartling, A., Henderson, C.M., and Hinds, R.C. 1994. Carboniferous strata of the Western Canada Sedimentary Basin. In: Geological Atlas of Western Canada Sedimentary Basin, G. D. Mossop and I. Shetsen (eds), Canadian Society of Petroleum Geologists and Alberta Research Council, p. 221-251.

Ricketts, B.D., Ed. 1989. Western Canada Sedimentary Basin - a case history. Canadian Society of Petroleum Geologists, Calgary, 320p.

Rostron, B.J. 1995. Cross-formational fluid flow in Upper Devonian to Lower Cretaceous strata, west-central Alberta, Canada. Ph.D. thesis, University of Alberta, 201p.

Rostron, B.J. and Tóth, J. 1997. Cross-formational fluid flow and the generation of a saline plume of formation waters in the Mannville Group, central Alberta. In: Petroleum Geology of the Cretaceous Mannville Group, Western Canada, Memoir 18, p. 169-190.

Rostron, B. J., Tóth, J. and Machel, H. 1997. Fluid Flow, hydrochemistry and petroleum entrapment in Devonian reef complexes, south-central Alberta, Canada. Basin-Wide Diagenetic Patterns: Integrated Petrologic, Geochemical, and Hydrologic Considerations, SEPM Special Publication No. 57. p. 139-155.

Russell, M.J. 1992. Plate tectonics and hydrothermal ore deposits. *In:* Understanding the Earth, G.C. Brown, C.J. Hawkesworth, R.C.L. Wilson (eds.), Cambridge, Cambridge University Press. Chapter 11, p. 204-221.

Sanford, W.E., and Konikow, L.F. 1985. A two-constituent solute transport model for ground water having variable density: U.S. Geological Survey Water-Resources Investigations Report 85-4279, 89p.

Schwartz, F.W., Muehlenbachs, K., and Chorley, D.W. 1981. Flow-system controls of the chemical evolution of groundwater. Journal of Hydrology, v. 54, p. 225-243.

Senger, J.M. and Fogg, G.E. 1987. Regional under-pressuring in deep brine aquifers, Palo Duro Basin, Texas. 1. Effects of hydrostratigraphy and topography. Water Resources Research, v. 23, p. 1481-1493.

Sharp, J.M., and Kyle, J.R. 1988. The role of ground-water processes in the formation of ore deposits. In: Hydrogeology. W. Back, J.S., Rosenshein, and P.R., Seaber, (eds.), Geological Society of America, p. 461-483.

Shi, Y. and Wang, C. 1986. Pore pressure generation in sedimentary basins: overloading versus aquathermal. Journal of Geophysical Research, v. 91, no. B2, p. 2153-2162.

Simmons, C.T. and Sharp, J.M., 2000. On variable-density groundwater flow in heterogeneous porous media. In: Groundwater: Past Achievements and Future Challenges, Sililo *et al. (eds),* Balkema, Rotterdam, p 425-430.

Spencer, R.J. 1987. Origin of Ca-Cl brines in Devonian formations, western Canada sedimentary basin. Applied Geochemistry, v. 2, p. 373-384.

Switzer, S.B., Holland, W.G., Christie D.S. and Graf, G.C. 1994. Devonian Woodbend to Winterburn strata of the Western Canada Sedimentary Basin. In: Geological Atlas of the Western Canada Sedimentary basin. G. D. Mossop and I. Shetson (eds.), Canadian Society of Petroleum Geologists and Alberta Research Council, p. 165-203.

Tóth, J. 1962. A theory of groundwater motion in small drainage basins in Central Alberta, Canada. Journal of Geophysical Research, v. 67, no. 11, p. 4375-4387.

Tóth, J. 1963. A theoretical analysis of groundwater flow in small drainage basins. Journal of Geophysical Research, v. 68, no.16, p. 4795-4812.

Tóth, J. 1978. Gravity-induced cross-formational flow of formation fluids, Red Earth region, Alberta, Canada: Analysis, patterns, evolution. Water Resources Research, v. 14, no. 5, p. 805-843.

Tóth, J. 1980. Cross-formational gravity-flow of groundwater: A mechanism of the transport and accumulation of petroleum The generalized hydraulic theory of petroleum migration. In: Problems of Petroleum Migration, W. H. Roberts and R. J. Cordell (eds.), American Association of Petroleum Geologists, Studies in Geology Number 10, p. 121-167.

Tóth, J. and Corbet, T.F. 1986. Post-Paleocene evolution of regional groundwater flow-systems and their relation to petroleum accumulations, Taber area, southern Alberta, Canada. Bulletin of Canadian Petroleum Geology, v. 34, no. 3, p. 339-363.

van Everdingen, R.O. 1968. Studies of formation waters in Western Canada: Geochemistry and hydrodynamics. Canadian Journal of Earth Sciences v. 5, p. 523-543.

Voss, C.I. 1984. SUTRA: A finite element simulation model for saturated-unsaturated, fluid-density-dependent groundwater flow with energy transport or chemically reactive single species solute transport. USGS Water Resources Investigation Reports 84-4369, 409p.

Voss, C.I., and Souza, W.R. 1987. Variable density flow and solute transport simulations of regional aquifers containing a narrow freshwater-saltwater transistion zone. Water Resources Research, v. 23, no. 10, p. 1851-1866.

Wendte, J.C. 1994. Cooking Lake platform evolution and its control on Late Devonian Leduc reef inception and localization, Redwater, Alberta. Bulletin of Canadian Petroleum Geology, v. 42, no. 4, p. 499-528.

Willett, S.D., Issler, D.R., Beaumont, C., Donelick, R.A., and Girst, A.M. 1997. Inverse modeling of annealing of fission tracks in apatite 2: Application to the thermal history of the Peace River Arch region, Western Canada Sedimentary Basin. American Journal of Science, v. 297, no. 10, p. 970-1011.

Wright, G.N., McMechan, M.E., and Potter, D.E.G. 1994. Structure and Architecture of the Western Canada Sedimentary Basin. In: Geological Atlas of the Western Canada Sedimentary basin. G.D. Mossop and I. Shetson (eds), Canadian Society of Petroleum Geologists and Alberta Research Council, p. 25-40.

Yeh, G.T. 1987. 3D-FEMWATER; a three-dimensional finite element model of water flow through saturated-unsaturated media, Oak Ridge National Laboratory, Publication No. 2904, 314p.

Appendix A

Culling Criterion of Formation Water Analyses

Culling Criterion of Formation Water Analyses

The Geofluids (Rakkit Petroleum Ltd.) database was used to compile the total dissolved solids (TDS) data of the MGA within the study area. TDS is determined by either the directly by the adding measured dissolved constituents or by weighing solid residues after evaporation or indirectly from electrical conductivity or spontaneous potential response.

TDS is calculated by:

$$TDS = Na + K + Ca + Mg + Ba + Sr + Cl + Br + I + HCO_3^{\;-} + SO_4^{\;2-} + CO_3^{\;2-}$$

The criterion for culling chemistry data has been well established. The Opus Petroleum Engineering publication of Formation Waters of Western Canada (Johnson, 1992) was a useful guide to the interpretation of the data. Other sources for culling criterion were Bustin's (1993) PhD on oil field hydrogeology and Hitchon and Brulotte's (1994) study on culling criteria for "standard" formation water analysis.

The method used in this thesis for mapping the TDS in the MGA involved flagging samples that were suspect for various reasons. Table 1.1 outlines the criteria used for culling the chemistry data. Each of these points were 'flagged', when a sample had more than one flag it was eliminated from the data set. Samples with one flag were compared to the adjacent data point and if they did not correspond they were also culled. Initially, within the study area, there were approximately 6000 data points. Using this culling criterion the number of data points was reduced to approximately 2000. The final step of culling the data involved cleaning up anomalous values.

There are many causes of erroneous chemistry data. The nature of sample collection makes it difficult to rely on the accuracy of the results (Johnson, 1992). The following paragraphs describe the common causes for invalid data as outlined by the Opus Petroleum Engineering publication of Formation Waters of Western Canada (Johnson, 1992). The majority of the samples are collected from drill stem tests but samples are also collected from well heads, treaters, separators, holding tanks and bailers. When

the samples are collected from surface facilities it is difficult to get a pure formation water sample since they will become contaminated by the mixing of formation waters sampled from different levels and should therefore be eliminated from the data set. The recovery description (drilling mud, etc) also helped in determining the origin and reliability of the sample.

When sampling from a DST, the location of the sample has a large effect. A sample from the top of the borehole will be mostly mud filtrate, in the middle will be a mix of mud filtrate and formation waters and at the bottom the best samples are collected since they will be mostly formation water. Stiff diagrams can be used to separate drilling mud from formation water. Stiff diagrams of drilling mud have a unique ‘creamer’ shape whereas formation waters stiff diagrams typically have a ‘crest’ shape.

Possible contaminates of the DST samples are caused by drilling mud, acid washes, washes from cement jobs, and possible water injections (Johnson, 1992). Drilling fluid is the most common source of contaminants. Most drilling mud is kept at a high pH of 8.0 or higher by the addition of Sodium Hydroxide. This addition helps to reduce the amount of corrosion of the drilling equipment. This also leads to high levels of sodium in relation to chloride (Na/Cl >1.0).

Hydrochloric acid is another common contaminant. The HCL reacts with carbonate in the reservoir producing Calcium and Chloride ions, plus Magnesium if the rock contains Dolomite. Acid contamination is found within a water sample by low pH values. This is not always the case since during production the pH will recover making the recognition of acid contamination more difficult, therefore, it may be determined by high Calcium ion concentration and if Na/Cl is less than 0.5 (Formation waters are expected to have a Na/Cl ratio of between 1.0 – 0 – 0.5).

Contamination from water injection is easier to determine in deep formations if meteoric water is used in the injection process. Since this is not always the case the most reliable way to judge if the sample is contaminated is to search the drill stem records at the time the sample was taking to determine if water injection occurred in that pool. Also having a stiff ‘type diagram’ of the formation of interest will make it possible to find samples that do not fit with that ‘type curve’ that may be a mix of formation waters.

Culling Criteria	Explanations
Acid Indicators	
pH<5.5	Acid washes lowers pH
Na/Cl (moles)<0.5	HCl acid adds Cl. No Na added
Ca+Mg>30% total cations (moles)	Dolomite dissolution adds Ca and mg May also see: High Fe: drill pipe /casing dissolution IBE>5%
Mud filtrate Indicators	
K>=0.75% of total cations (moles)	KCl mud/completion fluid
Ca+Mg<=4% total cations (moles)	All muds are low in Ca and Mg
pH>=8.3	All muds maintained at high pH
SO4>2% total anions (moles)	High SO4 may indicate: Surface water added to well Sodium sulphate added to well Gypsum/Anhydrite are possible natural sources
Na/Cl (moles)>1	NaCl mud has Na/Cl~1.0 and high SO_4 otherwise similar to formation waters NaOH added a mud dispersant
Cl<98.5% anions (moles)	This criterion indicates high concentration nigh concentration of CO_3 or SO_4 (both indicate mud)
"drilling mud" in recovery description	
Hydrocarbon Indicators	
Hydrocarbons in recovery	Any recovery of hydrocarbons
Iodide measured	Iodine used as hydrocarbon proximity indicator
Analytical Reliability	
IBE=0.0%	Probably indicates Na calculated by difference
IBE>5%	Analytical error or presence of "exotic" ions
CO3 presents at pH<8.3	pH measurement error
HCO3 present at pH<4.5	pH measurement error

Table A1.1 – Culling Criteria for used for TDS analysis of Mannville Group aquifer brines (modified after Barson, 1993)

University of Alberta Library
0 1620 1720 3082

B45528